NAVAL POSTGRADUATE SCHOOL
Monterey, California

THESIS

Ocean Thermal Analysis and Related Naval Operational Considerations in the Ionian Sea - June 1980

Laurent Monsaingeon

September, 1981

Thesis Advisors: C. N. K. Mooers
R. H. Bourke

Approved for public release, distribution unlimited

SECURITY CLASSIFICATION OF THIS PAGE (When Data Entered)

REPORT DOCUMENTATION PAGE

READ INSTRUCTIONS BEFORE COMPLETING FORM

1. REPORT NUMBER

2. GOVT ACCESSION NO.

3. RECIPIENT'S CATALOG NUMBER

4. TITLE (and Subtitle)
Ocean Thermal Analysis and Related Naval Operational Considerations in the Ionian Sea - June 1980

5. TYPE OF REPORT & PERIOD COVERED
Master's Thesis
September, 1981

6. PERFORMING ORG. REPORT NUMBER

7. AUTHOR(s)
Laurent Monsaingeon

8. CONTRACT OR GRANT NUMBER(s)

9. PERFORMING ORGANIZATION NAME AND ADDRESS
Naval Postgraduate School
Monterey, California 93940

10. PROGRAM ELEMENT, PROJECT, TASK AREA & WORK UNIT NUMBERS

11. CONTROLLING OFFICE NAME AND ADDRESS
Naval Postgraduate School
Monterey, California 93940

12. REPORT DATE
September, 1981

13. NUMBER OF PAGES
144

14. MONITORING AGENCY NAME & ADDRESS(if different from Controlling Office)

15. SECURITY CLASS. (of this report)

15a. DECLASSIFICATION/DOWNGRADING SCHEDULE

16. DISTRIBUTION STATEMENT (of this Report)
Approved for public release, distribution unlimited

17. DISTRIBUTION STATEMENT (of the abstract entered in Block 20, if different from Report)

18. SUPPLEMENTARY NOTES

19. KEY WORDS (Continue on reverse side if necessary and identify by block number)

Mediterranean Sea	Military Oceanography	Oceanic Rossby Waves
Ionian Sea	Regional Oceanography	
Maltese Front	Naval Operations	Oceanic Fronts
XBT Analysis	Oceanic Eddies	

20. ABSTRACT (Continue on reverse side if necessary and identify by block number)
A synoptic analysis of the Ionian sea in June 1980 showed thermal patterns of various scale sizes, and in particular, a warm core eddy which was comparable in size (ca. 30 km) and location with one found in MILOC-68. Spatial correlation functions of temperature were anisotropic in the southern part, with zero-crossings of 30 km in the EW direction and 40 to 80 km in the NS direction, commensurate with the (first mode) baroclinic Rossby radius of

DD FORM 1 JAN 73 1473 EDITION OF 1 NOV 65 IS OBSOLETE
S/N 0102-014-6601

SECURITY CLASSIFICATION OF THIS PAGE (When Data Entered)

Block 20 cont'd:

deformation of 23 km. There was a shallow main sound channel (axis at ca. 100m) and some secondary sound channels caused by temperature inversions. The spatial patterns of these sound channels were associated with synoptic scale and mesoscale oceanic phenomena, which in turn were influenced by bathymetry. The temporal patterns were influenced by atmospheric forcing. It may be possible to use features seen in satellite IR imagery to deduce zones with shoaler thermocline depth. With data sampling appropriate to the scales of atmospheric and oceanic variability, a valuable synoptic scale analysis can be derived from XBTs collected under operational conditions. Recommendations for a regional approach to military oceanography and XBT sampling procedures are made.

Approved for public release; distribution unlimited.

Ocean Thermal Analysis and Related Naval Operational Considerations in the Ionian Sea - June 1980

by

Laurent Monsaingeon
Lieutenant de Vaisseau, French Navy

Submitted in partial fulfillment of the
requirements for the degree of

MASTER OF SCIENCE IN OCEANOGRAPHY

from the

NAVAL POSTGRADUATE SCHOOL
September 1981

ABSTRACT

A synoptic analysis of the Ionian Sea in June 1980 showed thermal patterns of various scale sizes, and in particular, a warm core eddy which was comparable in size (ca. 30 km) and location with one found in MILOC-68. Spatial correlation functions of temperature were anisotropic in the southern part, with zero-crossings of 30 km in the EW direction and 40 to 80 km in the NS direction, commensurate with the (first mode) baroclinic Rossby radius of deformation of 23 km. There was a shallow main sound channel (axis at ca. 100m) and some secondary sound channels caused by temperature inversions. The spatial patterns of these sound channels were associated with synoptic scale and mesoscale oceanic phenomena, which in turn were influenced by bathymetry. The temporal patterns were influenced by atmospheric forcing. It may be possible to use features seen in satellite IR imagery to deduce zones with shoaler thermocline depth. With data sampling appropriate to the scales of atmospheric and oceanic variability, a valuable synoptic scale analysis can be derived from XBTs collected under operational conditions. Recommendations for a regional approach to military oceanography and XBT sampling procedures are made.

RESUME

L'analyse synoptique de la mer Ionienne en Juin 1980 révèle des structures thermiques variées, et en particulier, un tourbillon chaud comparable en taille et position à celui trouvé au cours de MILOC-68. Les fonctions de corrélation spatiale en température sont anisotropiques dans la partie sud, avec des échelles respectives de 30 et 40 à 80 km dans les directions Est/Ouest et Nord/Sud, comparables au rayon baroclinique de déformation (1er mode) de 23 km. Le chenal sonore est situé à environ 100m de profondeur, et des inversions thermiques créent des chenaux sonores secondaires. La distribution spatiale de ces chenaux sonores est liée aux phenomènes océaniques à échelle synoptique et moyenne, eux-mêmes influencés par la bathymétrie. Les variations temporelles sont liées aux effets atmosphériques. Il semble possible d'utiliser l'imagerie satellite infra-rouge pour déterminer la profondeur de la thermocline. Il est conclus qu'une analyse synoptique valable peut être effectuée avec des sondages bathythermiques prélevés en ambiance opérationnelle à condition que ce prélèvement tienne compte de la variabilité océanique et atmosphérique. Des recommendations sont émises, concernant une approche régionale de l'océanographie militaire et les procédures de collecte bathythermique.

TABLE OF CONTENTS

LIST OF TABLES

LIST OF FIGURES

LIST OF ACRONYMS

ART	Airborne Radiometer Temperature
ASW	Antisubmarine Warfare
AVHRR	Advanced Very High Resolution Radiometer
BC	Boundary Condition
EOTS	Expanded Ocean Thermal Structure
FNOC	Fleet Numerical Oceanography Center
LIW	Levantine Intermediate Water
PLD	Primary Layer Depth
SSP	Sound Speed Profile
SST	Sea Surface Temperature
XBT	Expendable Bathythermograph

ACKNOWLEDGEMENT

I wish to thank Prof. Christopher N. K. Mooers for his guidance during the conduct of this thesis. Our weekly meetings, which extended over several months, provided continuous help, constructive criticism and encouragements. Furthermore, it offered to me a masterly example in the conduct of scientific investigation.

I am also indebted to Dr. Robert H. Bourke for his very helpful support and technical advice, in particular in the field of thermal and acoustic analysis. I must also thank O. M. Johannessen, A. R. Miller and L. A. Mysak for their useful comments provided at various stages of this study.

The guidance of Prof. Gilles Cantin, of the Mechanical Engineering Department, was instrumental in developing the program which restored satellite pictures to a geographical grid. In fact his support went far beyond by introducing me to computer graphics and some modern mathematical techniques.

CDR R. Barry, CDR J. Bodie and LCDR W. Rogers, USN, provided data as well as technical support from the FNOC, regarding acoustics, EOTS and archives-related matters. Captain Beydon (French Navy) was a key supporter and gave me access to the French Meteorological Office data base, which provided satellite pictures as well as atmospheric

analysis charts. The EPSHOM (Brest, France) provided very useful XBT information and navigation charts.

Finally, I wish to thank the French naval officers who, as sponsors from the Etat-Major de la Marine and the CEPOC, counseled and encouraged me along this sojurn at the Naval Postgraduate School.

I. INTRODUCTION

A. FOREWORD

The history of naval warfare has often demonstrated the impact of the oceanic environment on combat capabilities. Until recently, little was understood of the behavior of the ocean. For centuries, the traditional answer had been to develop some kind of innate feeling for the environment, as successfully demonstrated by mariners or fishermen. In more recent years, with the growing sophistication of naval ships, there has been a temptation to ignore the environment and consider its effects as harmless to a powerful technology, or at least secondary. But reality seems to go precisely the other way, and the solution, if any, lies through an increased knowledge of atmospheric and oceanic processes, which is still a challenge to the scientific community. As partial answers start to appear, a demand arises to strengthen the links between ocean science researchers and the users of the sea. Naval officers need to be informed and convinced that oceanology can provide useful, practical help in a variety of activities, ranging from antisubmarine warfare (ASW) to search and rescue.

This informative role will be one of the author's responsibilities in his next assignment with the environmental/ operational group of the French Navy. With experience in

ASW and a newly acquired knowledge in oceanography, he felt the need to test and apply it to a practical environmental problem in a way that would include a scientific approach to data analysis as well as a goal of practical, operational output products.

B. OBJECTIVES

This study was, hence, designed as an attempt to:

- acquire a keen knowledge and understanding of a particular oceanic region, especially its dynamical processes.
- analyse a set of operational data, i.e., data collected by naval ships in the course of an exercise in that area.
- yield operational products in the field of acoustic propagation.
- compare the results of the analyses with other studies.
- develop and tailor analytical tools, mainly computer software, for future use.
- finally, to evaluate the validity of this kind of computer-assisted, but basically manual approach as a support to naval operations.

Fortunately, a set of data was found in an area of some interest to the French Navy, a fact that increased to some extent the benefits of this study.

C. SUMMARY

- Zone: 33 to 39N, 14 to 19E, the Western Ionian Sea in the Central Mediterranean Basin.
- Period: 8 to 20 June 1980
- Data:
  - 167 expendable bathythermograms (XBT) taken during a US Navy exercise (SHAREM 38).
  - 14 infrared AVHRR satellite pictures (from the Centre de Meteorologie Spatiale, Lannion, France)
  - daily wind field analyses (from the Fleet Numerical Oceanography Center, Monterey and Meteorologie Nationale, Paris, France)
  - 3 complete analyese (EOTS) of thermal structure by the Fleet Numerical Oceanography Center.
- Computational tools:
  - the IBM 3033 for the main computations (Computer Center, Naval Postgraduate School)
  - the Tektronix 4081 for most graphic applications (Dept. of Mechanical Engineering)
- Output:
  - Thermal analyses from the surface to the 400m level
  - Resolution of small scale anomalies
  - Spatial and temporal variability
  - Acoustic variables

D. CONTENTS

Chapter II of this study reviews the climatology of the area, with emphasis on the exchange of water masses between the Eastern and Western Mediterranean Sea. Chapter III describes in some detail the way data were checked for quality. Selection of subareas for detailed analysis of thermal features is also described. It defines the statistical indices (cross-correlation) which are used later, and then addresses the processing of "other" data, e.g., satellite pictures and wind field. The description of the analysed fields commences with Chapter IV. The atmospheric conditions and their possible effect on the oceanic thermal structure are explained. Chapter V evaluates the different processes which might have a contaminating effect on the synopticity of the XBT data set, i.e., advection and non-synoptic sampling, and concludes with a reasonable assumption of synopticity. Chapters VI and VII describe in much detail the thermal structure found in the XBT data set, and gives some statistical (cross-correlation) parameters. The thermal fields are next analysed to yield acoustic variables, as discussed in Chapter VIII.

Two comparisons are made with other analyses: Chapter IX evaluates the results, relative to the Fleet Numerical Oceanography Center (FNOC) analysis, and Chapter X evaluates the results in the light of a previous, extensive study made in 1968 in the same area (MILOC-68).

Chapter XI summarizes the oceanographic picture, and, in conclusion, Chapter XII examines diverse qualitative problems related to the use and conduct of oceanographic analyses for and by forces at sea.

II. GENERAL FEATURES

The Western Ionian Sea, a part of the Central Mediterranean Sea, is bounded to the north by the Italian peninsula, to the south by the African continent, to the west by the Strait of Sicily while its eastern part is open to the Levantine Basin (Fig. 1). Its most prominent characteristics are described below in terms of bathymetry, meteorology and oceanography.

A. BATHYMETRY

The Western Ionian Sea, the deepest basin in the Mediterranean Sea, has an average depth of 3300m. The main boundary is the Maltese Escarpment, a steep barrier which rises to the shelf, at an average depth of 200m (Fig. 2).

The only opening to the western basin lies between Malta and the Medina Bank, with a sill depth of 430m. Hence, no intermediate water can be exchanged with the Western Mediterranean basin below this sill. There is no other deep opening either north of Malta or in the Gulf of Syrta. East of the Escarpment lies a relatively flat area. However, there is one notable topographic feature near 35°N, 17° to 18°E: a significant ridge, which rises 1000m over a 10 km horizontal distance, and which is about 90 km long.

B. METEOROLOGY

The atmospheric regime of the Mediterranean Sea is characterized by an alternation between the summer and winter seasons, the spring and fall seasons being brief transitional periods. The winter season commences abruptly around October, with the invasion of cold air into the Western Mediterranean. Typical storm tracks originate in the Gulfs of Lion or Genoa and storms move southeast across Italy and Greece. Starting in February, the dominant storm tracks originate in the Atlas Mountains and move northeastward over the area [Brody and Nestor, 1980].

The summer season starts in May and lasts until September. As a result of a very stable situation where the Azores High extends well over Central Europe, this season is hot and relatively dry.

In June, the period in which this thesis is particularly concerned, winds are calm about 25% of the time and average 4 m/s from SW to NW 50% of the time [Naval Weather Service Command, 1970]. Sea breeze regimes are common in coastal areas. Cloudiness is low (less than 4/8) 80% of the time, which accounts for intense solar radiation over the sea, in conjunction with low wind stress, and offers exceptionally good conditions for passive satellite remote sensing.

C. OCEANOGRAPHY

1. General circulation in the Eastern Basin

Because of the hot, dry climate, the Mediterranean Sea acts as a concentration basin for the Atlantic surface water. Evaporation in the extreme eastern part greatly exceeds both precipitation and river runoff. The water budget and the general circulation features of the Mediterranean Sea are considered to be well established [Lacombe and Tchernia, 1960; Morel, 1971].

The slope of the sea surface, due to evaporative water loss at its eastern end, is the driving force for water renewal, with an estimated cycle of 100 years. Atlantic Water enters as a near-surface current through the Strait of Gibraltar and flows eastward (Fig. 3). In the summertime, the absorption of solar radiation exceeds, by far, the radiative and evaporative heat losses. Hence, this surficial Atlantic Water, about 100m thick, warms progressively as it moves along the Algerian coast. The salinity is approximately 37.5‰. A thermocline is formed around 20 to 40m depth. As this tongue of water moves eastward through the Strait of Sicily, it splits into two branches. In the Ionian Sea, one branch continues eastward, while the other flows southward and appears to be modified by the bottom topography [Morel, 1971; Grancini, 1972; Briscoe et al., 1974].

Temperature and salinity increase in the surface layer as it reaches the Eastern Basin. Below the thermocline the

Atlantic Water maintains its relatively low temperature and salinity characteristics, which can be traced to the eastern part of the Sea in the Levantine Basin. Hence, because of the very strong thermocline, the direct influence of atmospheric forcing and air-ocean interaction is concentrated in a shallow layer.

In fall and winter the thermal budget in the Eastern Basin becomes negative, i.e., the heat flux is from the ocean to the atmosphere. Sea-surface temperatures may exceed air temperatures by more than 10°C, and, thus, the air can be unstable. This atmospheric instability increases the air-sea thermal exchange and results in the high salinity layer of the sea becoming unstable. Hence, convective sinking occurs and the thermocline disappears.

This process, which is particularly noticeable in the Rhodes-Cyprus area, results in the formation of a Levantine Intermediate Water (LIW). It is a mixture of overturned surface water, Atlantic Water (which was sheltered by the summer thermocline) and the water formed in the previous year. This homogeneous water body is usually found initially at a depth of 150m, near its source, down to 400m. Following a cyclonic gyre in the Levantine Basin, the LIW flows through the Strait of Sicily, continuing towards the Western Basin and into the Atlantic Ocean. Between its source and the Strait of Sicily, it flows isentropically, with a change of its characteristic temperature and salinity

from 16.3°C, 39.15‰ at its source to 15.8°C, 38.90‰ in the Ionian Sea and 14.0°C, 38.74‰ in the Strait of Sicily [Oztugurt, 1976].

As described above in the Bathymetry Section, the Maltese Sill provides the most obvious passage for this return flow, which has been estimated to be 10 million m^3s^{-1}, with an excess of 4.5% of in-flow over out-flow. Miller [1972] suggests that the westward flow of LIW is more prominent in the northern part of the Strait, i.e., between Malta and Sicily, while the eastward flow of Atlantic Water dominates the southern part.

In addition to this main flow pattern, there is some evidence of summertime exchange between the Ionian Sea and the Adriatic Sea [Zore-Armanda, 1969]. Due to the continental character of the narrow, shallow Adriatic Sea, its water is lighter than Ionian Sea Water, with a noticeable input of fresh water from the northern rivers of Italy. This surficial water flows south into the Ionian Sea, and a compensation current is formed in the intermediate layer, with Mediterranean Water flowing into the Adriatic Sea at around 300m depth.

2. Frontal structures in the Ionian Sea

The Western Ionian Sea is an area of mixing. Within the upper 100m of the water column, which includes the thermocline, Atlantic Water spreads over the area while LIW flowing underneath is forced by topographical features

through the narrow sill of Malta (Fig. 3). As can be expected, thermal and salinity fronts occur as quasi-permanent features, although marked by great variability in position and strength. Several studies of these fronts have been made [Woods, 1972; Johannessen et al., 1971], some of the features noted are described below.

In May, July, and August, a front (called the Maltese Front) was found along the continental slope east of Malta, extending about 130 km from the southern tip of Sicily. Cross-front horizontal gradients reached 2°C over 33 km (20 nmi), with extensive vertical shear over a depth of 100m due to up- and down-welling processes along the interface. Surface water flowed through the front into the Ionian Sea.

The most characteristic features of the Front seem to be:

- its position is associated with bottom topography
- a salinity and temperature minimum lies to the west of the salinity and temperature front, and
- temperature inversions are highly probable [Briscoe et al., 1972].

Two studies of the Ionian Sea made in the late summer and fall [Levine and White, 1972; R. R. Miller, 1972] showed the existence of an oceanic, i.e., deep water, frontal structure, located several tens of kilometers east of the Maltese Front. Its main discontinuity was manifested in the presence of warm anomalies of LIW extending to a depth of

400m and presumably moving westward. The frontal features did not always appear in the sea surface fields, but they were mainly noticeable at depths between 50 and 400m.

It was later suggested that the Maltese Front undergoes seasonal variations and propagates eastward, from summer to winter, into the Ionian Sea [Johannessen, 1972].

Woods et al. [1977] have discussed a model of vertical circulation for fronts in this area which displayed the upward and downward displacements of water tongues. The shape of isotherms was described and related to features found commonly in the temperature transects, depending on the orientation of the cross-section with respect to the frontal axis.

Woods [1977] also examined the analysis made by Briscoe et al. [1974] to show that the assumed linear frontal zone, interpreted by Briscoe et al. as extending over 100 km, might possibly have derived from an erroneous interpretation. Woods emphasized that a 50cm/s southward drift was not taken into account, and that what was described as sections of an elongated front could just as well have been the repeated crossing of a water mass boundary of limited extent. As an alternative, Woods showed a preference for the concept of widely spread, but small scale, frontal structures, imbedded in a turbulent upper ocean.

III. DATA PROCESSING

A. BATHYTHERMOGRAPH DATA

The present study was initiated when a set of one hundred and sixty seven expendable bathythermographs (XBTs) were made available by FNOC after completion of the US Navy exercise, SHAREM 38, in the Western Ionian Sea in the middle of June, 1980.

The first step in evaluating this data set was to plot each temperature profile, its geographical location, and to contour temperatures at various depths.

1. Vertical temperature profiles

Vertical temperature profiles provided a visual estimation of the quality of the 167 XBTs. The quality of each XBT was examined according to the following characteristics:

- the number of points in each profile and maximum depth of the sounding.
- the smoothness of the profile, i.e., did the sounding include the small scale features generally expected, or had it been excessively "smoothed"?
- the presence of discontinuities, i.e., did they represent an actual thermal feature or merely a defective sounding?

The data set was then separated into three categories. The best quality category included those profiles which extended to at least 150m, had a large number of depth/temperature pairs and resolved reasonably well the 30 to 100m layer. Rejection of profiles was made on the basis of limited vertical extent (less than 40m), or an obvious anomaly. This constituted the category of rejected profiles. The remaining profiles constituted the second quality category. The best quality, second quality and rejected profile categories contained 74, 70 and 23 profiles, respectively. Figure 4 shows two XBT profiles that were classified, in spite of their similar shape, as best and second quality due to the absence, in one of them, of the typical inversion feature.

No effort was made to differentiate surface-launched SXBTs from air-launched AXBTs and the appelation XBT was used for both types of bathythermogram.

2. Geographical distribution

The geographical distribution of XBTs was found to be concentrated in two well-defined areas. This spatial pattern was supposedly due to a change of operational area during the exercise. Zone I was defined as covering 33°30' to 35° N, 17° to 19° E. Of the 67 soundings from Zone I, 45 were first quality, and 19 were second quality soundings. Zone II was defined as 35° to 38° N, 16°30' to 19° E, thus covering four times as much area as Zone I. Of the 85 soundings from Zone II, 23 were first quality and 47 were

second quality soundings. Finally, 15 soundings were widely spread over the rest of Western Ionian Sea. Table I summarizes these facts.

TABLE I

Quality and geographical distribution of XBTs

	Best quality	Second quality	Rejected	Total	Exploitable
Zone I	45	19	3	67	64
Zone II	23	47	15	85	70
Other	6	4	5	15	10
Total	74	70	23	167	144

Some disproportion seems to arise regarding the percent of first quality profiles in Zones I and II, respectively 67% and 27% of the total number. This disproportion is certainly due in part to the inherent subjectivity of the quality classification, but it points out that profiles in Zone II, which were more frequently classified as "exceedingly smoothed out, hence second quality" might in reality be smoother. Hence, Zone I could be expected to be an area with more variability in the vertical structure: inversions, sheets, layers, etc. In spite of this subjectivity, the quality classification was retained as a valuable aid in thermal field contouring.

3. Time distribution

The 70 XBTs in Zone II were acquired between June 6 and 24, with some concentration (64) from 13 to 20 June. Similarly, the 64 XBTs in Zone I were acquired between June 6 and 15, with some concentration (55) from 8 to 12 June.

The two data subsets:

- Zone I - 8 to 12 June
- Zone II - 13 to 20 June

were finally selected for independent thermal analysis based on the following criteria:

- good apparent quality of the individual profiles
- relatively high spatial density, and
- potential use as a synoptic set as discussed below.

Figure 5 summarizes the space and time distribution of profiles for the two selected subsets. The use of 'Zone I' and 'Zone II' in what follows is indicative of both the temporal and the spatial limits defined above.

4. Thermal analysis

An analysis was made for temperature structure at the surface, 100, 200, 300, and 400m. The thermocline depth and inversion depth were mapped. Confidence was given to singular points according to the qualitative estimation of each XBT, i.e., a best or second quality profile. For example, the absence of an inversion in a second-quality

sample was not considered significant when neighbouring first-quality soundings showed such a feature.

A cross section was evaluated to a depth of 400m where thermal features presented the greatest horizontal variation. A profile of thermocline depth and inversion depth was superimposed on this cross-section.

Discussion of this analysis, its validity and the results are presented in Chapter VI and VII.

B. CORRELATION COMPUTATIONS

A statistical approach was used in both Zones I and II to determine the horizontal structure of the perturbation field at different levels. It included the following steps:

1. A perturbation field was generated as the difference between a given XBT profile and the mean profile for the area using a vertical resolution of 5m.
2. XBTs were then taken 2 by 2, and a cross correlation coefficient was computed over three different layers: 0 to 60m, 60 to 150m, 150 to 400m. These layers were selected as representative of different physical processes in three regimes: the well-mixed layer, the zone of inversions, and the quasi-isothermal layer, respectively.
3. The cross-correlation functions were evaluated as a function of the spatial and temporal interval between

the two profiles, in an attempt to validate the assumption of synopticity.

4. The cross-correlation functions were also analysed as a horizontal field with respect to latitudinal and longitudinal spacing between the XBT pairs.

Details of the computational technique are given in Appendix A.

C. SATELLITE IMAGES

A set of daily Advanced Very High Resolution Radiometer (AVHRR) satellite images was obtained from the French Meteorological Office, covering the area of interest from mid-May to the end of June. The quality and cloud coverage varied widely throughout this period and ultimately 14 pictures were selected which gave a good estimation of skin SST gradients. These pictures were sometimes used in pairs, when they were not too separated in time and showed no evolution of the characteristic features, to make a composite image. The resolution between two tones of gray was 0.5°C and no correction was attempted for atmospheric absorption. Hence, the contours were taken as representative of SST contours, whenever atmospheric effects did not apparently blur the picture.

Since the satellite images obtained were direct enhancements, for oceanographic purposes, of raw IR pictures, they still had a grid distortion corresponding to the particular

geometry of the satellite (NOAA-6 or TIROS-N) scanning procedure. A computer program was written to rectify each immage on a geographical grid. The numerical technique included:

1. digitization of the image contour,
2. initialization of the scanning grid for each particular orbit,
3. point by point inversion using an 8-noded isoparametric mapping, and
4. output and plotting.

All of these steps were executed on the Tektronix 4081 of the Mechanical Engineering Department. The restritution was believed to have a sufficient accuracy to locate thermal features within a few kilometers.

D. WIND FIELD ANALYSIS

A set of daily wind observations at 1200Z (from 1-20 June) was obtained from FNOC, with wind vectors evenly distributed at 16 grid points throughout the study area. Surface pressure analyses with the same periodicity were received from the French Meteorological Office.

The wind stress at the surface was computed for each grid point and each day as $\vec{\tau} = \rho_a C_D \vec{u} |\vec{u}|$, ρ_a being the density of the air, $\vec{u}$ the wind velocity, using $1.5\ 10^{-3}$ for the dimensionless drag coefficient C_D. The curl of the wind stress was computed for 9 intermediate grid points, using

an elementary finite difference scheme. Using a result of Ekman theory based on the conservation of water mass and an evaluation of the mean horizontal mass transport, the vertical velocity at the bottom of the Ekman layer was computed as:

$$w = \frac{1}{\rho f} (\vec{\nabla} \times \vec{\tau})$$

where ρ is the density of sea water, f the Coriolis parameter and $\vec{\nabla}$ x the rotational operator.

IV. WEATHER SITUATION

A. DESCRIPTION

During early June, 1980 the synoptic weather situation was mostly determined by the Azores anticyclone, extending over western Europe, and a series of depressions over the Balkans and central Europe. Winds over the Ionian Sea were eastward, 5 to 10m/s (Fig. 6a). This situation remained steady until June 6, when the Azores high regressed and a series of depressions developed over Spain, the British Isles and Algeria. By June 8, this latter center of low pressure had caused the wind to veer to northward, 5 to 7m/s, and with a speed increase to 10m/s on June 10. During that two-day period, some cloudiness was present over the Ionian Sea.

After June 10, an anticyclone started developing over the central Mediterranean Sea, and winds were moderate and unstable in direction through June 12. On June 13 and 14, winds were steadily westward, 10m/s, while a strong depression developed over the Bay of Biscay and passed over northern Europe. The following period, June 16-20, was more typical of the seasonal pattern, with a moderate wind regime over the Western Ionian Sea. Winds were south- to southeastward, 2m/s on June 17, increasing to 8m/s by June 20. Air temperatures, as reported by the Malta weather station, were over 24°C throughout most of the month.

B. IMPACT OF WIND STRESS

Dynamical theory indicates that the surface wind stress increases turbulence in the upper layer and contributes to a downward redistribution of heat, i.e., deepening and cooling of the mixed layer, or steepening of the thermocline. Moreover, transient winds can generate inertial oscillations [Pollard, 1970], an effect which has been observed in the Mediterranean Sea [Perkins, 1972; Mittelstaedt, 1973]. This is most noticeable during the period of calm following a period of high winds [Gonella, 1971].

The Ekman "pumping" or "suction" due to the curl of the wind stress was evaluated (Fig. 6b) as a time series of daily vertical velocities, computed at the bottom of the Ekman layer (see Chapter III). The most striking event in this series is a very strong upwelling induced during the period 10 to 12 June, with mean values exceeding 0.02 cm/s (15m/day), a very high value indeed. This was followed by a more moderate, but still noticeable, downwelling during the period 13 to 15 June.

It is not known, from available observations, whether this vertical "pumping" or "suction" acutally interacted with mixed-layer processes or not. From theoretical considerations, it would raise or depress the water column, hence the thermocline, without heat redistribution. A very strong upwelling, possibly coupled with strong wind-mixing, might rupture the thermocline and account for the presence of

intermediate water at the surface. Since these estimations were not applied as corrections to the XBTs, any vertical displacement of isotherms by such an Ekman "pumping" or "suction" contributed to increase the noise level in the data.

V. SPACE AND TIME VARIABILITY

To validate the analysis of the thermal field, it was necessary for all XBTs taken in each of the two periods to be established as essentially synoptic with respect to a temporal scale of 8 days and a spatial scale of about 30 km. Eight days was the duration of the sampling effort in Zone II, the longest of the two data subsets, and 30 km was an average sampling interval in the densest area. Among the mechanisms which could possibly distort the analysis, i.e., falsify the synopticity assumption, were horizontal and vertical advection due to mean flows, internal waves, etc., surface heating, interleaving and mixing of water masses, all of which might have occurred during the sampling interval. It will be shown in the following sections that the above mechanisms did not violate the assumption of synopticity at the temporal and spatial scales specified.

A. VARIABILITY OF SURFACE FEATURES

1. Characteristics of satellite images

The series of seven satellite composite pictures (Fig. 7-13) was found to have the following features in common.

A persistent tongue of cold water oriented eastward from the sill, at 35°20'N, was distinguishable and observed as far east as 18°E. It presented a varying shape, either

straight (Fig. 11 and 13) or bent southward around longitude 17°20'E (Fig. 7, 10, and 12). In some cases it turned into a clockwise circular pattern, suggestive of an anticyclonic eddy (Figs. 8 and 9, and possibly Fig. 12).

The other dominant feature was a tongue of cooler water issuing also from the Maltese Sill, which tended to bend southward along the Medina Bank. It then followed the shelf break, along 16°E and bent eastward again along 34°N. This feature was seen on all seven satellite pictures and was separated from the tongue of cooler water mentioned above by an area of warm water, sometimes in anticyclonic eddy-type shape, centered approximately at 35°N, 17°E (Figs. 8, 9, 12).

In the northern part of the Ionian Sea, a persistent tongue of cooler water was observed flowing southward from the Strait of Messina. Upwelling structures could be seen along the eastern coast of Sicily, with occasional extensions offshore (Fig. 11). Within Zone II, the surface features seemed to be quite stable, and surface temperatures were notably warmer than in the southern part.

Based on the composite pattern from 4 to 30 June (Fig. 14), there are commonly two branches in the sea-surface temperature field, as found in earlier Airborne Radiometer Temperature (ART) studies, e.g., Briscoe et al. [1974; Fig. 1]. Using the same ART technique, Saunders [1972] established the existence of a tongue of cold water which

corresponded exactly, in season and geographical location, to the northern most of the two cold tongues found in the present study. Finally the branching of the cold tongues can be traced also from a salinity analysis [Morel, 1972; Fig. 8] along 15°E, i.e., across the sill, in which two shallow salinity minima (Atlantic Water) are found 45 km apart.

All these factors suggest a relation between this typical shape of SST contours and the circulation of water through the Strait of Sicily.

2. Surface temperature and water mass circulation

As noted by Saunders [1972,p473], "there are clear connections between the surface circulation and the surface temperature field." Although it was not possible to calibrate the satellite imagery, it was clear that such patterns of cooler and warm water, with their large scale and persistence, were mainly due to advection and not to loss of heat or redistribution of heat in the ocean. This observation was used by Miller [1972, p14] to assert that

> transient as the surface temperature may be, advective circulation could orient the distribution of surface temperatures in such a way as to indicate the superposition of intruding water masses from the anomalous features of the distribution, the apparent organization and horizontal coherence of isotherms, and the rapid changes of temperature with short distances.

It is also noted that double-tongued flows are not atypical downstream of the Straits of Sicily and Gibraltar, and, in a more general frame, of vortex patterns.

The SST pattern was thus interpreted as two flows of cold water from the Strait of Sicily, the southern tongue following a topographically controlled path along the shelf edge, while the northern tongue curled into an anticyclonic flow.

The eddy structure which existed on June 14 and 15 (Figs. 8 and 9) did not appear on June 22 and 23 (Figs. 10 and 11), but was found again on June 24-25 (Fig. 12). Hence, this pattern can be apparent, disappear, and appear again in 4 to 8 days. This time scale is typical of a nominal weather cycle; however, no definitive study has been made of this time scale of variability in the Ionian Sea. As an explanation, it could be hypothesized that the summertime heating of the upper ocean masks its deeper structure, until a weather event causes sufficient mixing to unveil this thermal structure. Hence, the atmosphere would not necessarily provide the generating force of these oceanic thermal features, but would act as a revelator.

3. The effect of advection

The velocity of water masses in the area has been estimated as follows [Saunders, 1972] from the MILOC-68 data set:

- along 35°N, i.e., in the tongue of Atlantic Water, currents are eastward at 10 to 20 cm/s
- around 37°N, 18°E, the currents are weak (5 to 8 cm/s) and northeastward.

These current estimates were based on geostrophic velocities computed relative to the 200dbar level. No indication of westward flow was found at the level of LIW. The surface flow seems to be rather sluggish in most of Zone II, while the mean flow is stronger south of 35°30'N. In the vicinity of frontal features, velocities are typically greater, with a magnitude of the order of 30 to 50 cm/s. Such velocities would occur in high shear situations, along water mass boundaries, which in this region are spread north-south, as shown by Johannessen [1971; 1977] and others. Given a spatial scale of 30 km and typical advection speeds of 5 cm/s (general case) and 35 cm/s (frontal areas), a tentative synoptic time scale was computed as the ratio of length scale to surface current speeds, yielding values of, respectively, seven and one day.

From this evaluation of the effects of advection only, it was inferred that the XBT data could be considered as synoptic over a seven-day interval as long as they did not show the characteristics of a fully formed frontal structure. In the presence of such a feature, a one-day interval should be held as a limit of synopticity, unless some corrections are made to account for advection, due to the high velocities and the variability of mesoscale features.

B. EVALUATION OF TEMPORAL VARIABILITY

This section describes an attempt to evaluate the importance of temporal variability in each of the two data subsets.

A mean temperature profile was computed for Zone I, as if all XBT profiles were co-located. This average profile is referred to, later in the text, as the areal mean profile. Similarly, a mean temperature profile was computed for each day, and the five daily mean profiles from the June 8-12 period were evaluated as a time series. Since it was difficult to separate visually such profiles when plotted on top of each other, the perturbation profiles, i.e., the arithmetic difference between each daily profile and the areal mean profile, were derived. The analogous procedure was performed in Zone II (Fig. 16).

In Zone I, there was a marked difference in the 8 June mean perturbation profile: it was significantly cooler than the average in the well-mixed layer, down to 100m. This was believed to express a geographical characteristic, i.e., a local cold area which could be the southernmost part of the tongue of cold water seen in Figure 7. It is not considered as representative of a temporal phase in the area. This interpretation is validated by the observation that the mean location (Fig. 5) for June 8 is significantly different from those of the other four days.

The mean profiles for June 9 and 10 are quite similar, with no major deviation from the areal mean profile. Similarly, the profiles for June 11 and 12 are within 0.25°C of the areal mean profile and can be regarded as a pair of similar data sets. But a comparison of the two pairs,

June 9 and 10 with June 11 and 12, in the upper 25m, shows that a significant (0.5°C) average heating occurred after June 10. This can be well related to the weather pattern described in Chapter IV, where June 10 was noted as a separation date between a period of strong winds with cloudy conditions, and a calm period with intense heating. In addition, the well mixed layer between 25 and 75m revealed markedly variable temperatures, as compared with the areal mean, although with no obvious time dependence. From this, it could be expected that spatial analysis of the thermal field in this upper layer would be difficult.

Temporal variability in Zone II was difficult to assess, because the initial assumption that all XBTs were co-located was far from true. On the average, the displacement of the sampling ships from June 13 to 20 was northward, about 30 km/day, although erratic. This is referred to below as the mean sampling speed. There was an apparent heating of the surface layer, with mean surface temperatures increasing in the following time sequence: 13, 14, 16, 15, 17, 20, 19, 18 June (Fig. 16). At this point, it was not possible to separate spatial from temporal effects without an alternative source of data. The satellite images could not help, since they were not calibrated. Moreover, as the spatial density of the XBTs was low, no small scale resolution could be expected in Zone II, in contrast with Zone I. Hence, it was not possible to separate the real heat gain in the surficial

layers, which occurred most probably, from the apparent warming due to the mean direction of sampling, from cooler to warmer waters. In the subsurface thermal field, some grouping of the perturbation profiles is observed around 200m, with June 17, 18, and 20 being warmer than the areal mean and June 13, 14, 15, 16 and 19 being cooler. Given the depth of this grouping, this is not believed to represent an effect of surficial heating, but more probably an indication of the spatial distribution of water masses or some internal process, i.e., large-scale wave or eddy.

C. TEMPORAL VERSUS SPATIAL CORRELATION

The following section describes an attempt to use the cross-correlation computations (see Chapter III and Appendix A) to enlighten the respective roles of temporal and spatial variability. The following reference system is defined: one axis describes the time difference, in increments of days, between XBT pairs; the other axis describes the distance in increments of 10 km between pairs. In a perfect steady-state situation, the cross-correlation coefficients between XBTs would vary only with distance. Hence a plot of these coefficients in the reference system would show iso-correlation contours lying parallel to the time axis (Fig. 17a). Conversely, the variation with time of a homogeneous temperature field would be revealed by iso-correlation contours lying parallel to the distance axis (Fig. 17b).

1. Observation in Zones I and II

In Zone I the correlation decreased with distance (Fig. 17c) but it was quite constant with time. This is dramatically illustrated by the fact that two profiles separated by 30 km correlated at a 0.5 level, even when sampled at a four-day interval.

By contrast, in Zone II there was a clear dependence of iso-correlation contours in both time and space (Fig. 17d). The 0.3 correlation level existed as far as 80 km for a pair of XBTs acquired on the same day, and as far as 30 km for XBTs acquired two days apart, but not for any larger time separation. Similarly, the zero-correlation contour, which occurred at a distance of 150 km for same-day samples, was found at a four-day separation for co-located samples.

From Figure 17c Zone I was essentially in steady state over the five-day period, even in the presence of strong advection. This concept of synopticity applies relative to a length scale of, typically, 30 km. It was consistent with satellite pictures which showed an average temporal scale of three-to-eight days for the tongue of Atlantic Water and related patterns.

In Zone II, as was seen in the preceding section, it was not possible to separate the various effects which may have affected the temporal vs. spatial correlation: advection, heating processes and mean speed of sampling. From Figure 17d, the speed scale is 150 km/4 days for the

0.0 correlation contour, i.e., 37 km/day, and 90 km/3 days for the 0.3 correlation contour, or 30 km/day. These two values are fairly close to the mean sampling speed. It is believed that the temporal distribution of samples over an eight-day period in Zone II represents the main cause in the loss of correlation with time. Hence, the physical processes involved could be expected to have a longer time scale, implying a true synopticity in Zone II, even though it should ideally be analysed as a time succession of smaller synoptic "analysis spaces."

VI. THERMAL ANALYSIS IN ZONE I

A. DESCRIPTION OF THERMAL STRUCTURE

This section describes the thermal structure found in Zone I and refers to Figs. 18 through 24.

There was a core (diameter of ca. 30km) of warm surface water (20.2°C) centered at 34°20'N, 18°15'E surrounded by water approximately 0.5°C colder (Fig. 18). The northwestern part of the area was somewhat colder (19.2°C), and seemed to correspond to the cold water tongue, or its distant influences, intruding eastward. The distribution of XBTs in that part of the zone was not adequate to resolve the two tongues of water appearing in the satellite imagery.

The SST analysis was made much easier by using an "interpolated SST": the Expanded Ocean Thermal Structure (EOTS) model run by FNOC provides a grid analysis of thermal structure from input XBTs, following a scheme that is briefly described below (Chap. IX). A by-product of this analysis is a geographical interpolation of the SST analysis, which provides an analysed SST at each XBT location interpolated from SST values analyzed at EOTS grid points. This interpolated SST is generally believed to smooth out small scale structure and only retain well correlated features. In this respect, it seems to overestimate the warm water core described above rather than average it out (Fig. 19).

The analysis at 25 and 50m did not show any consistent pattern. Since these depths are located above or in the average thermocline, it is not surprising to find extreme variability there.

Below the thermocline, the analyses at 200, 300, and 400m showed a warm core area 35 km eastward of the equivalent surface feature; this displacement increased with depth (Figs. 18-22). Average horizontal gradients through this discontinuity were of the order of 1°C/50 km.

The thermocline depth, defined as the depth with a maximem temperature gradient, has a zone of transition between a shallow depth (less than 40m) in the western part of the area to a deeper depth (greater than 60m) in the eastern part. The thermocline depth had strong variations in the region of the warm anomaly, including an area where the mixed layer seems to vanish.

Most XBT profiles in the best quality subset of data showed inversions, i.e., the presence of warm water underlying cool water. Such a feature is typical of regions where the salinity gradient has a dominant role in the density stratification. The inversion depth increased from the northwest corner (50m) to the southeast corner (125m) (Fig. 23). Again, the warm anomaly was associated with perturbations in the inversion depth, which decreased sharply over a short horizontal distance (from 100 to 50m in about 10 km), just east of the warm anomaly and precisely where the thermocline seemed to vanish.

A transect was construced from ten XBTs spanning 120 km, with a greater concentration of XBTs in the perturbed area. The characteristics of the horizontal and vertical temperature fields are summarized below (Fig. 24):

- a deep (200m and more) warm anomaly was present, which was characterized by a large isothermal (15°C) body of water, whereas the 15°C isotherm is found above 150m depth throughout the remainder of the area (Fig. 25).
- a strong thermocline was present west of the warm anomaly;
- the temperature variability was relatively great in the surface layer;
- layered inversion zones were present;
- relatively warm surface water was present on the western edge of the warm anomaly.

B. COMPARISON OF SATELLITE AND XBT SEA-SURFACE ANALYSES

An attempt was made to compare thermal features observed in the satellite IR images (Figs. 7 and 8) with those seen in the surface XBT analysis. The comparison did not prove very successful, due to a paucity of XBTs where the satellite imagery presented the most characteristic eddy-shaped feature. However, the satellite IR image (Fig. 8) shows a cool (1.5°C) anomaly[1] where the interpolated XBT SST shows a warm anomaly.

---

[1]Although this satellite image is a composite made of two actual images, only the June 14 picture showed that particular feature.

Several factors suggest that the satellite anomaly might be due to some atmospheric effect: its size, the fact that it appears on one IR image only (no persistence), and its transparence to some of the surrounding oceanic features. The development of marine fog or stratus from a warm water patch has been observed and modeled [Rogers and Hanley, 1980], and could explain the phenomenon described above. No attempt was made to verify this hypothesis from local atmospheric observations.

C. CORRELATION COMPUTATION

It can be recalled from Chapter III that a correlation coefficient was defined to allow for quantitative comparisons of a pair of XBT profiles. The number-density contours of XBT correlation pairs in each 10 by 10 km square generally have a E-W stretching (Fig. 26). Hence more profile pairs had a east-west than a north-south orientation.

The cross-correlation of near-surface temperatures (Fig. 27) has a wavy pattern of significant (+0.5) positive correlation in the N-S direction, at distances of 25 and 60 km. Zero-crossings occurred at 30 km in the E-W direction and 40 km in the N-S direction.

The N-S pattern exhibited in the surface layer was even more notable in the intermediate (60-150m) level (Fig. 28). but there was also an area of significant negative correlation at a distance of 70 km east and west of the center.

Similar patterns were found in the deep (150-400m) layer (Fig. 29).

Due both to measurement noise and the impossibility of resolving details within the averaging grid size of 10 km, all three correlation diagrams had values less than +1.0 at zero spatial lag.

The thermal structure in the area was clearly anisotropic. Choosing the deep layer as the most stationary, two distinct patterns are distinguished:

- in the E-W direction, where the zero-crossing yeilded a correlation scale of 50 km, physical phenomena seemed to occur with a typical separation distance of 200 km. In fact, the correlation fields (Fig. 27) displayed in a different fashion the most apparent features described in the thermal analysis section, in which one could observe (Fig. 18):
  - a warmer area in the east
  - a colder area in the west
  - a strong thermal gradient area with isotherms oriented in the N-S direction.
- in the N-S direction, the spatial scale of variability was larger. With a separation as large as 80 km, XBTs still showed a significant positive correlation. Superimposed on this positive correlation field was a wave pattern, with a length scale of approximately 40 km, i.e., similar to the length scale in the E-W direction.

Hence, similar wave or eddy processes occurred in all directions, though they were superimposed on a strong positive E-W pattern. This result is also in good general accordance with the thermal structure analysis. A natural axis of symmetry, along 340°T, is apparent and could represent, with the general E-W axis, a preferential axis for advection or baroclinic wave propagation.

VII. THERMAL ANALYSIS IN ZONE II

The location and the circulation of water masses in Zone II are basically similar to those in Zone I, as described in Chapter II. Zone II's bottom topography is somewhat flatter than Zone I's. Zone II is more sheltered from the Western Mediterranean Sea, but it seems to be more exposed to the westward LIW flow, as well as possible exchange with the Adriatic Sea. The data density was one profile per 1650 sq km, as compared to one per 550 sq km in Zone I. These factors led to a separate analysis in Zone II, while expecting a lesser resolution than in Zone I.

A. DESCRIPTION OF THERMAL STRUCTURE

The SST pattern demonstrates a general NW-SE orientation of isotherms, with temperature increasing in the NE direction (Fig. 30). There was a "tongue" of cool (1°C) water along 36°N which bent southward along 17°30'E. It could not be accurately matched with satellite IR images, although its sourthern boundary correlated quite well with the eddy-shaped structure of Figs. 8 and 9. The XBT data were sparse SE of this feature; hence, the positive temperature gradient is only significant to the NE.

The interpolated (EOTS) SST field (Fig. 31) shows the same basic features, and, in particular, the 20° and 21°C

isotherms are almost identical to the XBT-derived SST. However, the EOTS SST does not accurately depict the 22°C isotherm, nor does it depict well the cool anomaly near 38°N, 17°40'E in the north of Zone II. Analyses were conducted at the 100, 200, 300, and 400m levels and showed little change with depth. Hence, the subsurface temperature field is only shown here at the 100m level (Fig. 32).

At all levels, there was a warm anomaly in the NE of Zone II, with a general orientation of isotherms more N-S than in the surface analysis. There was a band of cool water at all levels between 16°E and 17°E, and it seemed to widen as it reached 36°N. Here, it joined the cool area centered at 35°30'N, 17°30'E, which was the subsurface expression of the surficial tongue of cool water described above. This cool tongue of water could be interpreted as a local frontal structure, whereas the elongated band extending northward could indicate exchange with the Adriatic Sea, at an intermediate level.

The correlation technique described previously was applied to Zone II. The horizontal cross-correlation diagrams were of little value, due to the high "noise" level in the data. The analysis was, hence, made non-directionally (Fig. 33), as an averaging of the time vs. space correlation (Fig. 17d) along the zero lag time axis for the eight-day period. The zero-crossing correlation distance was 50 km in the 150 to 400m layer, in good agreement with the results in Zone I.

VIII. ANALYSIS OF ACOUSTIC FEATURES

The goal of the acoustical analysis was twofold. First, some particular oceanic features might be best revealed by sound speed profiles. This is usually true when looking at extrema; e.g. sound speed maxima or minima, maximum gradients, etc. Second, some understanding of the impact of these features on ASW detection capabilities might develop; e.g., how tactical parameters (surface duct, deep sound channel, critical depth, etc.) relate to easily accessible oceanic variables.

A. PRELIMINARY REMARKS, DEFINITIONS

The spatial and temporal distribution of XBTs has been described extensively above. The following analysis does not deal explicitly with physical processes, and the data are presented regardless of previously defined time intervals, subzones, etc. Moreover, some previously ignored XBTs, sparsely distributed southwest of 36°N, 17°E, have been incorporated.

The Leroy [1969] equation was used to convert the XBT profiles into sound speed profiles (SSP). Because of the absence of salinity data associated with the temperature profiles, a single climatological salinity profile from FNOC archives was used. The effects of this approximation were

checked and it proved to have no significant effect on the shape of the SSP, nor on the depths of its characteristic features. The largest deviation in absolute sound speed from a test profile was 1 m/s at the surface and deviations decreased with depth.

The more typical sound speed profile (SSP) characteristics were defined below (Fig. 34) in terms of their nature (gradient, extrema), their physical origin (inversion, mixed layer), or their effect on sound propagation (duct, sound channel):

- a near-surface positive gradient[2] which is due to a surficial isothermal layer and relates to the acoustical surface duct.
- a strong negative gradient, which occurs where the temperature decreases most strongly with depth, and defines the thermocline depth.
- the main sound channel, or summertime channel, whose existence is due to the seasonal heating of the surface layer above a deep near-isothermal water mass. Its axis coincides with the absolute sound speed minimum. Its thickness is the difference between the depth of the absolute near-surface sound speed maximum and the depth at which this same sound speed is encountered below the axis.

---

[2] the sign convention adopted here is common to underwater acousticians, (as opposed to the oceanographers' convention), whereby depth is positive downward.

- one or several secondary sound channels, which are due to the presence of thermal inversions or isothermal water masses, and are characterized by an axis, a thickness and a mean gradient. Axis and thickness are defined as above, but the sound speed maximum is, in this case, the nearest (to the minimum) relative sound speed maximum. The mean gradient is defined as $2\Delta S/\Delta Z$, where ΔS is the difference between local sound speed extrema, and ΔZ is the channel thickness.
- a deep positive gradient due to the dominant effect of pressure on sound speed.

B. DISTRIBUTION OF VARIABLES

Subareas were re-defined to increase the contrast from one subarea to another, in order to facilitate the study of the distribution of sound channels. The water mass properties and the topography were taken into account. This led to the definition of five subareas, A through E, A being located on the continental shelf, B and C in Zone I, D in the coastal part of Zone II and E in the oceanic part of Zone II.

The thermocline depth was a systematic variable, i.e., its depth could be defined almost unambiguously and changed smoothly from one location to another (Fig. 35). Its mean value was about 40m in Zone II, and varied between 30 and 70m in Zone I. Greater variability was again found in Zone I along 18°E. The most striking feature is an elongated,

narrow zone of shallow thermocline depth, oriented NW to SE across most of the domain. This is believed to be an effect of the main branch of Atlantic Water flowing into the Ionian Sea. It corresponds reasonably well with the "tongues" of cool water found on the satellite IR images. In some areas, the main thermocline showed a step-like structure, yielding two different depths of maximum gradient. These areas were well-defined, but they seemed to be unrelated to any other particular thermal features.

Surface ducts, due to a shallow isothermal layer, were present almost exclusively in Zone I. More interestingly, their temporal distribution was related to atmospheric forcing events. They appeared on June 9, persisted until June 14 and reappeared for a short period of time on June 18 and June 20 (Fig. 36). Their average depth was 20m.

A main sound channel was found all over the area, with an axis depth typically at 80 to 120m (Fig. 37). In subarea D, the distribution of the main sound channel was bimodal, with more than 50% of the axis depths shallower than 75m (see Table II). Subarea A had a deeper-than-average sound channel axis, about 130m. The thickness of the main sound channel varied from 800 to 1200m. Given the average bottom depth of 3000m, the "depth excess" criterion [Urick, 1975, p152] was met at almost every location in the Ionian Sea away from the shelf and the ridge, thus allowing the use of convergence zone detection. Ray tracing would indicate a convergence zone spacing of 34 km.

TABLE II

Frequency of occurrence of sound channel axis in each area. For the main channel, this frequency is indicated in percent for each layer, adding to a total of 100% for each area considered individually. The secondary channels are described by a rate of occurrence in each individual area, regardless of the depth at which it was found. Hence, it is an estimate of the probability of occurrence in that area.

	AREA				
	A	B	C	D	E
No. of XBTs	14	35	26	20	49
DEPTH ZONE	MAIN SOUND CHANNELS				
35-75m	0	19	14	56	10
75-122m	23	54	46	44	80
122-180m	77	20	13	0	10
180-250m	0	7	27	0	0
	SECONDARY SOUND CHANNELS				
% occurrence	47	53	33	0	5

The common presence of temperature inversions below the thermocline is the key factor which explains the existence of secondary sound channels. Some of these small scale discontinuities were too tenuous to be accounted for, and the following limits were set, although somewhat arbitrarily, to filter the data: inversions were retained when their thickness was larger than 10m and the mean gradient larger than 0.01 m/s m^{-1}. In terms of sound propagation, the effect of such filtering was to reject sound channels usable at

frequencies higher than 5kHz (the low frequency cut-off for a 10m-thick channel) and, at these high frequencies, diffractive leakage losses higher than 13db/km (computed from [Bourke, 1973]) would occur. Such restrictions would only apply to a limited number of operational situations.

Secondary sound channels were almost nonexistent in subareas D and E, which constitute Zone II, giving further evidence of the low variability there, as demonstrated previously (Table II). The geographical distribution of the secondary features, overlayed on the main sound channel, provide further insight into the location of intense mixing (Fig. 37).

The limitations of some equipments, in terms of accessible depth, might make the secondary sound channels appear attractive as an alternative to the deeper main channel. Some of these secondary channels were continuous over extensive distances (greater than 100 km), although many of them were only isolated (short-lived?) features. Several difficulties may arise when trying to insure the navigation of an acoustic array within such a channel, with an accuracy of about 5m in depth, in areas where intense vertical current shear might render the behavior of towed systems somewhat uncertain. Moreover, many factors could act on the thermal inversion to alter its characteristics: internal waves as well as inertial oscillations are the most common of these and have typical

periods of a few minutes to 20 hours (the local inertial period). The amplitude of vertical oscillations can be over 10m. Under such variable conditions, one might not be able to track the oscillations and keep an array in the selected sound channel.

IX. COMPARISON WITH THE EOTS ANALYSIS

A. EOTS

To allow some comparison between the present analysis and the EOTS (Expanded Ocean Thermal Structure) analysis , the following characteristics of EOTS are summarized. EOTS is a numerical scheme designed for the analysis of oceanographic data, mainly BT profiles and sea-surface temperatures. It is produced by FNOC, for use in the Fleet Oceanography Centers and forces at sea. It uses a climatological data base with both temperature and salinity as well as real-time XBTs. The Mediterranean Sea is covered by two analysis zones, each on a 63 by 63 grid, with a mean grid spacing of 40 km. The longitudinal boundary between the western Mediterranean analysis (MEDW) and the eastern analysis (MEDE) is approximately 18°E. The analyses are run three times a week. Each input datum is weighted according to its nature and age, and blended with climatology. The most common outputs are horizontal charts of temperature at various levels, as well as the primary layer depth (PLD). Isotherms are contoured at 1°C intervals.

The profiles used in the present study were among those used as input to the EOTS, which may have used other inputs. The thermal analyses made in Zones I and II were compared with EOTS temperature analyses at the surface and 100, 200,

300, and 400m, obtained for June 11, 13, and 20 (Figs. 18-22 (Zone I) and Figs. 30-32 (Zone II)).

Not all figures display a synoptic scale feature, an indication that nothing was found or resolved by the EOTS analysis at that location. The deeper levels, 300 and 400m, in particular, were devoid of any features. When features are present in EOTS, they have an obviously coarser resolution, with a minimum radius of 40 km. This can be attributed to the numerical technique, which does not allow the resolution of features smaller than two grid lengths, i.e., 80 km in diameter.

The present study, which spans an area from 14° to 19°E, required the use of both MEDW and MEDE analyses. It was observed that the two zones, where they overlapped, did not always show the same distribution of isotherms (Fig. 32). This was attributed to the fact that input profiles were selected geographically before each analysis, hence eliminating the remote influence from data present on the other side of the boundary.

Similarly, the primary layer depth (PLD) contours from EOTS were overlayed on the present thermocline analysis (Fig. 35). The comparison shows more consistency and better resolution than the temperature analyses. In particular, the limits of the elongated contours, which delineate a shallow PLD area, agree fairly well. However, the absolute values differ by 20m from one analysis to the other, the EOTS

showing shoaler values. This deviation is explained by the fact that the thermocline depth of this study is a contour of maximum temperature gradients, whereas EOTS computes the PLD as the depth of maximum gradient discontinuity, i.e., the top of the thermocline.

B. EOTS INTERPOLATED SEA SURFACE TEMPERATURE

Referring to Chapter VI (Figs. 18 and 19) and Chapter VII (Figs. 30 and 31), the EOTS interpolated SST was very helpful, and easier to contour than the XBT-derived SST. This demonstrates that at least this portion of the EOTS analysis schemes has excellent resolution and smoothing effects, allowing an accurate and consistent contouring. A quantitative comparison, which was not possible at depth due to the nature of the analysis grid, was made at the surface between EOTS- and XBT-derived SSTs. The average difference was -0.15°C (EOTS cooler than XBT), the standard deviation of this difference was 0.7°C, and the correlation of the two fields was 0.75.

The author does not feel competent to analyze the numerical processes through which the interpolated profiles are smoothed out and the information is lost when analysed on the 40 km grid scale. Whether it comes from grid averaging or from an excessive time-decay constant in the model is not relevant to this study. However, the quality of the interpolation scheme is probably sufficient to justify an attempt to analyse the thermal field at a smaller grid scale, e.g., 5 or 10 km.

X. COMPARISON WITH THE MILOC-68 INVESTIGATION

MILOC-68 is the name of a NATO oceanographic investigation which took place in the Western Ionian Sea during the spring of 1968. It provided a number of STD casts as well as XBTs. The data reported by Miller [1972] were concentrated in a 220x220 sq km area, during the 20-day period from May 14 to June 2, 1968. This area represents the southern half of Zone II and the most northern part of Zone I (Fig. 5). The similitude in both space and season with the present study was of great interest. In addition, the MILOC-68 report was received after the present analyses in Zone I and II were completed, which prevented the introduction of any subjective influence.

A. THE MILOC-68 RESULTS AND COMPARISON

The MILOC area spanned two very different subareas: the northern half was dynamically inactive while the southern half was dynamically active. The border between these two areas, lying along 36°N, was identified as a "high density thermal front" [Miller, 1972; p18]. The salinity and sound speed distributions exhibited the same basic patterns (Fig. 38a-d).

A transect along 34°50'N showed the presence of a warm anomaly (Fig. 39a). From a perpendicular transect along 18°E (Fig. 39c), this anomaly was centered around 34°50'N,

18°E with a radius of 45 km, although some additional sampling south of 34°40'N would have been necessary to confirm the circular shape.

As pointed out by Miller, the depth of the 15°C isotherm is the most widely variable isotherm, a characteristic that has been found in the present study. The study by Saunders [1972] mentioned in Chapter V was made during MILOC-68, and is hence consistent and simultaneous with, if not identical to Miller's analysis. The freshest water was in the southwestern part of the area (Fig. 38e) and correlates remarkably well with the tongue of surface water, i.e., Atlantic Water, flowing eastward. To the north, high salinity LIW "encroached upon the shelf at the entrance to the Sicily passage between Malta and Sicily" [Miller, 1972] as an identifiable water mass. Both temperature and salinity fields can be related to the present study, and the characteristic 21°C surface isotherm (Figs. 30 and 31) can be taken as a limit between the stationary warm area (north of 36°10'N), presumably with a higher surface salinity, and the more perturbed area. To the south, the mixing area showed the following common features:

- the cool tongue seen on satellite pictures (see Figs. 14 and 38a-e)
- the cool tongue (20°C isotherm) found in Zone II (36°N 17°E) (see Figs. 30 and 38a-e)

- the warm eddy found in Zone I (34°30'N 18°30'E) and quite similar to the MILOC-68 "eddy" (34°50'N 18°E) (see Figs. 24 and 39).

B. THE INTEREST OF THE MILOC-68 STUDY

From the comparison made previously, it can be stated that:

- there is a considerable consistency between the two studies,
- the present study was more sketchy, due to the random sampling, the non-synopticity in Zone II, and the lack of salinity data.

A data base such as MILOC-68 is very valuable in many respects. First, it can provide the analyst with an initial impression on which he can build, by successive approximations, a contemporary description of the area, provided the seasonal and spatial domains and oceanic and atmospheric conditions are similar. Second, it provides a high quality case study, more carefully checked than is usually done operationally with XBTs. Finally, it has salinity profiles which, although not essential to sound speed computations, are important to any investigation of dynamical processes.

C. APPLICATIONS

Given the similitudes described above, the MILOC-68 data were used for some additional analyses, assuming they applied reasonably well to the present study. The first application

attempted to relate the T-S characteristics of 13 CTD profiles to their surface and subsurface structure. The second application was a computation of baroclinic modes and the Rossby radius of deformation.

1. Correlation between surface and subsurface structure

The 14 profiles present in the 34°50'N transect (Fig. 39a) were analysed on a TS diagram (Fig. 40). The profiles were numbered from 1 to 14 from west to east, profiles 9 to 12 being the warm anomaly. (Profile 14 was withheld from the analysis due to a suspicious anomaly in salinity at the 70m level.)

At the surface, there is a dense grouping of profiles 1 to 8 (Group 1) around 20°C, 37.6‰. Similarly, profiles 9 to 12 (Group 2) are concentrated around 21°C, 37.9‰. Profile 13 is singular, at the same temperature as Group 1 but with a somewhate lesser salinity.

Between 50 and 100m, almost the same grouping is present, but profiles 1 and 3 are in Group 2, which is still more saline and warmer than Group 1. Around 100m, all profiles merge towards the local LIW water type at 14.6°C, 38.83‰ .

Such a grouping of profiles is not random; in fact, it can be associated closely with the structure found in the transect and provide some knowledge about the composition of the upper part of the warm anomaly. The profiles in Group 1, in the 50 to 100m layer, are indicative of mixing between

surficial Atlantic Water and local LIW. By contrast, Group 2 is representative of mixing of local LIW with a warmer, more saline surficial water type. This is characteristic of surface water found to the east. The upper layer of the warm anomaly could have been formed in a mixing event to the east, a hypothesis which suggests a westward drift of this warm anomaly as an isolated dynamical entity. The layer considered here is below the thermocline, and a dynamical process (overturning, mixing, etc.) is more likely to have produced it than penetration of heat across the thermocline.

Furthermore, profiles 9 and 12, located on the edges of the warm anomaly, were closer to Group 1 than were profiles 10 and 11. These two profiles, being located in the core of the anomaly, could possibly have suffered less mixing than profiles 9 and 12. Profile 13 was even less saline than Group 1, which indicates the presence of a surficial lens of fresher water, for which no physical explanation is advanced.

To explain the behavior of profiles 1 and 3, which demonstrated characteristics similar to those of profiles 9 to 12 at the 50 to 100m level, one can refer to the temperature and salinity transects which indicate the edge of a trough-like perturbation. It is accordingly hypothesized that they might represent the same water mass composition as profiles 8 to 12, but did not show a tendency toward a "Group 2" composition at the surface because of some surficial transformation.

2. Internal (baroclinic) wave computation

"Internal waves are fluid motions which are under the influence of variations in the ocean density (buoyancy) field and the earth's rotation; i.e., both these influences provide restoring forces" [Mooers 1975, p1067]. The baroclinic low-frequency wave propagation in a rotating fluid is governed by the following equation:

$$N^2(z)\, W_{xx} + f^2\, W_{zz} = 0$$

with $\sigma^2 << f^2$ where $W(x,z)$ represents the vertical velocity, $N(z)$ the Brunt-Vaisala frequency, σ the wave frequency, and f the Coriolis parameter. Assuming that $W(x,z)$ can be modeled as:

$$W(x,z) = Z(z) \cdot \exp(kx),$$

the previous equation becomes:

$$Z'' + k^2 N^2 f^{-2} Z = 0$$

This eigenvalue equation was solved for k with the following kinematic boundary conditions (BC):

$$Z(0) = Z(-D) = 0$$

i.e. the vertical velocity vanishes at the surface and bottom. A Brunt-Vaisala frequency profile was computed from profile 11 (MILOC-68), the center of the warm eddy. Once the problem was solved for the first five modes, the eigenfunctions Z(z) were evaluated (Fig. 41) and the baroclinic Rossby radius of deformation computed as R = 1/k (Table III). Values of R are commonly interpreted as typical scaling lengths for dynamical processes. The eigenfunctions also give some information about the vertical dependence of velocity fields, and show in particular the depths where maximum shear and horizontal velocity reversal occur. Details of the computational algorithm are given in Appendix B.

TABLE III

Values of the baroclinic Rossby radius of deformation (modes 1 to 5).

Mode Number	1	2	3	4	5
Rossby radius (km)	23	12	9	7	5

Assuming that most of the energy of an eddy is associated with the barotropic and the first baroclinic mode, 23 km is, hence, assumed to be a reasonable first-order scaling length for the perturbation field. This value can be related to the e-folding distance of the correlation

functions found in Zone I and II, i.e., 30 and 45 km, respectively. However, a visual comparison of the second-mode vertical structure with the isotherm perturbation field (Fig. 39) shows that the main 15°C isotherm perturbation occurs at the same depth as the maximum of the second mode vertical speed. Hence, the second mode may also be important to describe the spatial structure, with a Rossby radius of deformation (second mode) of 12 km. Given the inherent approximations, including the fact that the Rossby radius of deformation was computed from a totally different data set at the center of the most notable anomaly, and with no data below 400m, the agreement is fair. The question is raised as to whether the local computation of the Rossby radius of deformation[3] could be used as a valuable operational index of horizontal variability.

The development above was limited to the f-plane, i.e., to an ocean with no latitudinal change of the Coriolis parameter. On the β-plane, where f is allowed to vary with latitude ($\beta = \partial f/\partial y$), the theory indicates that a class of long waves, called planetary or Rossby waves, is allowed to propagate in the (baroclinic) ocean. The wavelength (L) of such waves is of the order of $2\pi R_n$, the period (T) is greater than the inertial period:

$$T = (2\pi)^2 \frac{[R_n^{-2} + L^{-2}]}{\beta L^{-1} \cos\theta} \quad ,$$

---

[3] If actually treating a baroclinic wave, the appropriate scale is the horizontal wavelength, which is of the order of $2\pi R_n$ or about 72 km in the case of a second mode wave.

where θ is the direction of propagation relative to east and the phase speed has a typical order of magnitude of a few cm/s for an internal Rossby radius of deformation of about 10 km, which always has a westward component.

XI. OCEANOGRAPHIC SUMMARY

The various analyses reported in the previous chapters led to a description of some oceanic characteristics of the Ionian Sea. None of these characteristics seemed to differ from the commonly accepted picture of the region, but some of them bring a clearer focus to specific points, and suggest new questions.

The series of satellite IR images provided some quantitative estimates of the temporal variability and the geographical extent of the surface advection patterns, as the surficial water flows from the narrow Strait of Sicily into the more open Ionian Sea. Questions arise regarding the factors that influence and determine the characteristic double-tongued flow: where is the generation area and what are the triggering factors for this splitting? Is there a vortex pair (a cyclonic and an anticyclonic eddy) formed? What processes govern the anticyclonic curling of the northern tongue? What is the influence of bottom topography; e.g., the continental shelf and the ridge? Once this flow pattern is confirmed and its seasonal variability evaluated, a laboratory simulation could be undertaken to assess some of these factors, in a way similar to that which has been done recently for the Strait of Gibraltar [Whitehead and Miller, 1979]. A dynamical (numerical) approach could also be attempted to verify, for

each of the water tongues, whether the flow pattern could be affected by the release of absolute potential vorticity (baroclinic instability) as it reaches the deeper ocean [Mysak, 1977].

The satellite IR imagery correlated well with two subsurface features. First, the distribution of the thermocline depth had a good visual correlation with the advection patterns of surficial Atlantic Water. A relatively shoal thermocline depth can be expected in these tongues of cooler water. Second, the presence of a warm anomaly was revealed by the satellite IR imagery, as a transient atmospheric boundary layer effect, with the occurrence of low level stratus. Boundary layer theory indicates that such events would be most likely in the early morning and in the presence of higher winds. The observation of such a feature, if correctly interpreted as an atmospheric "second-order" effect, can be a first suggestion of the presence of such a feature, and may allow its (discontinuous) tracking.

The XBT analysis revealed - or confirmed - some contrast between the northern zone (Zone II) and the southern zone (Zone I). On one hand, Zone II is a relatively quiescent area in which the superposition of water masses has no dramatic consequences, and little apparent (synoptic scale) horizontal variability; on the other hand, Zone I is directly exposed to the entering surface flow from the Strait of Sicily, which seems to create geophysical turbulence and baroclinic

instability, as revealed by the occurrence of temperature inversions and layering. One particular feature was a warm core eddy, about 60 km in diameter, characterized by a strong (200m) deepening of the 15°C isotherm. A warm core eddy was also found in another study (MILOC-68); hence, it suggests that eddies could characterize the synoptic scale turbulence in that region, although with possible seasonal variation. Questions arise regarding the origin of this warm anomaly, which has a different water mass composition from the ambient water. It was suggested that this anomaly could have been formed by mixing to the east of its location. This hypothesis would rewuire further investigation to explain the westward migration of this isolated feature, perhaps as a Rossby wave, or eddy, and its associatin with depressed isotherms at the 200m level. Such an investigation could be possible, at first approximation, using a two-layer[4] model of the ocean and disregarding any bottom topographic effect [Leblond and Mysak, 1978] or using a more sophisticated approach [McWilliams and Flierl, 1979]. Scales for wavelength and phase speed could be estimated for comparison with observations as in Ozturgut [1976].

---

[4] If the second mode structure noted earlier is predominant, a three-layer model would be needed.

Finally, the statistical study of spatial and temporal scales of variability showed a clear anisotropy in Zone I. How typical these correlation functions are, and how permanent they are over an annual cycle could not be assessed, and would require a larger data base. It is suggested that such two-dimensional spatial-lag correlation functions would be useful to better define the spatial scales required for sampling and analysis. Clearly, additional analytical techniques are needed to allow for a systematic separation of the different processes that distort the synopticity of the data, which hence, decrease the quality of the analyses.

XII. OPERATIONAL CONSIDERATIONS

A. TWO OBJECTIVES FOR OPERATIONAL ANALYSIS

The basic methodology used in the present study can be described as an attempt to analyse and interpret a temperature data set in the light of the regional oceanology. It is the belief of the author that such an approach should be used as a routine technique to provide navies with environmental products.

It is a usual procedure for a group of naval ships to organize a bathy(thermograph) watch by assigning a guard ship with the task of sampling at regular intervals, usually 4 or 6 hrs, and broadcast each profile to other units, as well as to the environmental facilities ashore. Units then process this single profile to obtain the variables they need: predicted range, optimum depth, etc., for the appropriate sensors. In some tactical situations, the spacing between units might be re-evaluated as well.

But the sampling is seldom organized according to the ocean itself, its variability, the atmospheric forcing processes or the location of previous data samples in the region. Moreover, airplanes and helicopters have their own procedures, which they most often follow independently of the surface units. In fact, the error in such an approach is to reduce a four-dimensional problem (time, space) to a

two-dimensional one (time, depth). This procedure has two major deficiencies:

First, it makes sampling a random operation, with a loss of information when areas of strong variability are crossed and not sampled, and an increased expenditure when XBTs are redundant in unstructured areas.

Second, it encourages ASW forces to regard the ocean as a horizontally homogeneous water mass, with a temperature structure varying incrementally every 4 or 6 hours. It most certainly causes a lack of accuracy in sonar range predictions. But worse, it precludes the ability to use such inhomogeneities in the ocean for tactical purposes: hiding a unit, optimizing a silent transit, enhancing detection capabilities, etc.

Ashore, prediction facilities do not have the appropriate tools to conduct a more thorough analysis of the ocean structure, at a scale compatible with operational requirements. For example, at FNOC computational techniques are currently used which blend a variety of input variables through weighting of these variables [Holl et al., 1979] over extensive areas. This approach might be of some interest as a method of producing an input to global atmospheric models. However, it does not seem to be, as yet, well adapted to meet naval operational ocean prediction requirements, which involve typical scales of 5 to 100 km, suggesting a need to resolve, at least, the 20 to 60 km scale, so commonly found in the ocean.

Finally, reasonable objectives for ASW forces in this attempt to better understand and exploit the ocean would be:

1. to routinely include the horizontal variability, through a more appropriate sampling procedure, and
2. to request synoptic scale analyses from shore prediction facilities, which implies a regional approach to oceanography.

These two points are addressed in the following sections, with the idea that the next step in this development would be the implementation of short term, on-board prediction tools.

B. IMPROVING DATA COLLECTION

1. Four complementary systems

A variety of systems are available currently for monitoring the oceanic structure in a region:

- XBT profiles are well known for their ability to describe the temperature and, hence, sound speed structure, in the upper layers. This study has shown a potential capability to evaluate the horizontal fields.
- Satellite remote-sensing is available to provide a variety of variables, among which SST is the most common. The main interest in such data is to provide the analyst with a perception of synoptic scale and mesoscale features, and their approximate location.

- Drifting buoys, even a single one, could bring some dynamical clues in the evaluation of time variability (heating and turbulence of the upper layer), as well as advection, by continuous tracking.
- Continuous SST (and salinity) measurements from surface ships, if accurate, could clearly indicate anomalies such as fronts or eddies, and aid in the interpretation and "calibration" of satellite IR images. Furthermore, they could better orient XBT sampling in real time and encourage a better perception of horizontal variability.

2. Recommendations for XBT sampling

It is not known what type of XBT sampling procedures were implemented during the SHAREM 38 exercise from which the present data set was acquired. The limits of the exercise zone were also not known. Hence, no appreciation could be gained as to how well the actual XBT sampling covered the zone. In fact, the sampled area might have been somewhat smaller than the operating area, a situation which commonly occurs due to obvious priorities and limitations in mobility.

Fifty-five XBTs constitute the coverage in Zone I, an area of 30,000 sq km. Some pairs of XBT profiles were positioned quite close, in both time and space, and could be termed as a redundancy in the data set. This redundancy could be prevented and yield a better coverage within the limits of a planned sampling effort.

The correlation diagrams presented in Chapter VI suggest an order of magnitude for spacing of XBTs, since it evaluates the amount of common information present in two profiles. In particular, it suggests very strongly that sampling should not be isotropic. Since the Ionian Sea is clearly much more variable in the E-W direction, sampling should be made at closer intervals in this direction. The +0.5 correlation contour could be used as a satisfactory level of cross-correlation, suggesting that 20 km in the E-W direction might be adequate (Figs. 27 to 29). Spacing in the N-S direction depends on the layer of interest: adequate spacing would be from 30 to 60 km.

This type of approach, where correlation functions in a layer are used to estimate adequate sampling intervals, should be consistent with requirements for resolving features in the sound speed field. This is a factor which depends on sensor characteristics, mainly frequency and depth. Assuming that the depth of minimum sound speed, which is between 100 and 200m in this region, might be of interest, a sampling distance of 60 km would be adequate in the N-S direction (Fig. 29). Under such a procedure, Zone I could have been adequately covered with 26 XBTs. In other words, the same XBT expenditure would have permitted sampling the entire area twice within the same five-day period. The term "adequate coverage" implies here an attempt to resolve synoptic scale features, in order to track them and take

them into account in naval operational planning. This does not suggest that XBT sampling at short (a few hours) intervals is irrelevant, especially if IR imagery is used to guide the pattern of XBT deployments, but it emphazises the interest of well planned spatial sampling and analysis, by contrast with a temporally regular/spatially random procedure. In the upper layer of interest to hull-mounted sonars, more attention must be devoted to the transient physical processes and closer sampling will hence be required, until the driving processes are better understood and forecasted.

Clearly, the analysis grid, just like the sampling grid, should be determined carefully with respect to the thermal structures that one tries to resolve. The present study used the sampling grid as an analysis grid, since the data were not overwhelming, and the thermal fields were evaluated and smoothed manually. It is nevertheless interesting to proceed faster, and more objectively, i.e., consistently, with computer assistance, and objective analysis techniques (using weighting factors based on the correlation functions) are currently developed for such purposes [Bretherton et al, 1976].

C. AN APPROACH TO REGIONAL OCEANOGRAPHY

The suggestions developed in the following section apply to a geographical region where continuous monitoring of the oceanic variables is required, whether it is for harbor defense, the control of vital shipping lanes or the surveillance of submarine traffic. It could be adapted to the

transit of a task force, which usually covers a long track through a variety of oceanic regimes.

First, areas of operational interest should be delineated, and their boundaries should be kept consistent with the oceanic regime and local processes.

Second, a compilation of experimental studies should be made for each area, to provide the oceanographer with the initial material, a step which is instrumental in the regional approach. Such a study should be physical as well as statistical and describe processes such as formation of deep water, circulation, mixing of water masses, typical variables or products representative of these processes, etc. Atmospheric forcing variables should not be overlooked, and in fact need to be closely associated, especially with respect to mixed layer processes, Ekman transports, and formation of deep water. Such a compilation of local information can be compared, at a different scale, with forecasters' handbooks that are developed by meteorologists to provide coverage of local conditions, particularly near airports [Brady and Nestor, 1980].

Third, the sampling should be organized and adapted to the region, i.e., to both spatial and temporal scales of dominant processes. This point has been more fully developed in the previous section.

Fourth, a set of standard tools should be made available to help the analyst to process incoming data and relate them

to the climatological picture. The evaluation of how far the computer software must be involved in the data processing is precisely one of the steping stones of this method. These programs should not be used beyond the point where they start removing the essential information from the input data, leaving only the climatological picture. In fact, some computer-assisted manual evaluation is very likely to remain useful for a long time, which applies to quality control, field contouring and any other non-mechanical technique, a fact which is acknowledged in their own field by many experienced meteorologists.

Lastly, more specialized analytical tools should be developed as research progresses, and could be expected in the near future in such fields as data integration, dynamics of frontal regions, Rossby wave propagation, or mixed layer evolution. There would be the main tools necessary for operational analysis and forecasting.

D. THE MEDITERRANEAN SEA, NATURAL LABORATORY

The Mediterranean Sea offers an interesting potential as a natural laboratory for coupled environmental/tactical experiments:

1. Being surrounded by continental masses, its synoptic weather situation is well monitored and does not suffer much from data gaps.

2. Topographical peculiarities like straits, sills or basins are abundant, and create a variety of regimes in both the regional and dynamical sense.
3. The conditions for the use of satellite IR remote-sensing for the determination of thermal properties and other surface variables are exceptional, due to low cloud coverage throughout most of the year.
4. The "moderate" size of its basins, and their clear physical separation could allow for synoptic-scale, three-dimensional, numerical modeling which is within the reach of current computer capabilities once the dominant physical processes are properly determined.

Given these natural qualities, the Mediterranean Sea appears as an ideal region where new oceanographic techniques and tactics could be tested and improved, prior to their application, mutatis mutandis, to other regions of ocean, where the conditions are less exceptional.

LIST OF REFERENCES

Note: Due to a homonymy, the reference mentioned in the text as "R. R. Miller" implies the second Miller's document listed below. Any other reference to "Miller" implies A. R. Miller's publications, i.e., the MILOC-68 experiment.

Bell, T. H. (1971), Numerical calculation of dispersion relations for internal gravity waves, Naval Research Laboratory, Report 7294

Bourke, R. H. (1973), The ASRAP III acoustic forecast model, (unpublished document)

Briscoe, M. G., Johannessen, O. M., Vincenzi, S. with Furness, G. (1974), The Maltese oceanic front: a surface description by ship and aircraft, Deep-Sea Res., vol 21; 247-262

Bretherton, F. P., Davis, R. E. and Fandry, C. B. (1976) A technique for objective analysis and design of oceanographic experiments applied to MODE-73, Deep-Sea Res., vol 23; 559-582

Brody, L. R. and Nestor, M. J. R. (1980), Regional forecasting aids for the Mediterranean Basin, TR 80-10, Naval Environmental Prediction Research Facility, Monterey, California

Gonella, J. (1971), The drift current from observations made on the Bouee Laboratoire, Cah. oceanogr., 33 (1); 29-33

Grancini, G., Lavenia, A., and Mosetti, F. (1972), A contribution to the hydrology of the Strait of Sicily, Conference Proceedings 7, SACLANT ASW Research Center, La Spezia, Italy: 68-81

Holl, M. M., Cuming, M. G. and Mendenhall, B. R. (1979), The Expanded Ocean Termal-Structure analysis system: a development based on the fields by information blending methodology, MII Project nr M-241, Meteorology International Incorporated, Monterey, California

Johannessen, O. M., de Strobel, F., and Gehin, C. (1971), Observations of an oceanic frontal system east of Malta in May 1971 SACLANT ASW Research Centre, Tech. Memo. 169

Johannessen, O. M. (1972), A review of oceanic fronts, SACLANTCEN Conference Proceedings 7

Johannessen, O. M. (1977), Observation of an oceanic front in the Ionian Sea during early winter 1970, J. Geophys. Res., 82(9); 1381-1391

Lacombe, H. and Tchernia, P. (1960), Quelques traits généraux de l'hydrologie méditerranéenne Cahiers Océanograph. XII(8); 528-547

Lacombe, H. and Tchernia, P. (1971), Caractères hydrologiques et circulation des eaux en Méditerranée, in The Mediterranean Sea: a natural sedimentation laboratory, ed. by D. J. Stanley, 25-36

Leroy, C. C. (1969), Development of simple equations for accurate and more realistic calculations of the speed of sound in sea water, J. Acoust. Soc. Am., 46; 216-231

Levine, E. R. and White, W. B. (1972), Thermal frontal zones in the eastern Mediterranean Sea, J. Geophys. Res., nr 77(6); 1081-1086

McWilliams, J. C. and Flierl, G. R. (1979), On the evolution of isolated, nonlinear vortices, J. Phys. Oc., vol 9; 1155-1182

Miller, A. R. (1972), the distribution of temperature, salinity and sound velocity in the Western Ionian Sea during Spring, 1968, WHOI Tech. Rep. nr 72-5, Unpublished Manuscript

Miller, R. R. (1972), Current regime of the MALTESE oceanic frontal zone, Naval Underwater Systems Center, TR 4381

Mittelstaedt, E. and K. Huber (1973), Inversions beneath the thermocline in the north-western Mediterranean, Deutsche Hydrogr. Zeitschrift, (4); 145-154

Mooers, C. N. K. (1975), Sound velocity perturbation due to low-frequency motions in the ocean, J. Acoust. Soc. Am., vol 57(5); 1067-1075

Morel, A. (1971), Caractères hydrologiques des eaux échangées entre le bassin oriental et le bassin occidental de la Méditerranée, Cahiers Océanograph., XXIII; 329-342

LeBlond. P. H. and Mysak, L. A. (1978), Waves in the ocean, Elsevier oceanography series

Mysak, L. A. (1977), On the stability of the California Undercurrent off Vancouver Island, J. Phys. Oc., vol 7; 904-917

Ovchinnikov, I. M. (1966), Circulation in the surface and intermediate layers of the Mediterranean Oceanology, 6; 48-59

Naval Weather Service Command (1970), Summary of snyoptic meteorological observations; Mediterranean marine areas, vol 6 (AD 713 295)

Ozturgut, E. (1976), The sources and spreading of the Levantine Intermediate Water in the Eastern Mediterranean, SACLANT ASW Research Center, SM 92

Perkins, H. (1972), Inertial oscillations in the Mediterranean, Deep-Sea Res., vol 19; 289-296

Pollard, R. T. (1970), On the generation by winds of inertial waves in the ocean, Deep-Sea Res., vol 17; 795-812

Rogers, C. and Hanley, J. (1980), Deformation of the marine inversion and the development of marine fog and stratus resulting from warm water patches: numerical modeling and verification with satellite imagery, CR 80-01, Naval Environmental Prediction Research Facility, Monterey, California

Saunders, P. M. (1972) Space and time variability of temperature in the upper ocean, Deep-Sea Res., 19; 467-480

Urick, R. J. (1975), Principles of underwater sound (2nd ed.), Mc Graw Hill

Whitehead, J. A. and Miller, A. R. (1979), Laboratory simulation of the gyre in the Alboran Sea, J. Geophys. Res., vol 84 C7; 3733-3742

Woods, J. D. (1968), Wave-induced shear instability in the summer thermocline, J. Fluid Mech., 32(4); 791-800

Woods, J. D. (1972), the structure of fronts in the seasonal thermocline. In Oceanography of the Strait of Sicily, Conference Proceedings 7, SACLANT ASW Research Center, La Spezia, Italy; 144-152

Woods, J. D., Wiley, R. L. and Briscoe, M. G. (1972), Vertical circulation at fronts in the upper ocean. In A voyage of Discovery, ed. by M. V. Angel, Pergamon Press; 253-275

Wust, G. (1961), On the vertical circulation of the Mediterranean Sea, J. Geophys. Res., 66(10); 3261-3271

Zore-Armanda, M. (1969), Water exchange between the Adriatic and the eastern Mediterranean, Deep-Sea Res., vol 16; 171-178

APPENDIX A

XBT STATISTICS

A.1 DEFINITION

The following notation is defined:

- n the total number of synoptic XBTs in a zone
- i,j the indicies defining particular profiles
- k the index for depth for a given profile

Hence $T_{i,k}$ represents the temperature at level k, i.e., at depth 5(k-1) meters from profile at position i.

A.2 METHOD

Each profile was digitized by 5m increments from surface (k = 1) to 400m depth (k = 81). A mean profile was then computed by averaging the temperature at each digitized depth over the whole set of n XBTs:

$$\overline{T}_k = 1/n \sum_{i=1}^{i=n} T_{i,k}$$

Given a pair of XBT profiles, a cross-correlation coefficient was computed for each previously defined layer:

$$(\rho_{ij})_{0\text{-}60m} = \frac{\sum_{k=1}^{k=13} (T_{i,k} - \bar{T}_k)(T_{j,k} - \bar{T}_k)}{\sqrt{\sum_{k=1}^{k=13} (T_{i,k} - \bar{T}_k)^2 \cdot \sum_{k=1}^{k=13} (T_{j,k} - \bar{T}_k)^2}}$$

in the 0 to 60m layer; and similarly in the 60 to 150m layer (with summation from k = 13 to 31) and the 150 to 400m layer (with summation from k = 31 to 81).

Given a set of n profiles, the number of cross-correlation coefficients generated in the process is $n(n-1)/2$. The geographical location of each profile in a pair yields a ΔX_{ij}, ΔY_{ij}, defining the horizontal E-W and N-S distance between these two profiles. Whenever ΔX_{ij} is found to be negative, both signs of ΔX_{ij} and ΔY_{ij} must be changed. This is essentially the same as limiting the azimuth between XBTs to the 0-180° range without loss of generality.

The set of values (ρ_{ij}, ΔX_{ij}, ΔY_{ij}) were related to the time interval in the following fashion: the distance ΔD_{ij} between the two profiles was computed and associated with the difference in days between the two profile dates. Distances were quantified and averaged by 10 km increments, whereas time intervals were expressed in an integral number of days, from zero to four (Zone I) or seven (Zone II). The

cross-correlation coefficients were plotted in this time-space coordinate system.

Next the sets of values (ρ_{ij}, ΔX_{ij}, ΔY_{ij}) were quantified by 10 km intervals, and values of the cross-correlation coefficient falling in a given 10 by 10 km square were averaged, yielding a single coefficient.

Finally, these averages were plotted on a 10 km square grid and contoured, for each of three layers. The number of cross-correlation values in each square was also plotted to give a measure of the density of information. Clearly, these plots are symmetric with respect to the origin, since it does not make any difference whether profile i is considered to be at the center, and profile j in the ΔX, ΔY grid, or the converse.

APPENDIX B

NUMERICAL CALCULATION OF BAROCLINIC INTERNAL WAVES

B.1 EIGENVALUE PROBLEM

Solving equation (1), with its associated boundary conditions (BC), is an eigenvalue problem:

$$Z(z) + N^2(z)\, k^2\, f^{-2} Z(z) = 0 \qquad (1)$$

$$Z(0) = Z(-D) = 0$$

A solution for k and Z can be found for an infinite number of modes. N(z) is a geophysical variable, the Brunt-Vaisala frequency, which represents the natural frequency of oscillation of a water particle under the influence of the buoyancy force:

$$N^2(z) = -g/\bar{\rho} \left(\frac{\partial \rho}{\partial z}\right)_{adiab} = -g/\bar{\rho} \left(\frac{\partial \rho}{\partial z}\right)_{insitu} - g^2/c^2,$$

where $\rho(z)$ is the density of water, g the gravitational acceleration and c(z) the sound speed at depth z.

B.2 NUMERICAL METHOD

For the Brunt-Vaisala frequency profile N(z) encountered, an analytical solution to equation (1) is not possible. A

numerical technique obtained from Bell [1971] was used as follows:

The Brunt-Vaisala profile is digitized from the surface to the bottom, yielding n values N_1, N_2, ...N_n at n levels z_1, z_2, ...z_n. These levels need not be at evenly spaced intervals. An approximate quadratic form for Z(z) is assumed for each depth interval spanning two increments of depth.

$$Z_{i-1} = a_{0i} + a_{1j}\, z_{i-1} + a_{2i}\, z_{i-1}^2$$

$$Z_i = a_{0i} + a_{1i}\, z_i + a_{2i}\, z_1^2$$

$$Z_{i+1} = a_{0i} + a_{1i}\, z_{i+1} + a_{2i}\, z_{i+1}^2$$

The second derivative Z''(z) is equal to $2a_{2i}$, and the system of equations above can be solved for a_{2i}, as a linear function of Z_{i-1}, Z_i, Z_{i+1}: $a_i = \phi(Z_{i-1}, Z_i, Z_{i+1})$

Hence, equation (1) becomes:

$$Z_i'' + k^2N^2f^{-2}Z_i = 0$$

or

$$2\phi(Z_{i-1}Z_i, Z_{i+1}) + k^2N^2f^{-2}Z_i = 0$$

This can be solved for Z_{i+1} :

$$Z_{i+1} = \frac{-1}{\Delta i} \{[\tfrac{1}{2}k^2N_i^2f^{-2}\det X_i - \Delta_{i+1} - \Delta_i] Z_i + \Delta_{i+1} Z_{i-1}\} \qquad (2)$$

where $\Delta_i = z_{i+1} - z_i$

and

$$\det X_i = \begin{vmatrix} 1 & z_{i-1} & z_{i-1}^2 \\ 1 & z_i & z_i^2 \\ 1 & z_{i+1} & z_{i+1} \end{vmatrix}$$

B.3 THE ITERATION SCHEME: A SHOOTING METHOD

The theory of eigenvalue (Sturm-Liouville) problems asserts that the wave number which yields solutions satisfying the BCs must lie in the interval:

$$0 < k_1 < \ldots < k_{\ell-1} < k_\ell < k_{\ell+1} \ldots$$

Also, the first mode eigenfunction has one and only one extremum between the boundaries, hence no zero-crossing, the second mode has two extrema and one zero-crossing and so forth.

The shooting method for the first mode is designed as follows: An initial value for k is guessed; given a value for $Z_1 = 0$ (surface BC) and $Z_1 = 1$ (normalized value), the

Z_i's are computed from equation (2) by iteration to the nth level, i.e. the bottom. If the axis Z = 0 is crossed before reaching the nth level, a new lower value for K_1 is tried. Otherwise, the value of Z_n is examined, as the bottom BC. A larger value is tried for k until Z_n gets reasonably close to zero. When the iteration is stopped, k is the numerical solution for the first mode wave number, and the set of Z_i's (i = 1,n) is the eigenfunction.

The next mode is initiated with a guess value $k_2 = 2k_1$. The iterative process is conducted to allow for the proper number of axis crossings, and to obtain a value $Z_n = 0$; and so forth for the other modes. The eigenfunctions obtained are also representative of the density eigenfunctions, and the general theory of baroclinic waves show that the horizontal velocity and the pressure eigenfunctions are proportional to the first vertical derivative of the eigenfunction Z [LeBlond and Mysak, 1978]. These vertical profiles were computed from each eigenfunction Z by a simple centered differentiation scheme.

APPENDIX C

FIGURES

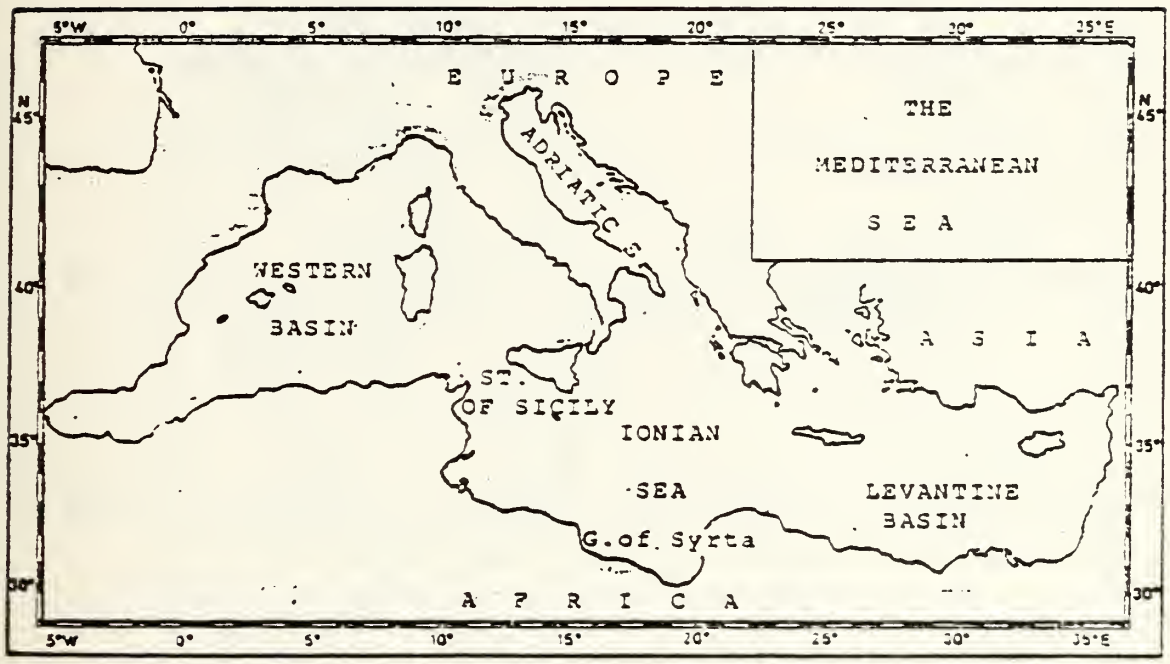

Figure 1. Toponymy of the Mediterranean Sea.

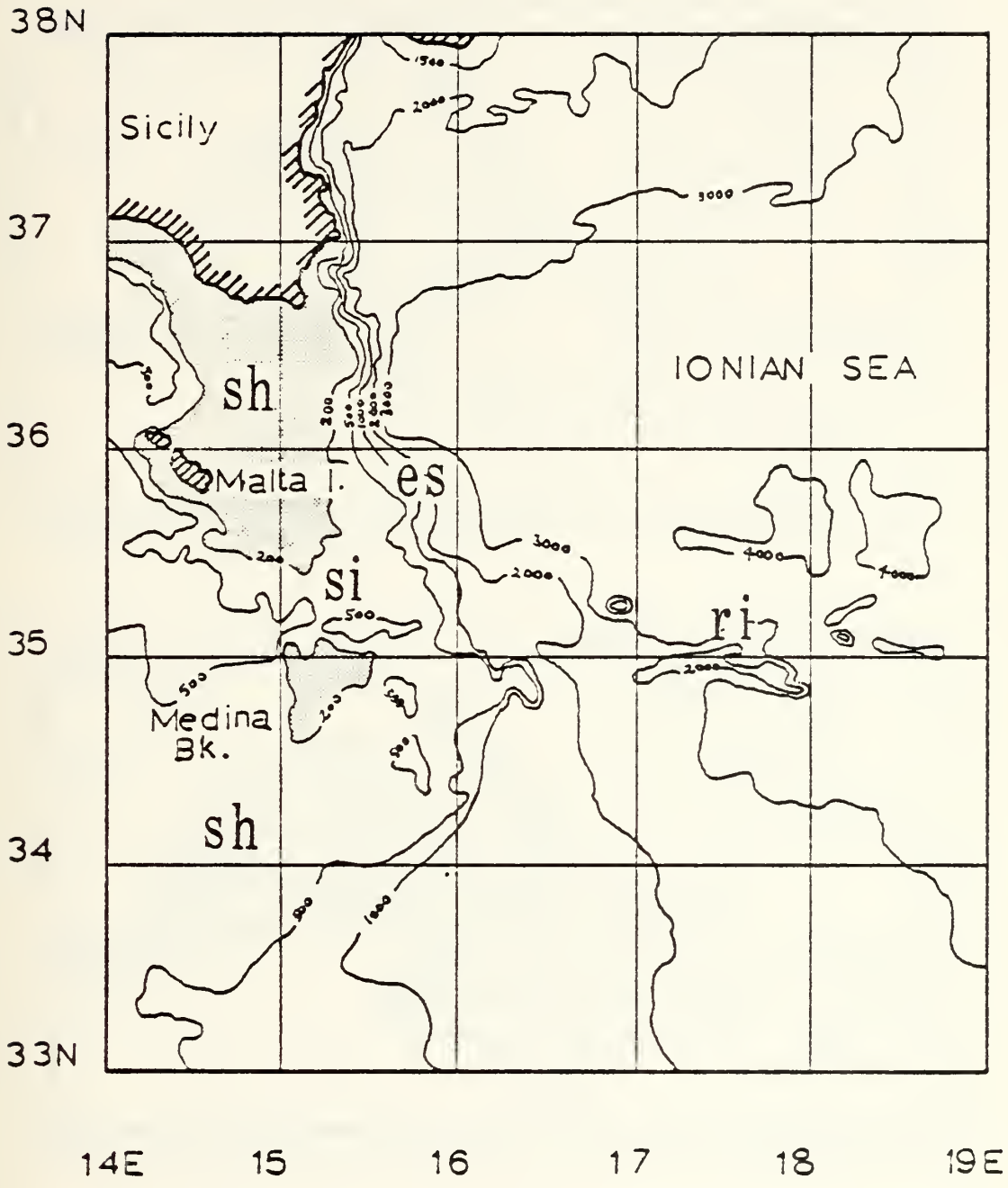

Figure 2. Bathymetry of the Ionian Sea. The main topographic features are: sh-the shelf, si-the sill south of Malta I., es-the escarpment descending from 200m to a depth of 3,000 to 4,000m, ri-the more than 1,000m high ridge along 35°N.

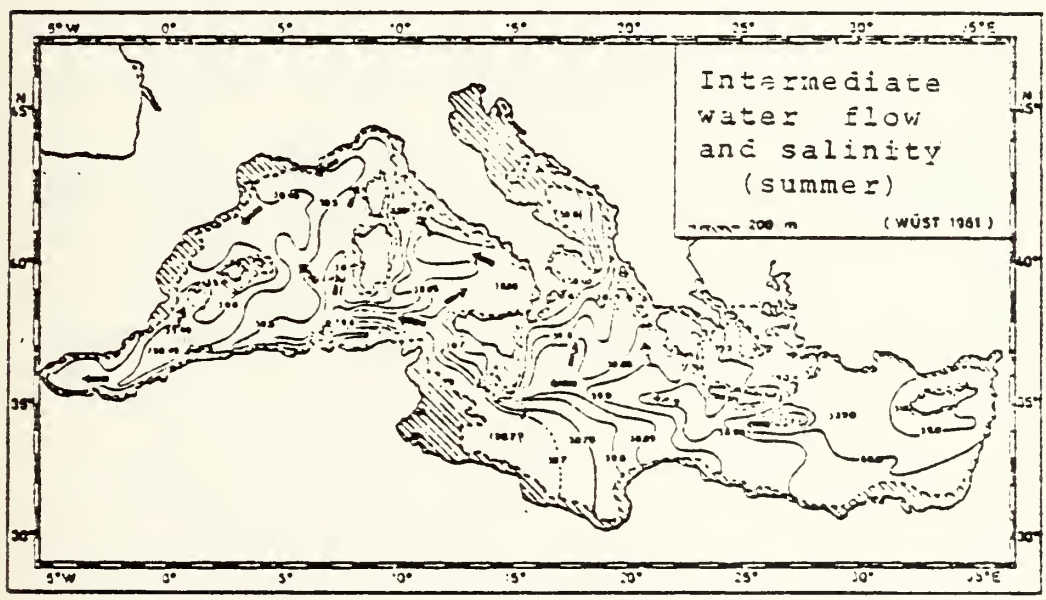

Figure 3. Surface and intermediate circulation in the Mediterranean Sea: a) the surface flow of Atlantic water is eastward b) the return flow of LIW is westward.

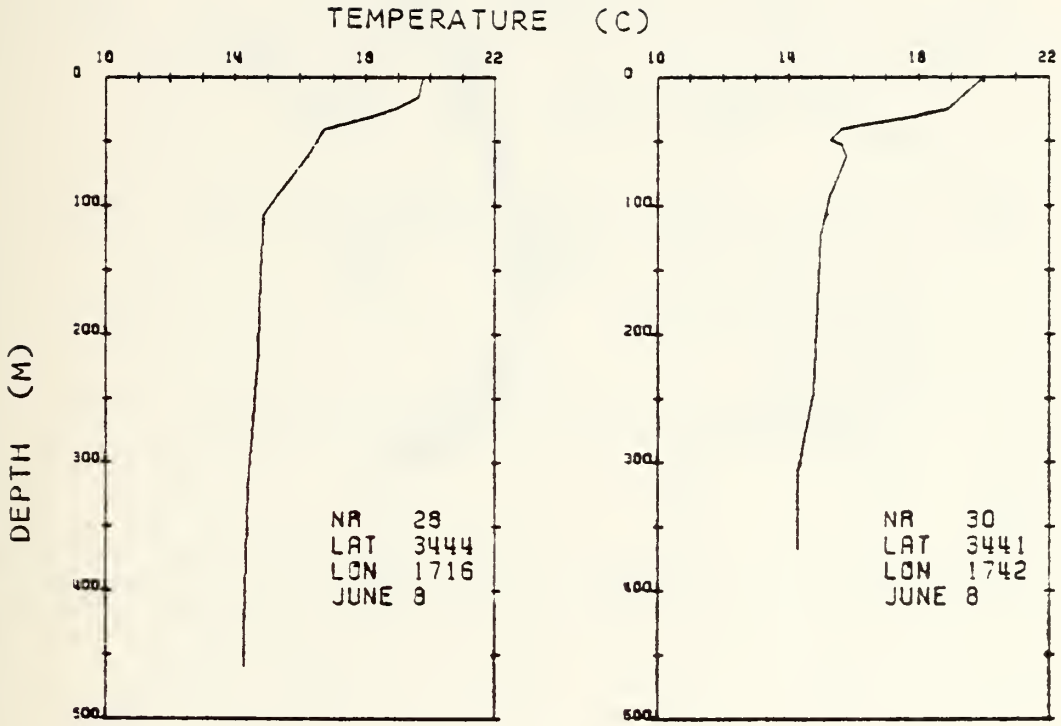

Figure 4. Example of XBT quality discrimination. Although these two sample profiles are less than 35km apart, the profile on the right shows a better resolution in the 50 to 100m layer ("mixing layer"). It is presumed that the profile on the left had a similar inversion, but it may have been overly smoothed.

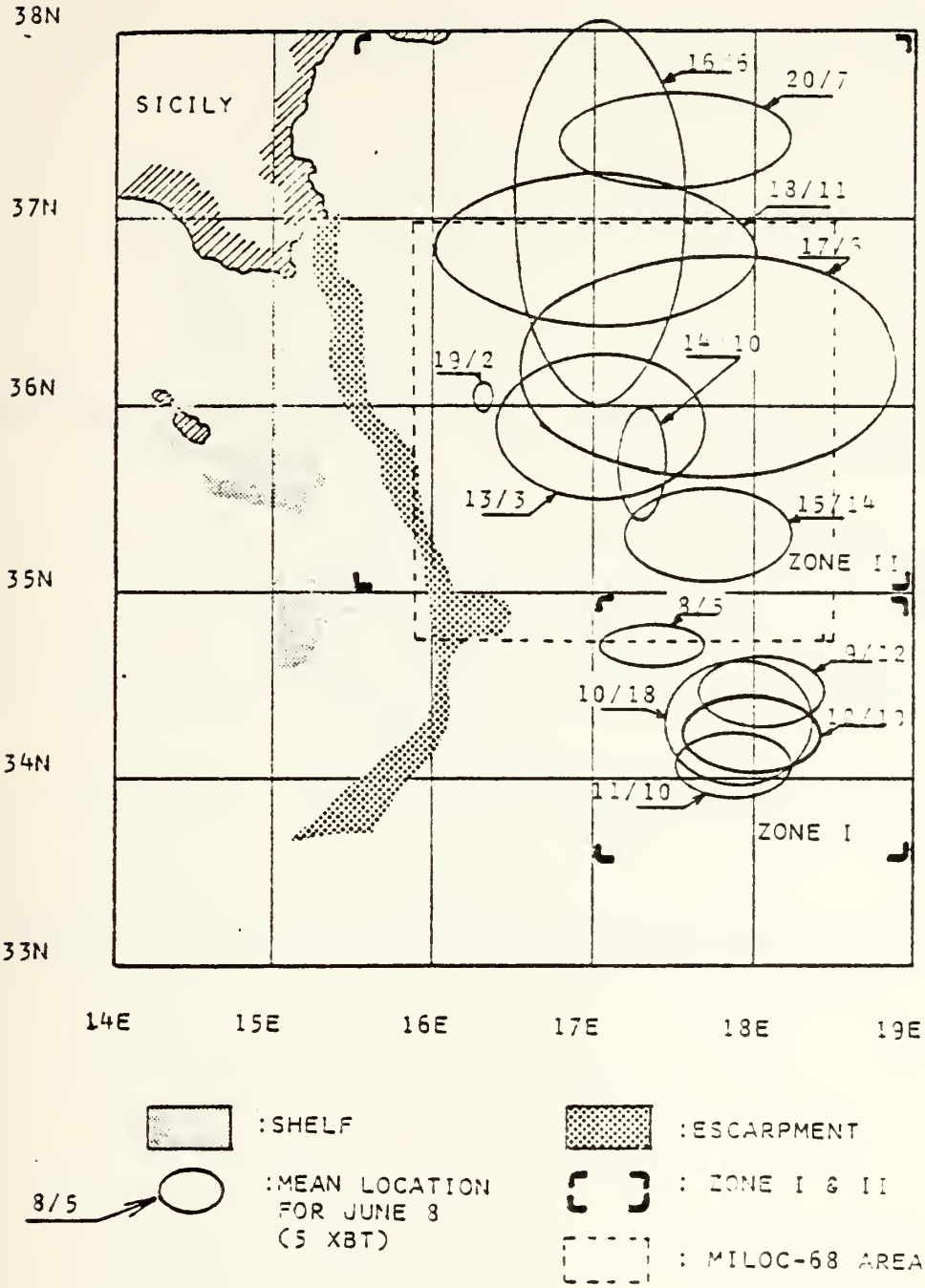

Figure 5. Distribution of XBT profiles in space and time, including the limits of Zones I and II, used for thermal analysis, and the limits of the MILOC-68 study. Each ellipse represents the centroid and spreading of one day of data, with the date and number of XBTs.

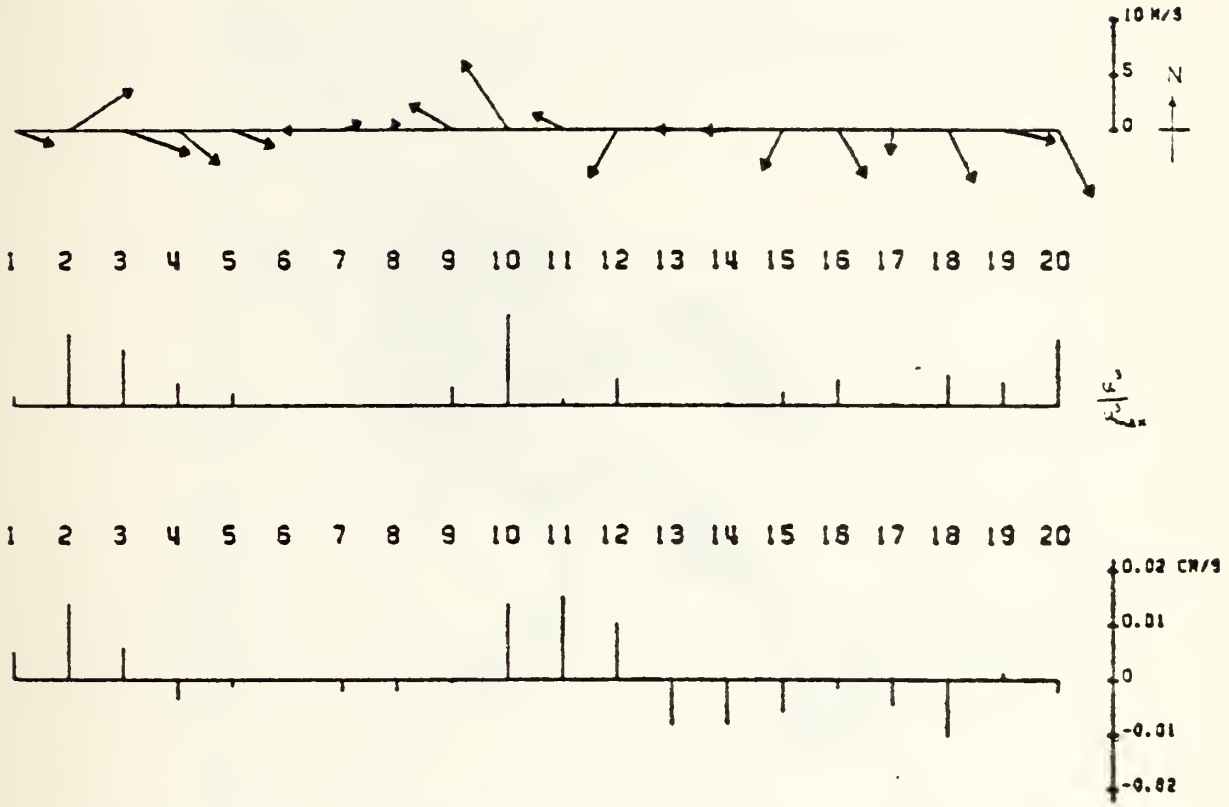

Figure 6. Time series of wind stress and Ekman pumping with the daily mean values for June 1 to 20 of a) wind velocity, b) normalized cube of the wind speed, c) Ekman "pumping" vertical velocity.

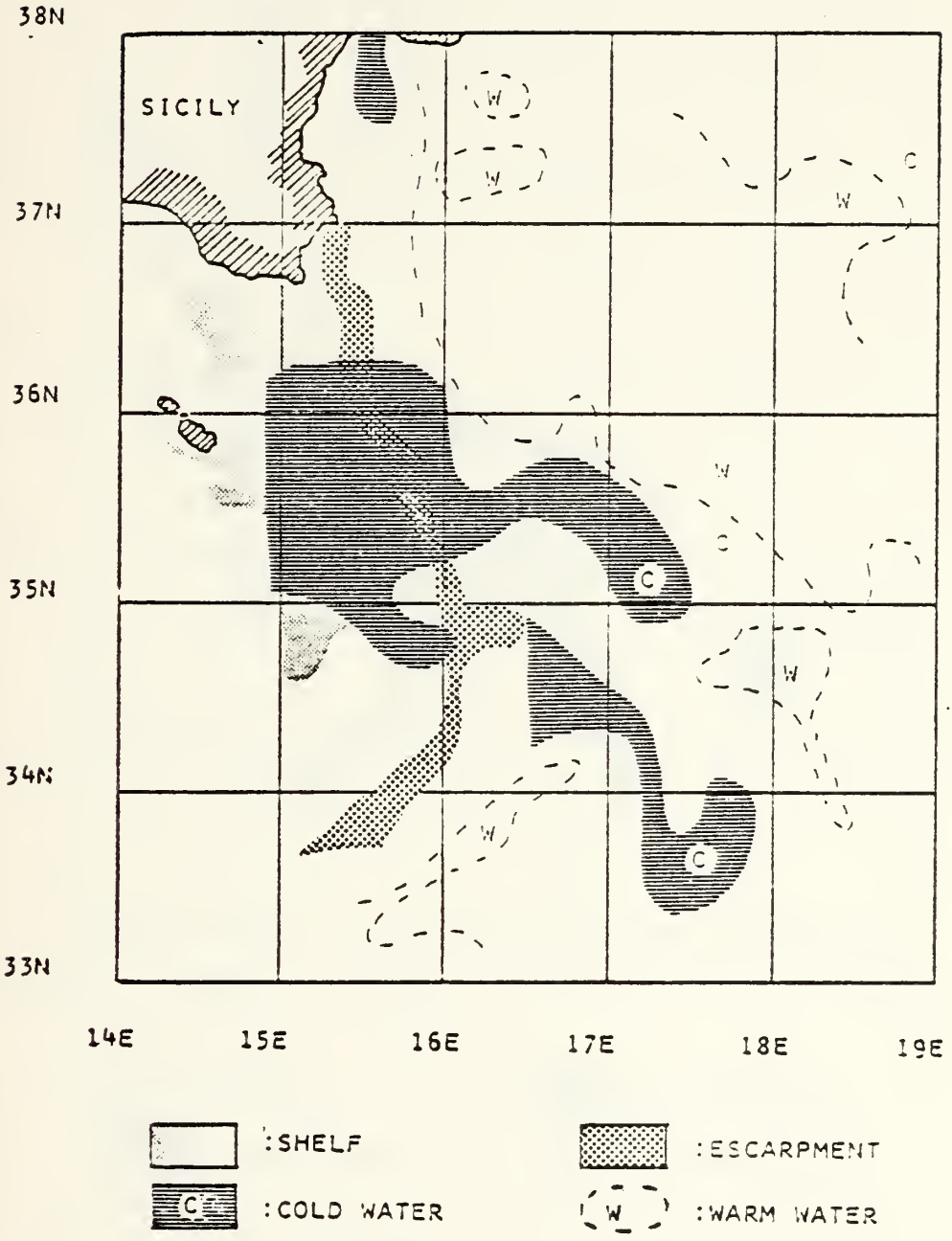

Figure 7. Composite satellite images 5 to 7 June. The two cold water "tongues" are representative of the surface advection from the Strait of Sicily into the Ionian Sea.

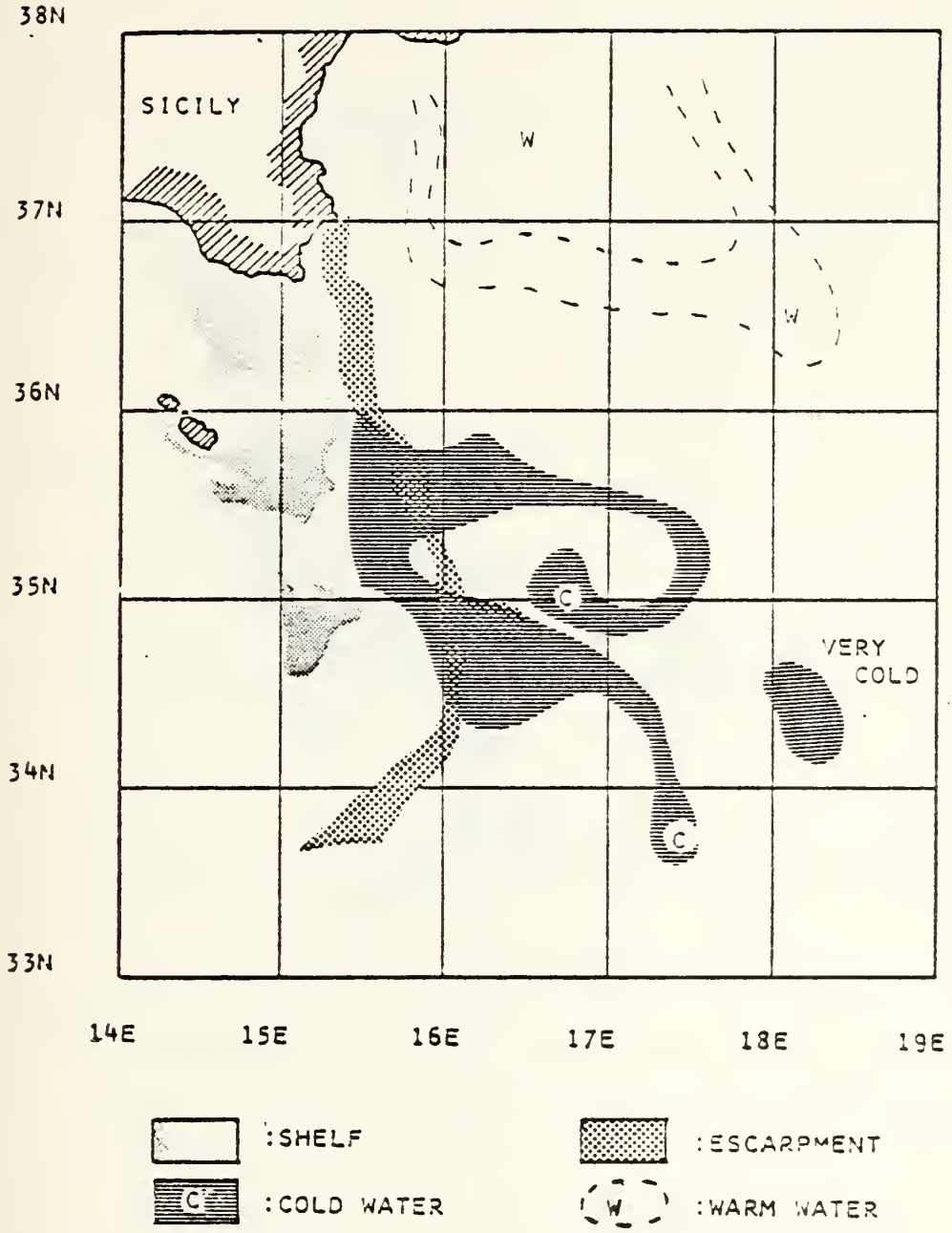

Figure 8. Composite satellite images 10 to 14 June. The northern "tongue" of cold water has curled into an anticyclonic pattern. See section VI.3 for explanations about the "very cold" patch.

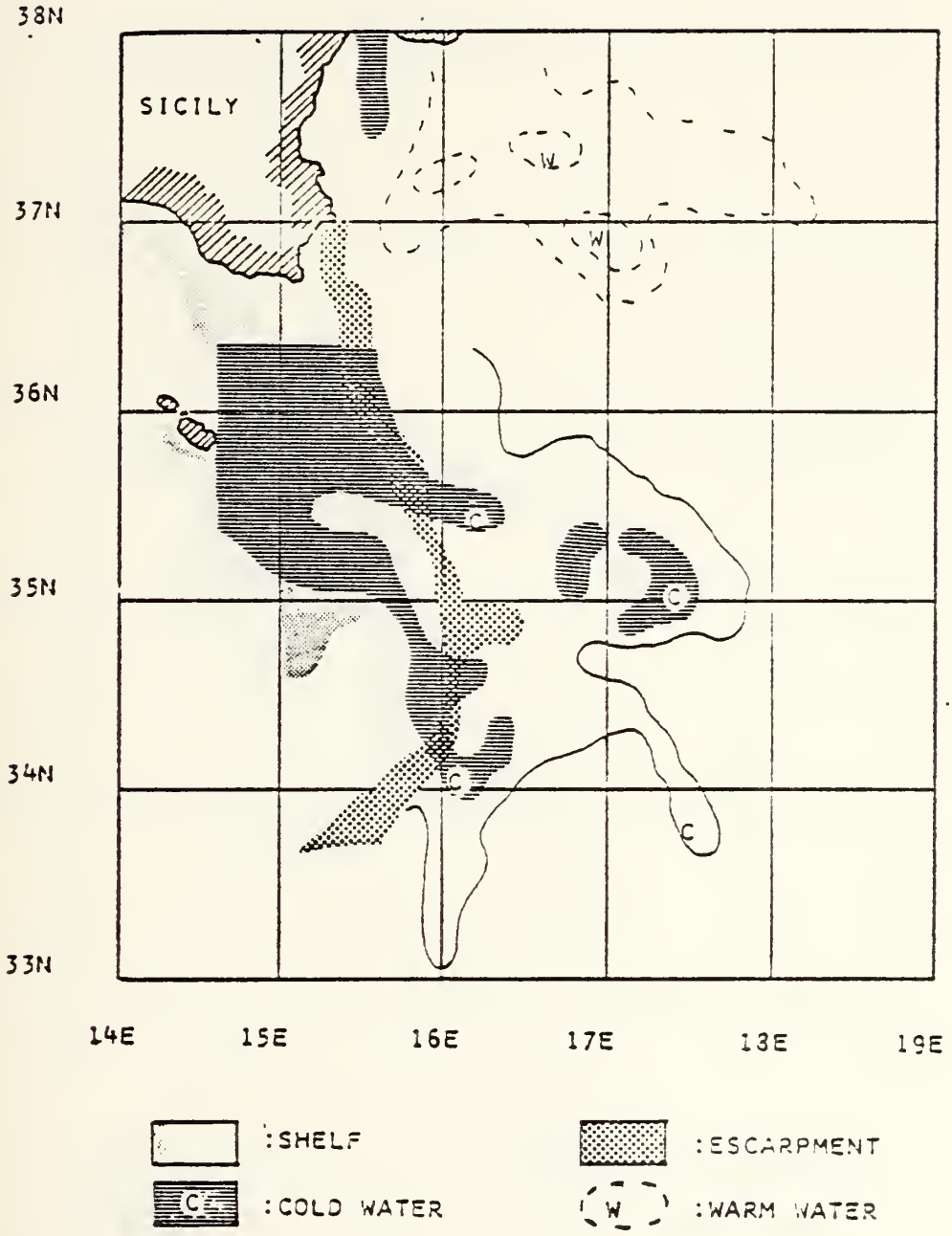

Figure 9. Composite satellite images 15 to 17 June. The anticyclonic flow has separated from the cold water "tongue" which lies at the latitude of Malta I.; the southern "tongue" follows the topography.

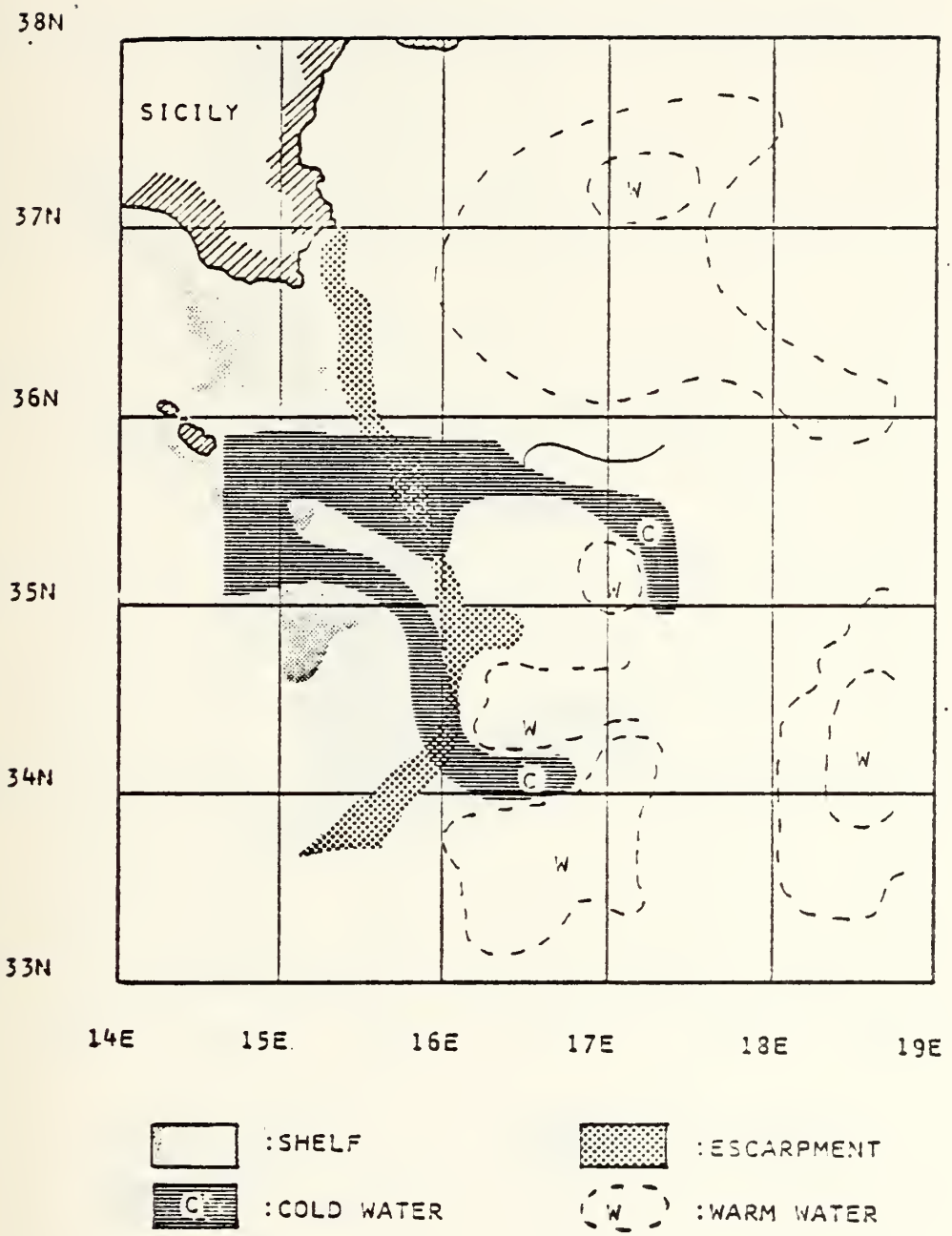

Figure 10. Satellite image of 22 June. Both cold water "tongues" have regained their extension into the Ionian Sea.

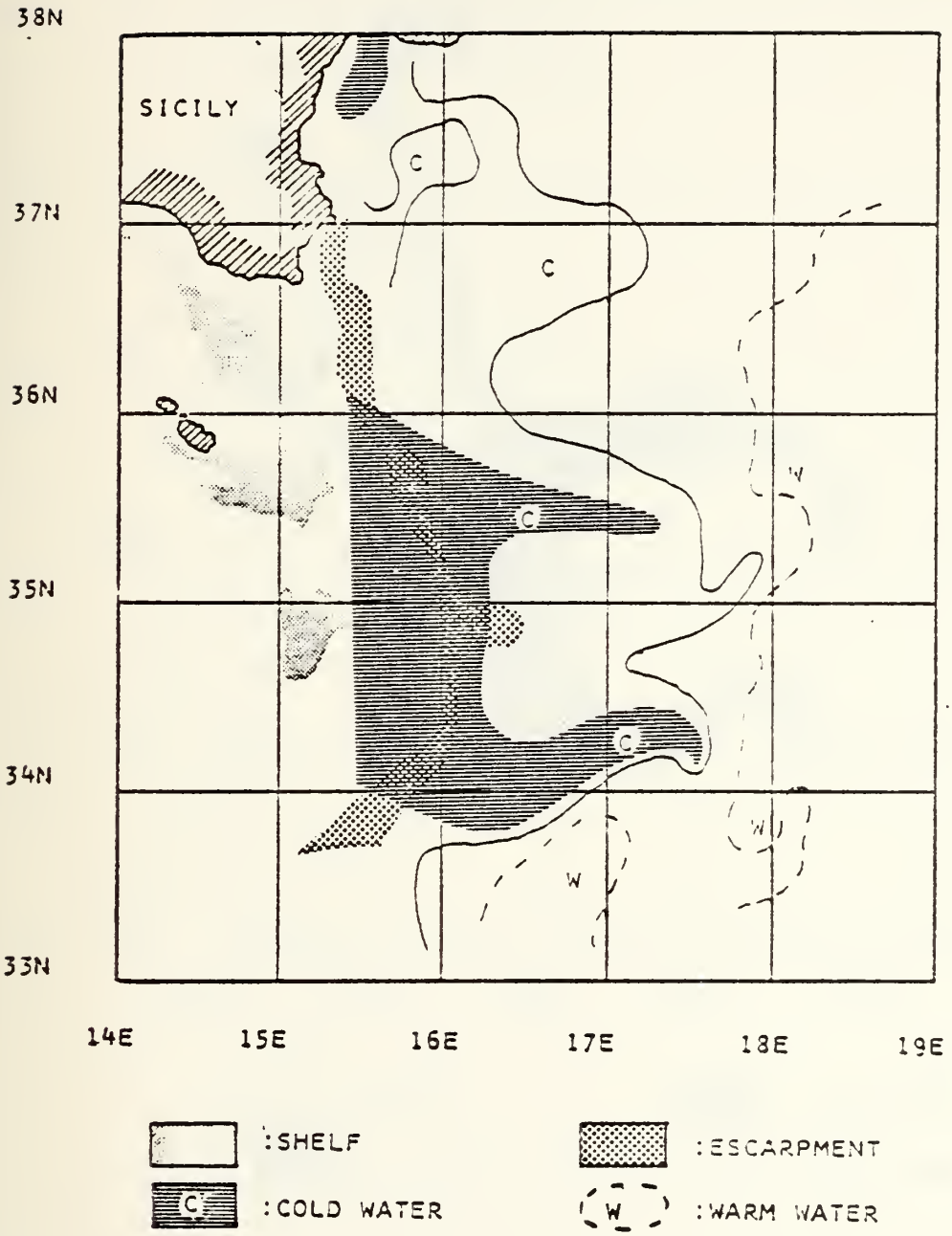

Figure 11. Satellite image of 23 June. (See previous figure).

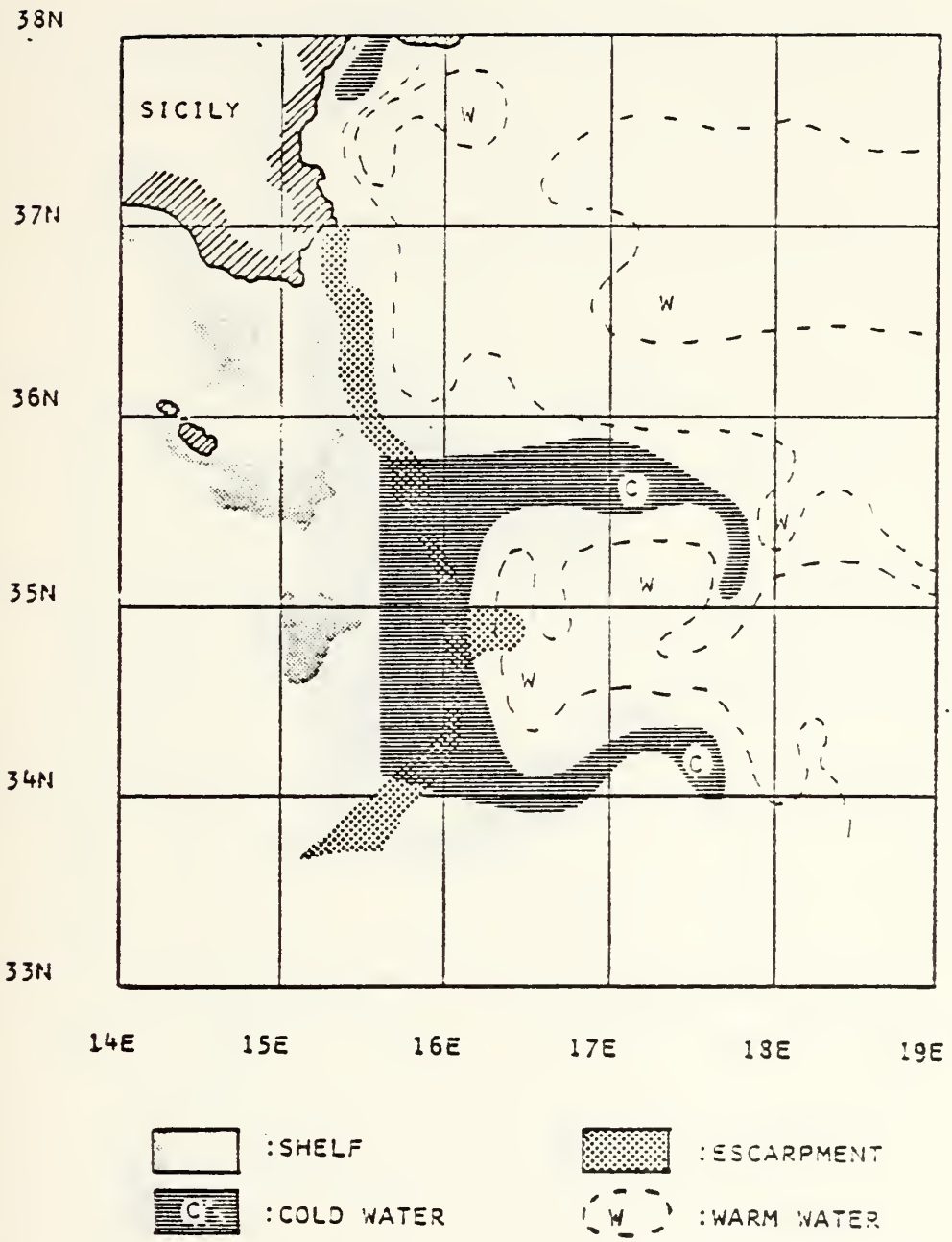

Figure 12. Composite satellite images 24 to 25 June. The northern cold water "tongue" has again curled into an anticyclonic flow. Comparison with Fig. 8 indicates a 10-day time scale.

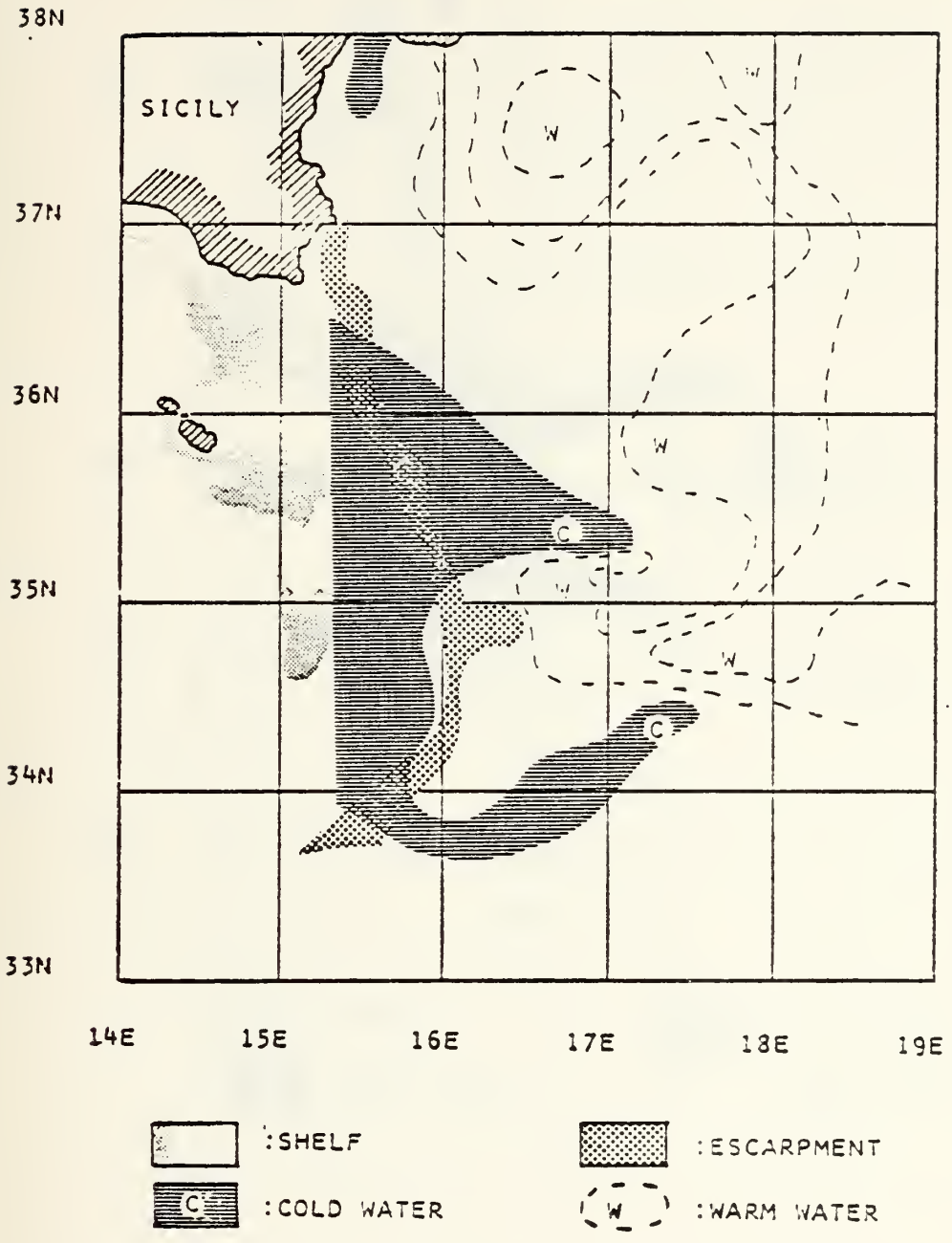

Figure 13. Composite satellite images 29 to 30 June. (See previous figure)

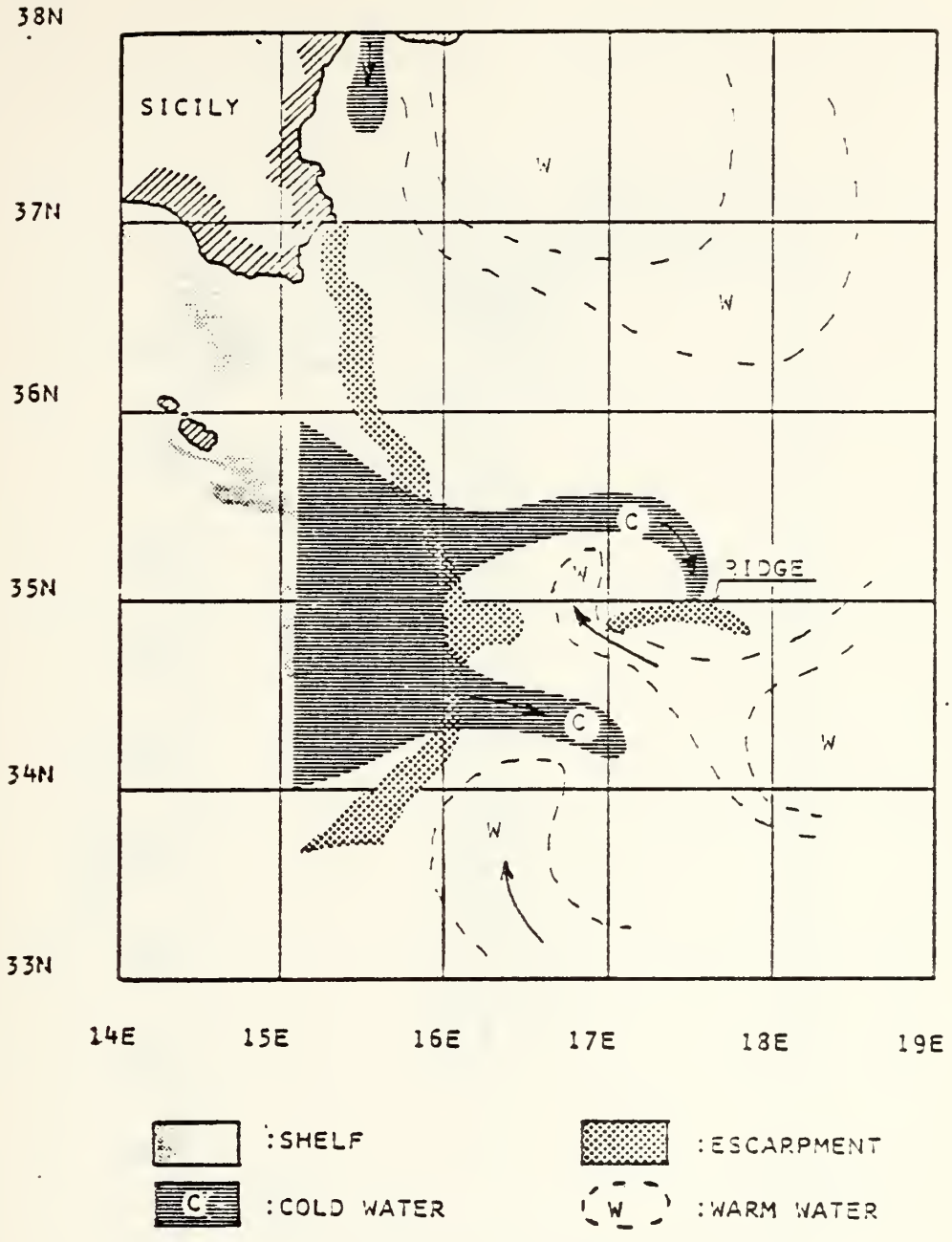

Figure 14. Thirty-day composite surface thermal pattern based on satellite images. This interpretative figure summarizes the surface flow pattern. Cold water flows eastward from the Strait of Sicily into the Western Ionian Sea. The northern part of the area is warmer with no visible distortion of temperature patterns by advection. A cool water flow of limited extent (and coastal upwelling, not represented on this figure) are present near the Strait of Sicily.

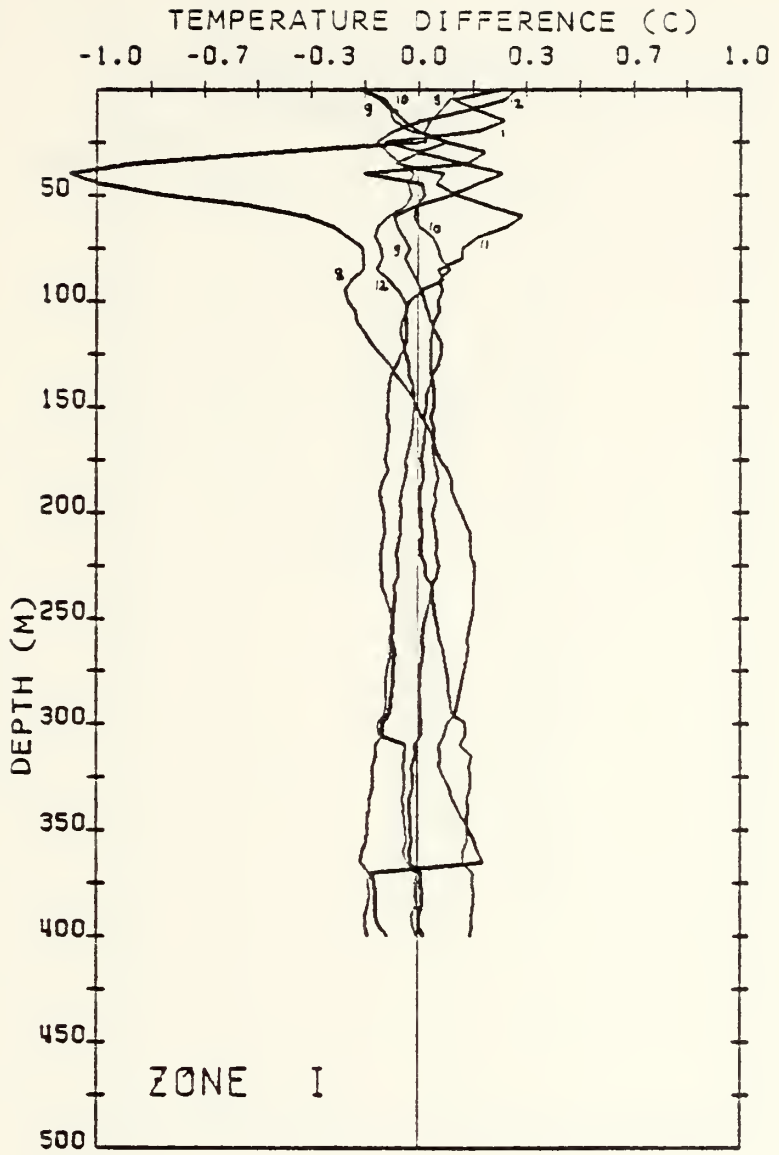

Figure 15. Zone I: Difference between areal mean and daily mean profiles. The number on each profile represents the date. The profiles for the 9 to 12 June period are similar below 25m. Above 25m, they suggest a progressive heating of the surface layer. Step discontinuities in the lower part of the graph correspond to a larger numerical variance at the depth where one of the averaged XBTs is discontinued.

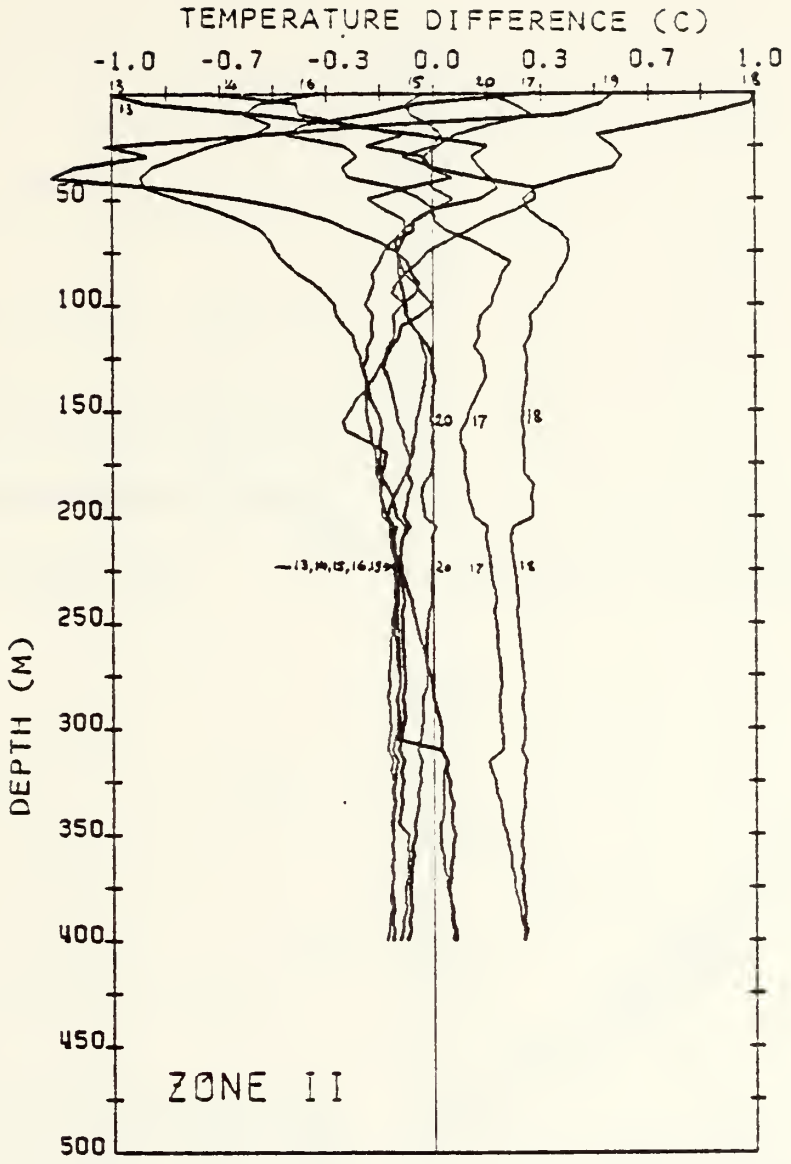

Figure 16. Zone II: Difference between areal mean and daily mean profiles. The number on each profile represents the date. Above 25m, the sequence suggests a heating. At 225m, there is a good grouping of, on the warm side, profiles 17,18 and 20 and, on the cool side, profiles 13 to 16 and 19. The three warmer profiles are located to the NE of the others.

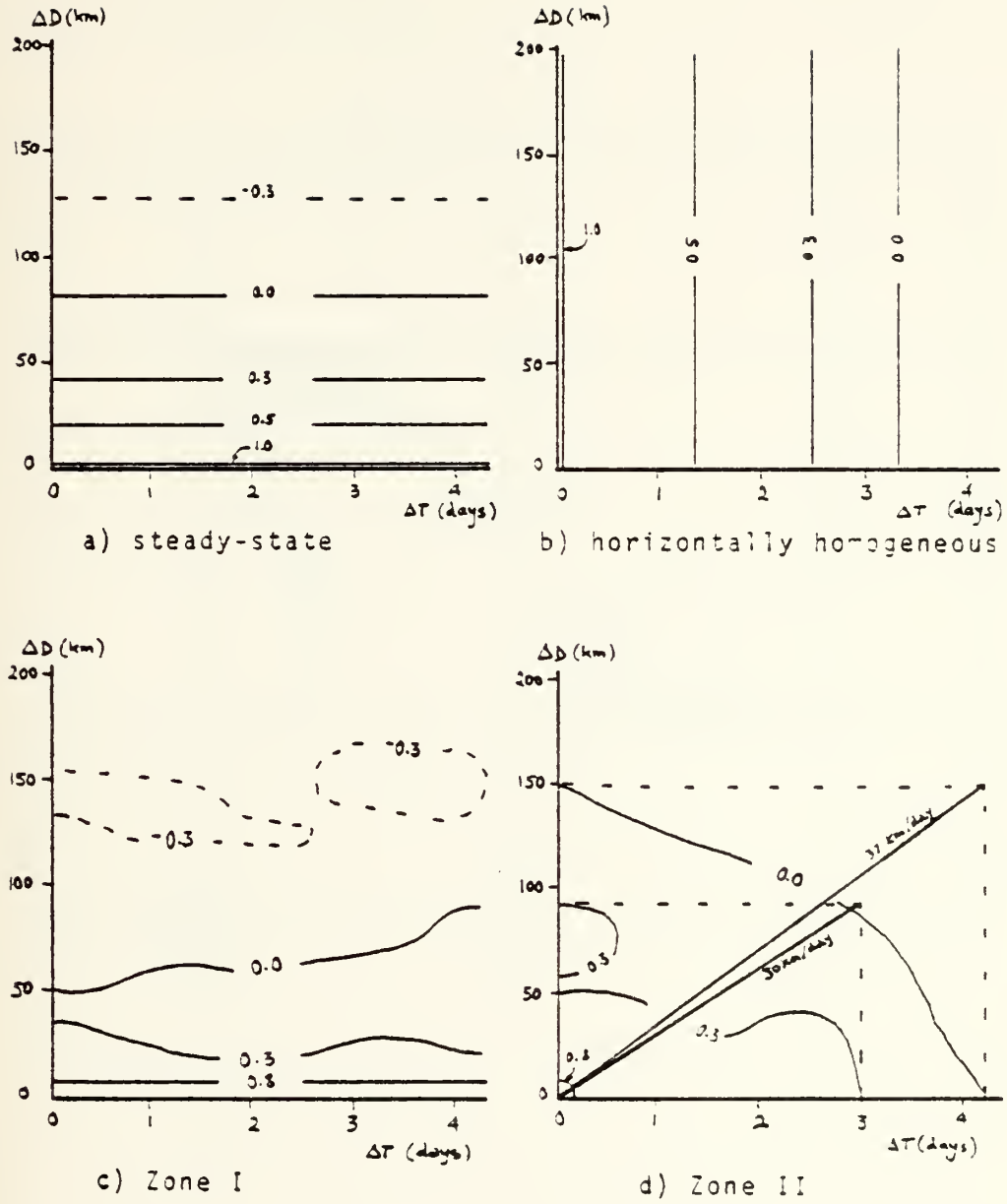

Figure 17. Evaluation of synopticity by space vs. time correlation diagrams. a) Hypothetical steady-state b) Hypothetical horizontally homogeneous state c) Correlation function for Zone I d) Correlation function for Zone II

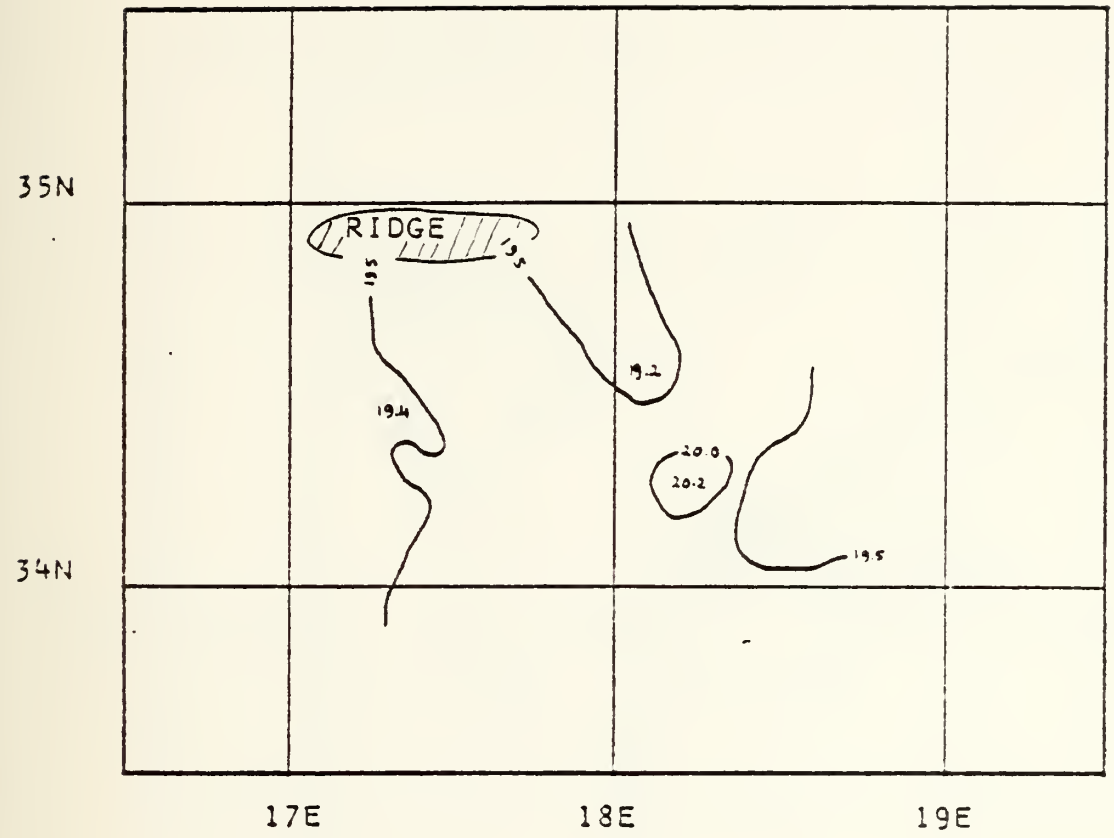

Figure 18. Zone I, June 3 to 12: XBT sea surface temperature (C).

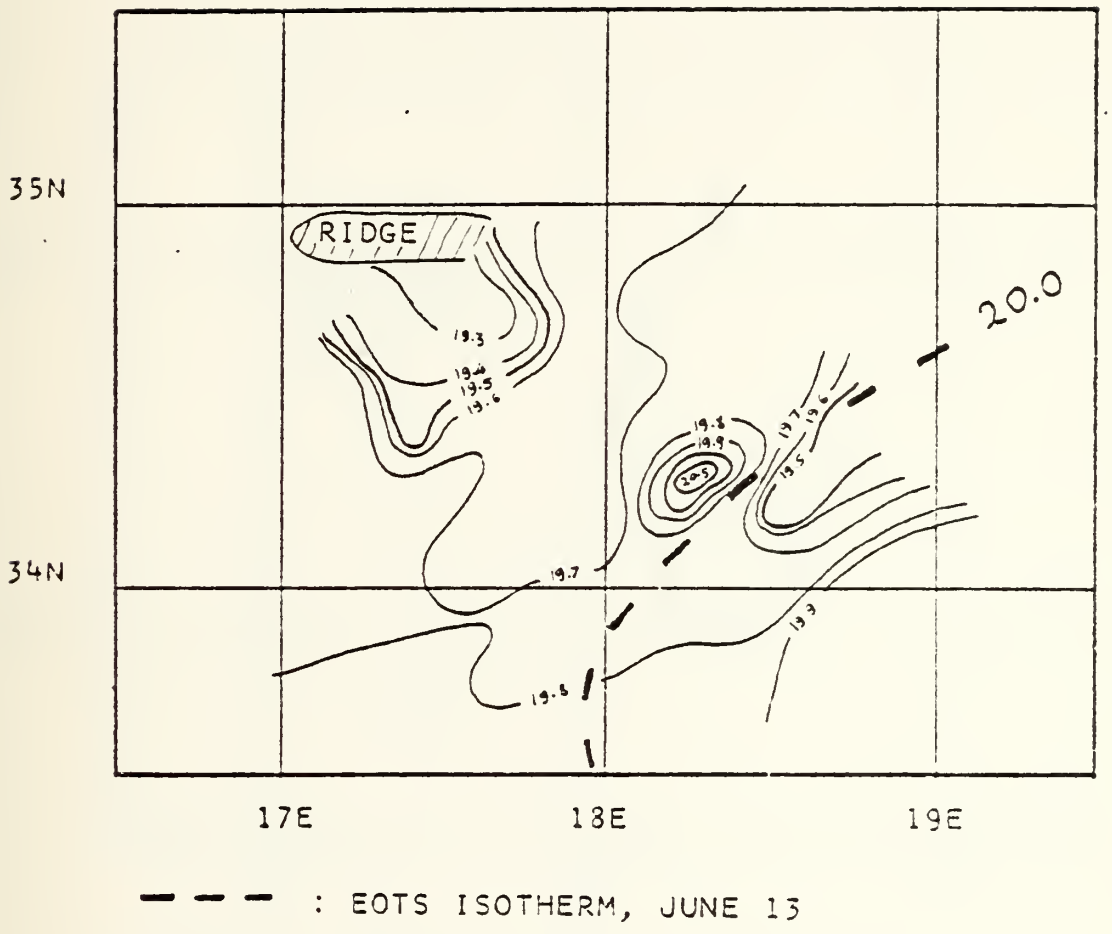

Figure 19. Zone I, June 8 to 12: XBT EOTS interpolated sea surface temperature (C) and final EOTS SST analysis (dashed line)

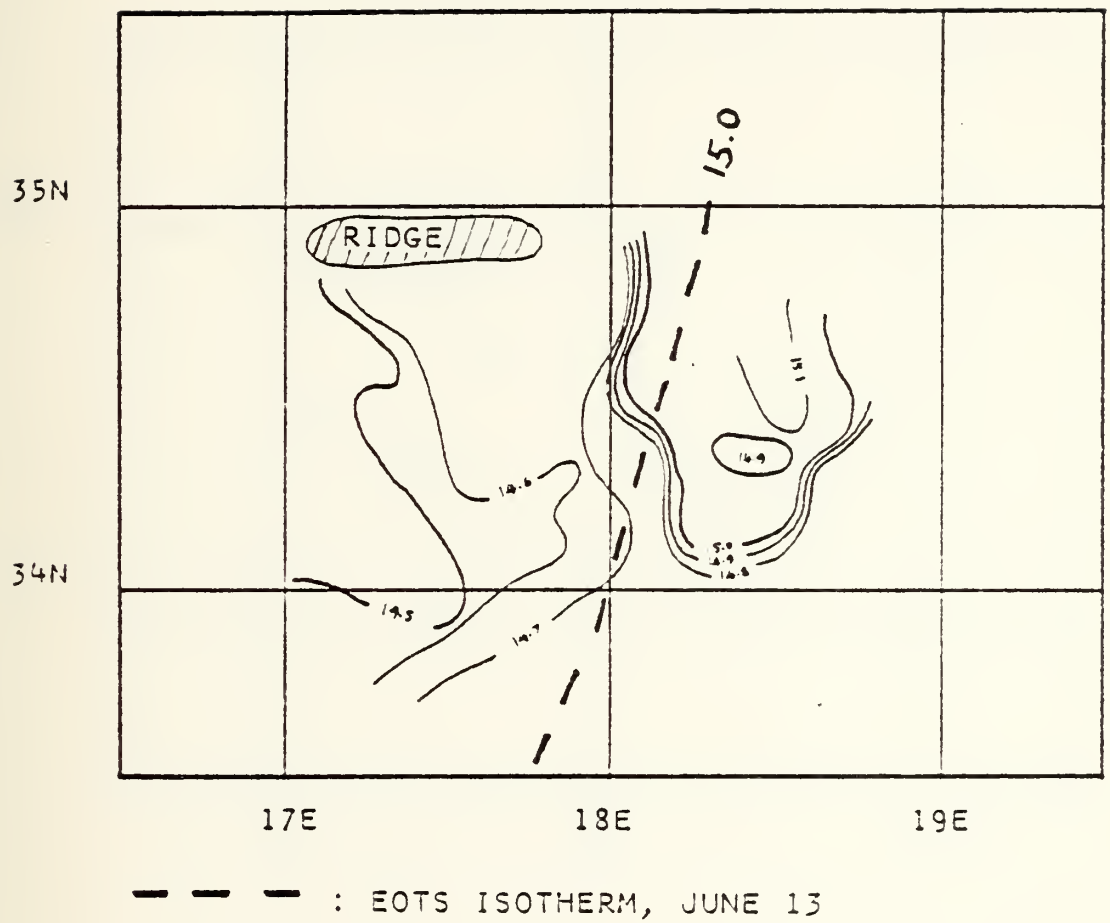

Figure 20. Zone I, June 8 to 12: XBT temperature (C) at 200m depth showing a warm anomaly east of 18°E. The EOTS analysis is the dashed line.

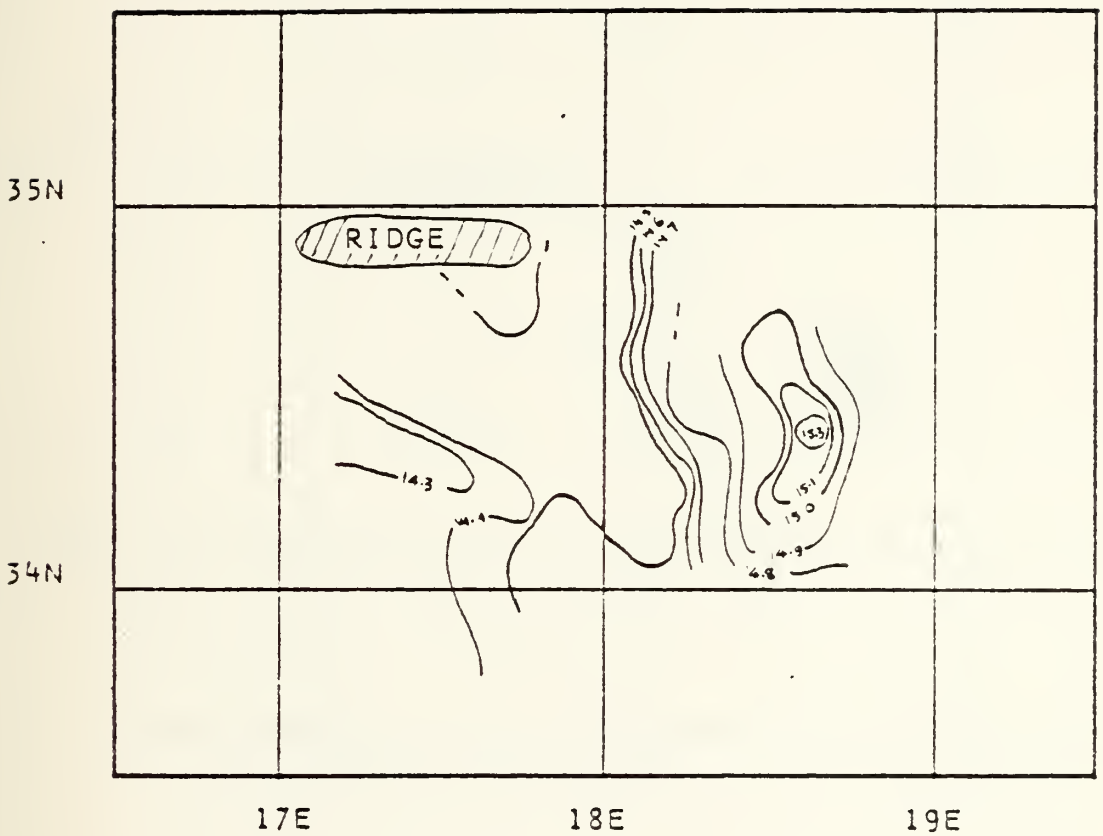

Figure 21. Zone I, June 8 to 12: XBT temperature (C) at 300m depth. No feature is resolved by EOTS at this depth.

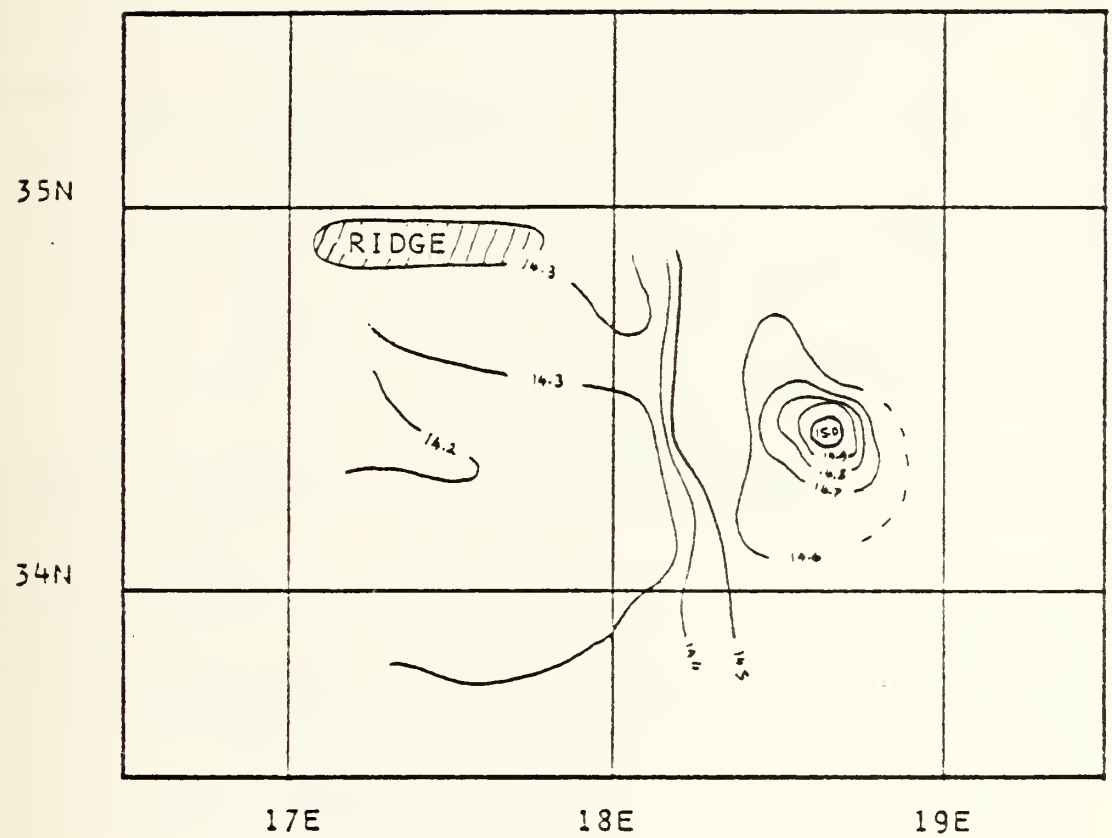

Figure 22. Zone I, June 8 to 12: XBT temperature (C) at 400m depth. The warm anomaly has a smaller size than at the 200 and 300m levels. No feature is resolved by EOTS at this depth.

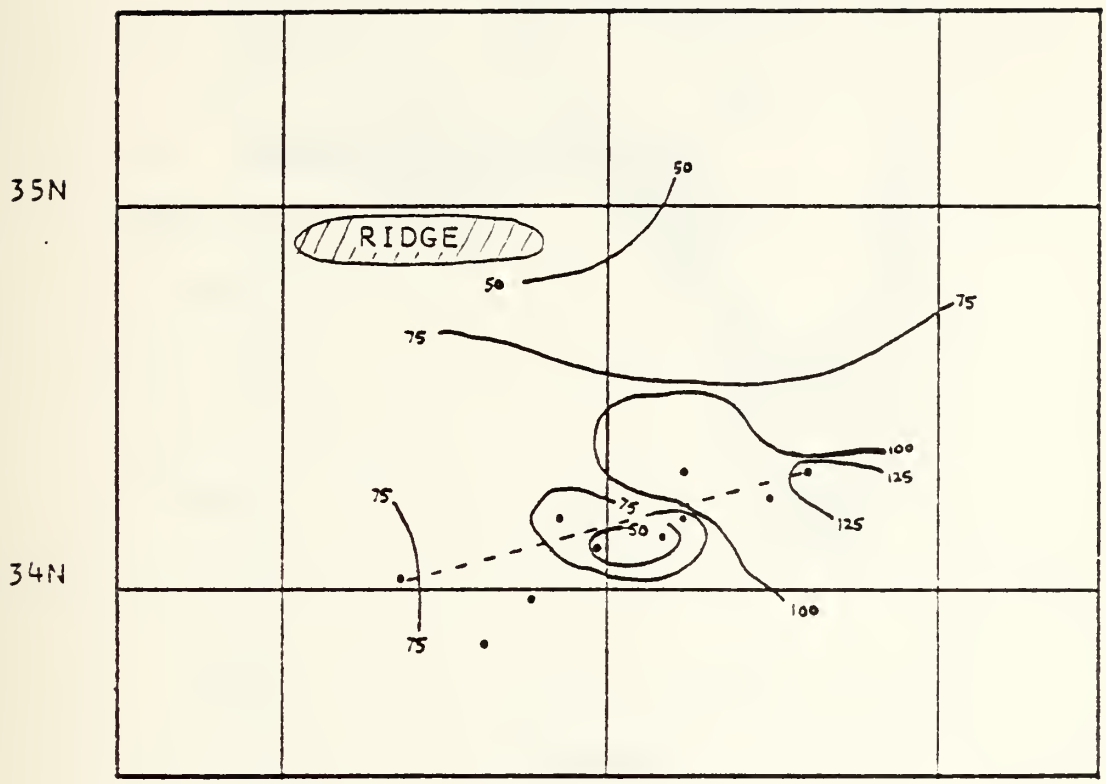

Figure 23. Zone I, June 8 to 12: Inversion depth (m). The inversion depth is almost continous. The change in depth of the inversion is strongest in the vicinity of the warm anomaly.

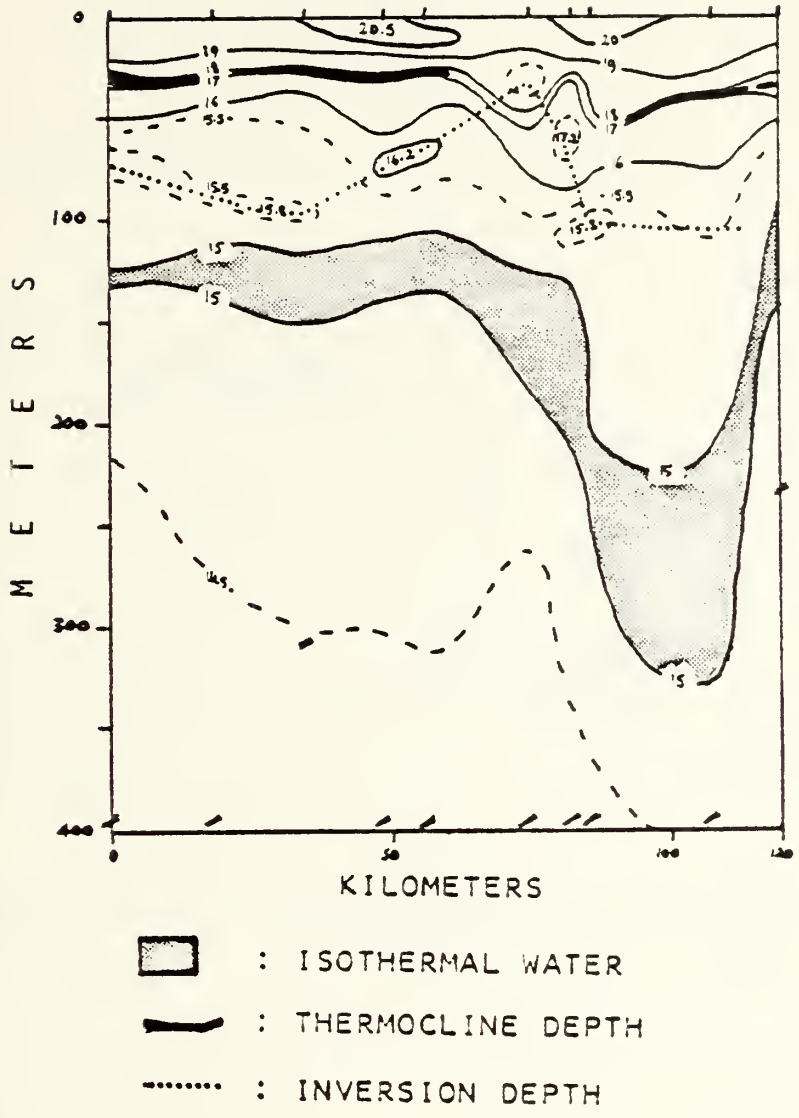

Figure 24. Zone I, June 8 to 12: Temperature (C) transect of the warm anomaly characterized by the 15°C isotherm, with indication of the thermocline depth and the inversion depth. Both of these features are discontinuous on the western edge of the anomaly.

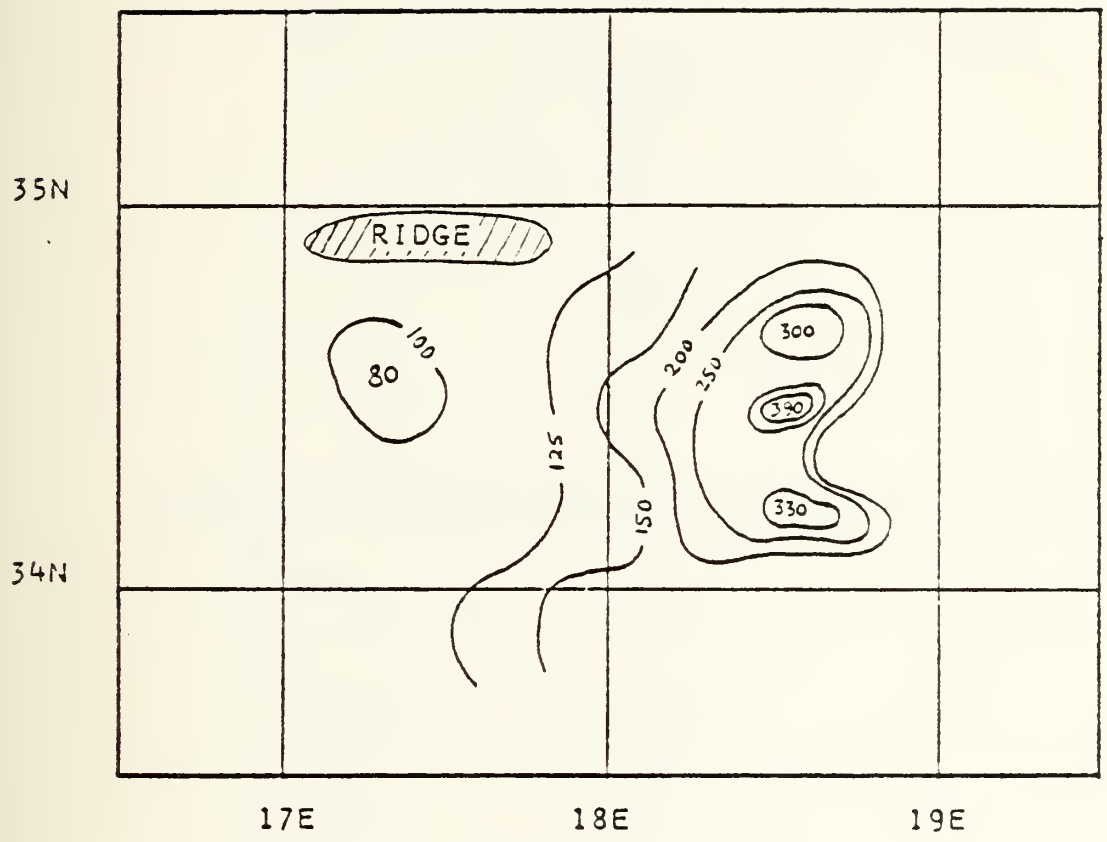

Figure 25. Zone I, June 3 to 12: 15°C isotherm depth (m).

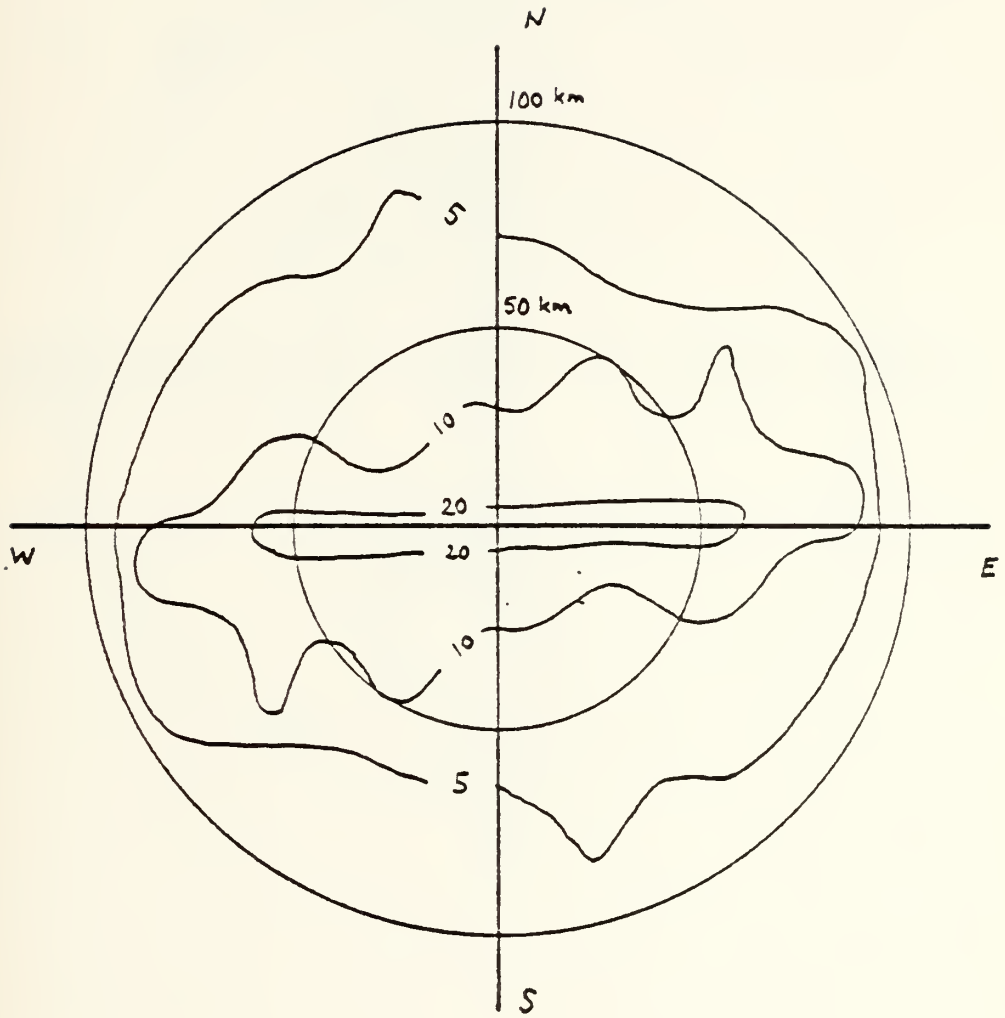

Figure 26. Zone I, June 8 to 12: Number of XBT correlation pairs per 100 sq km indicating a general E-W stretching of the data density.

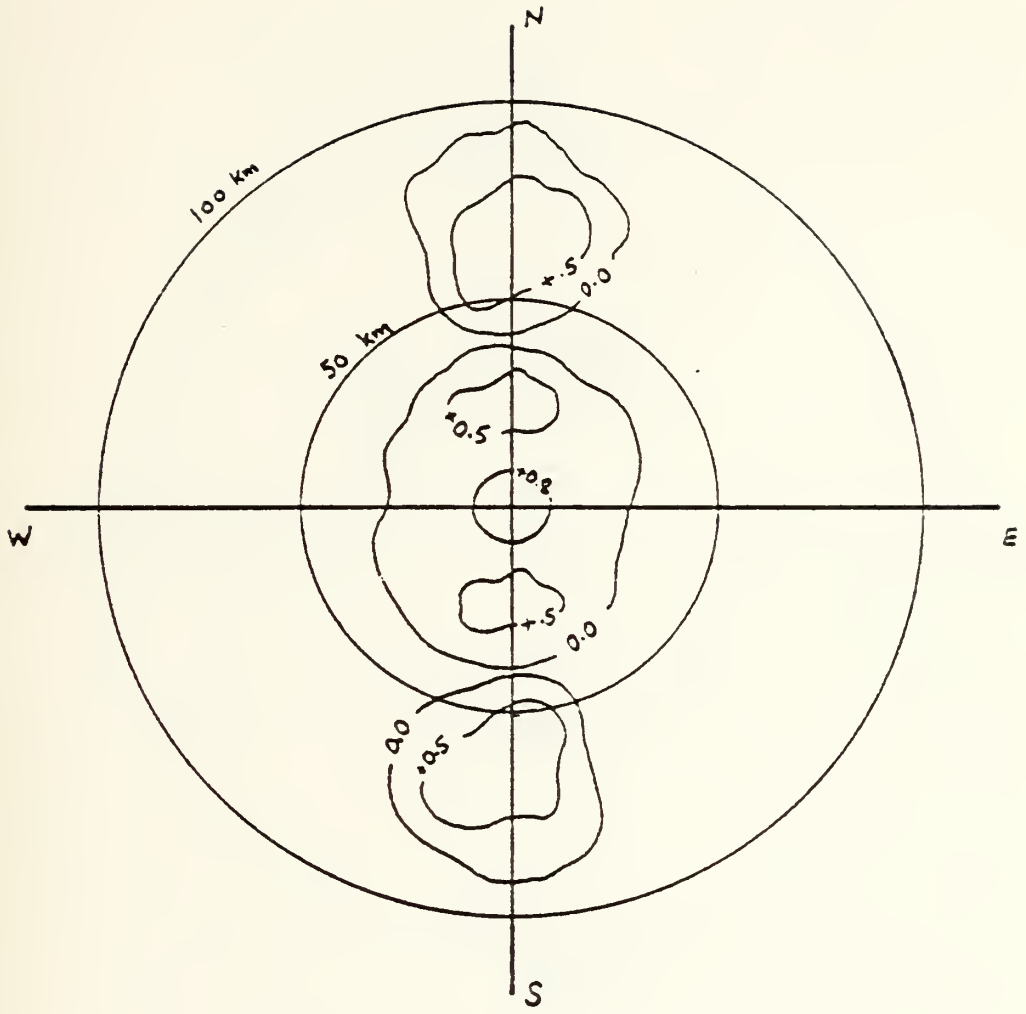

Figure 27. Zone I, June 8 to 12: Horizontal correlation function in the 0 to 60m layer. Zero-crossing occurs at 30 km in the E-W direction, plus a "wavy" N-S perturbation.

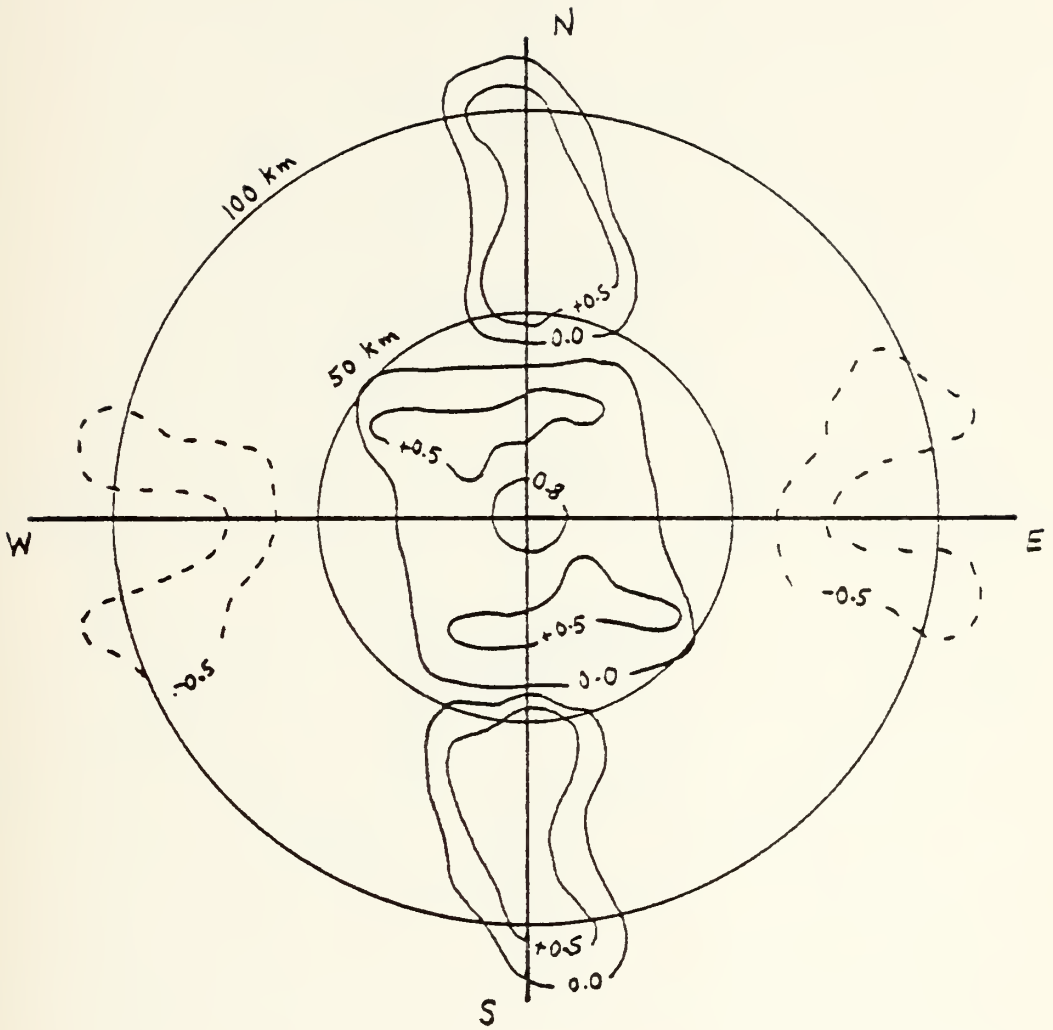

Figure 28. Zone I, June 8 to 12: Horizontal correlation function in the 60 to 150m layer. It is similar to the surface layer pattern, with an increased (negative) correlation in the E-W direction at a distance of 70 km.

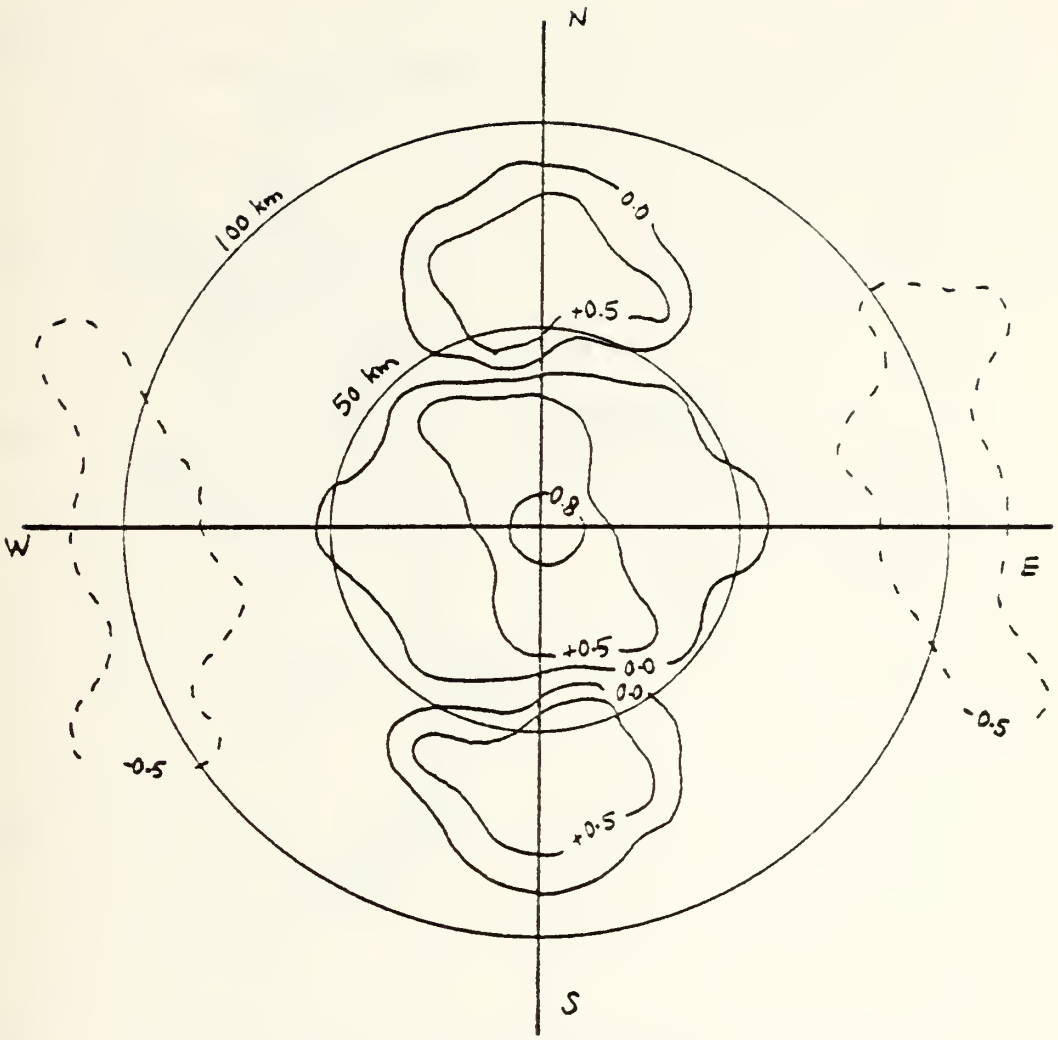

Figure 29. Zone I, June 8 to 12: Horizontal correlation function in the 150 to 400m layer. Similar to the preceding figure, but with a generally stronger correlation attributable to the lesser influence of surface variables. There seems to be an axis for better-than-average correlation along 340T.

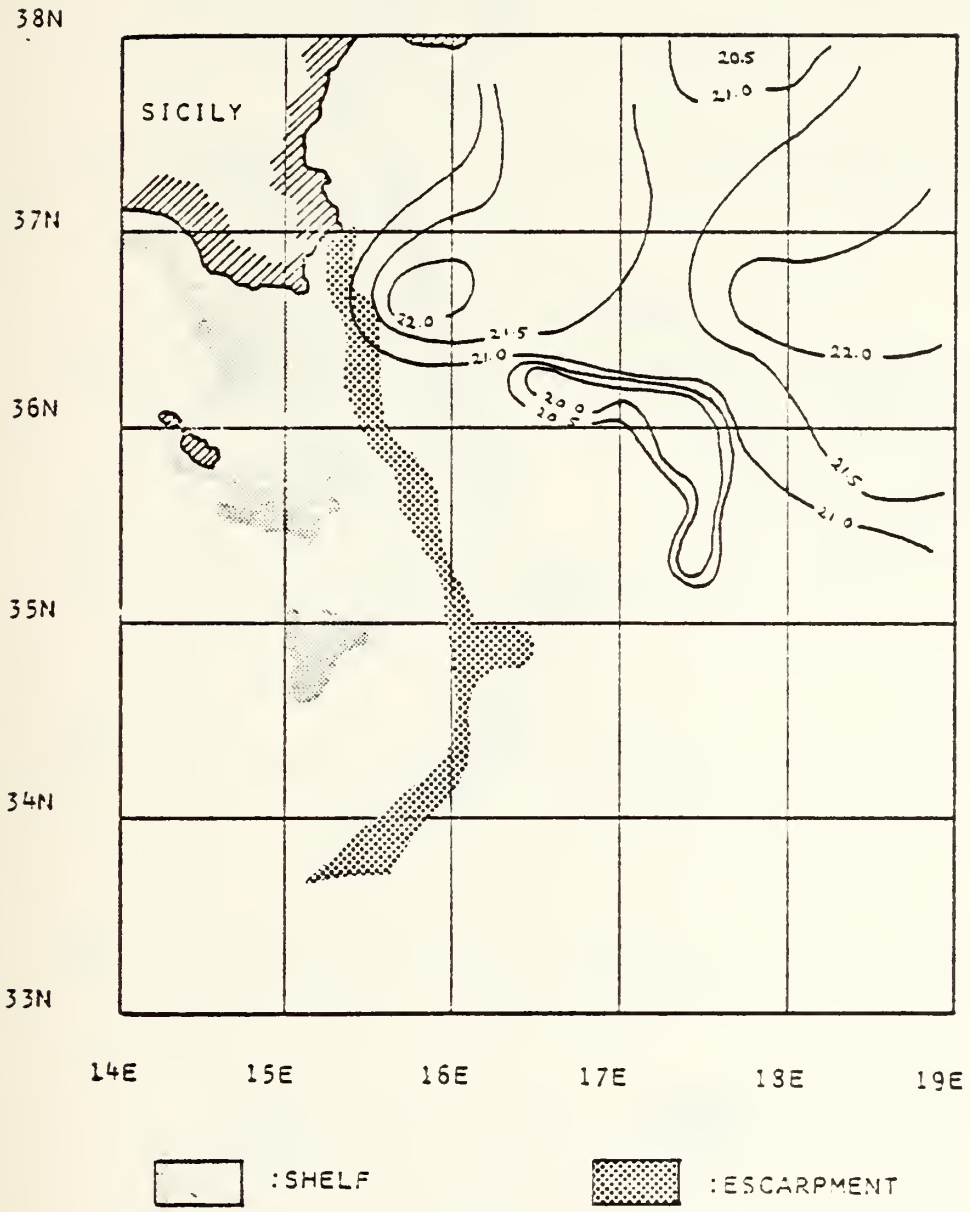

Figure 30. Zone II, June 13 to 20: XBT sea surface temperature (C).

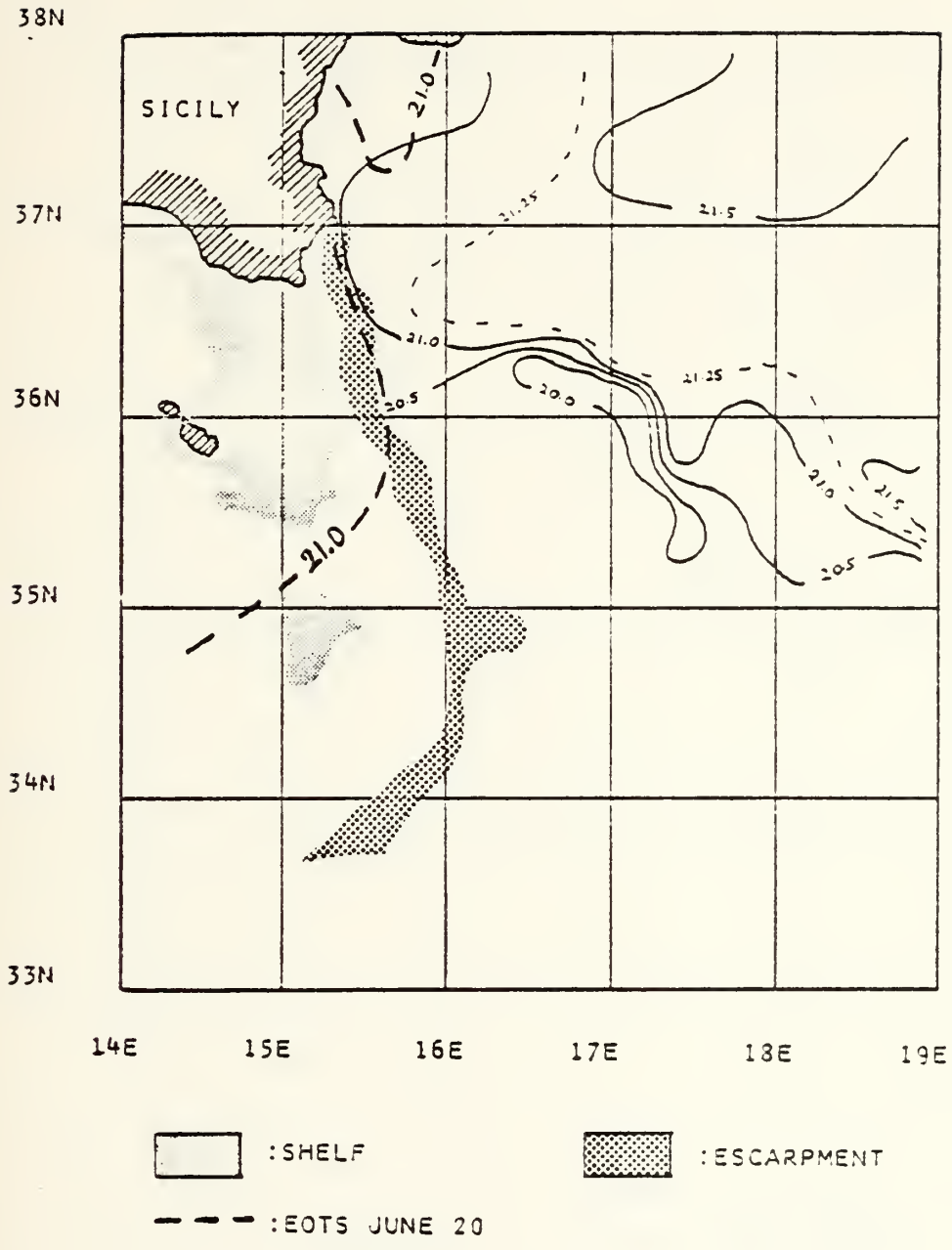

Figure 31. Zone II, June 13 to 20: XBT EOTS interpolated sea surface temperature (C) and final EOTS SST analysis (dashed line).

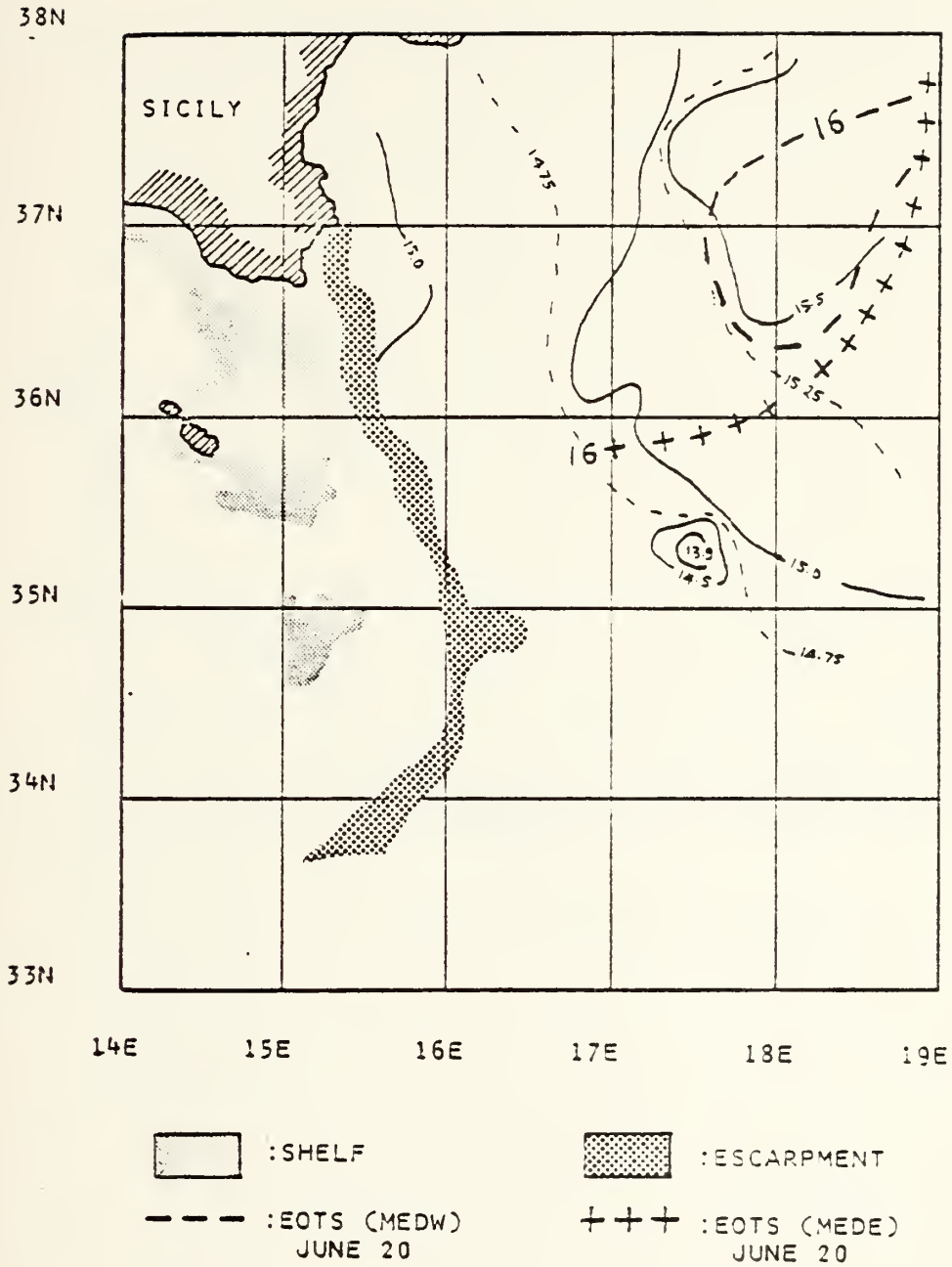

Figure 32. Zone II, June 13 to 20: XBT temperature (C) at 100m depth. There is some dissimilitude between the Eastern and Western Mediterranean Sea EOTS analysis.

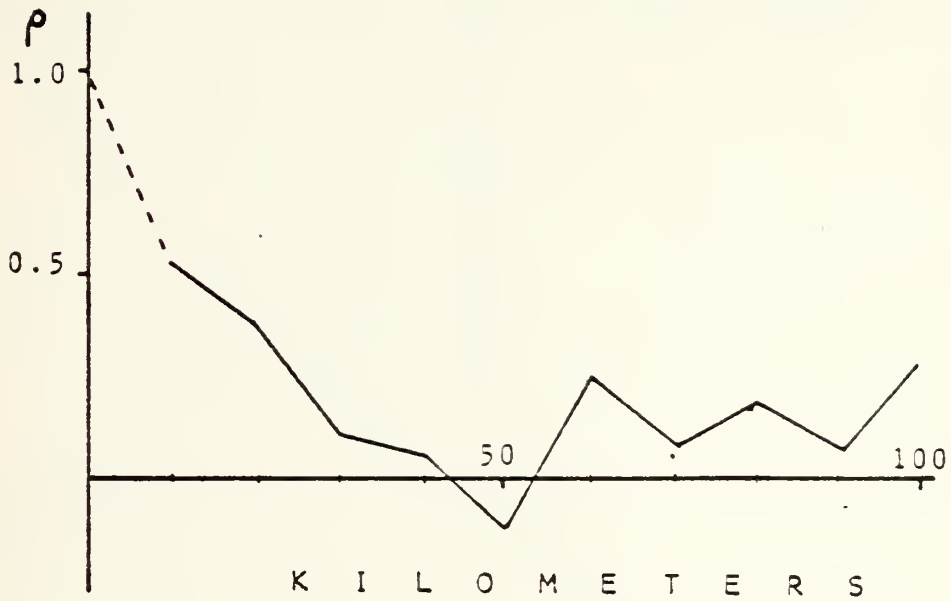

Figure 33. Zone II, June 13 to 20: Spatial correlation function in the 150 to 400m layer. It has a zero-crossing at a distance of 45 km.

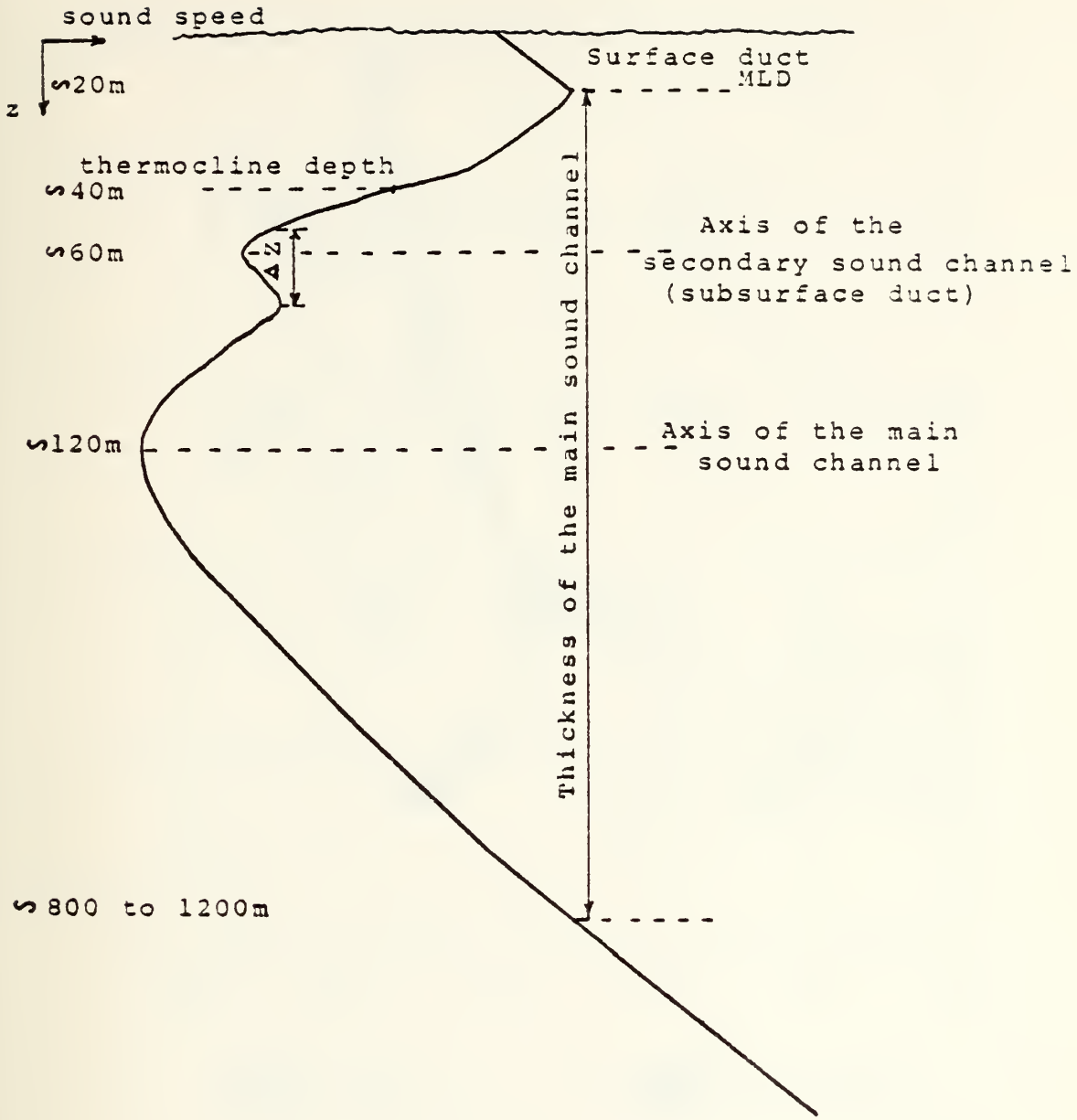

Figure 34. Sound speed profile: definition of characteristic features.

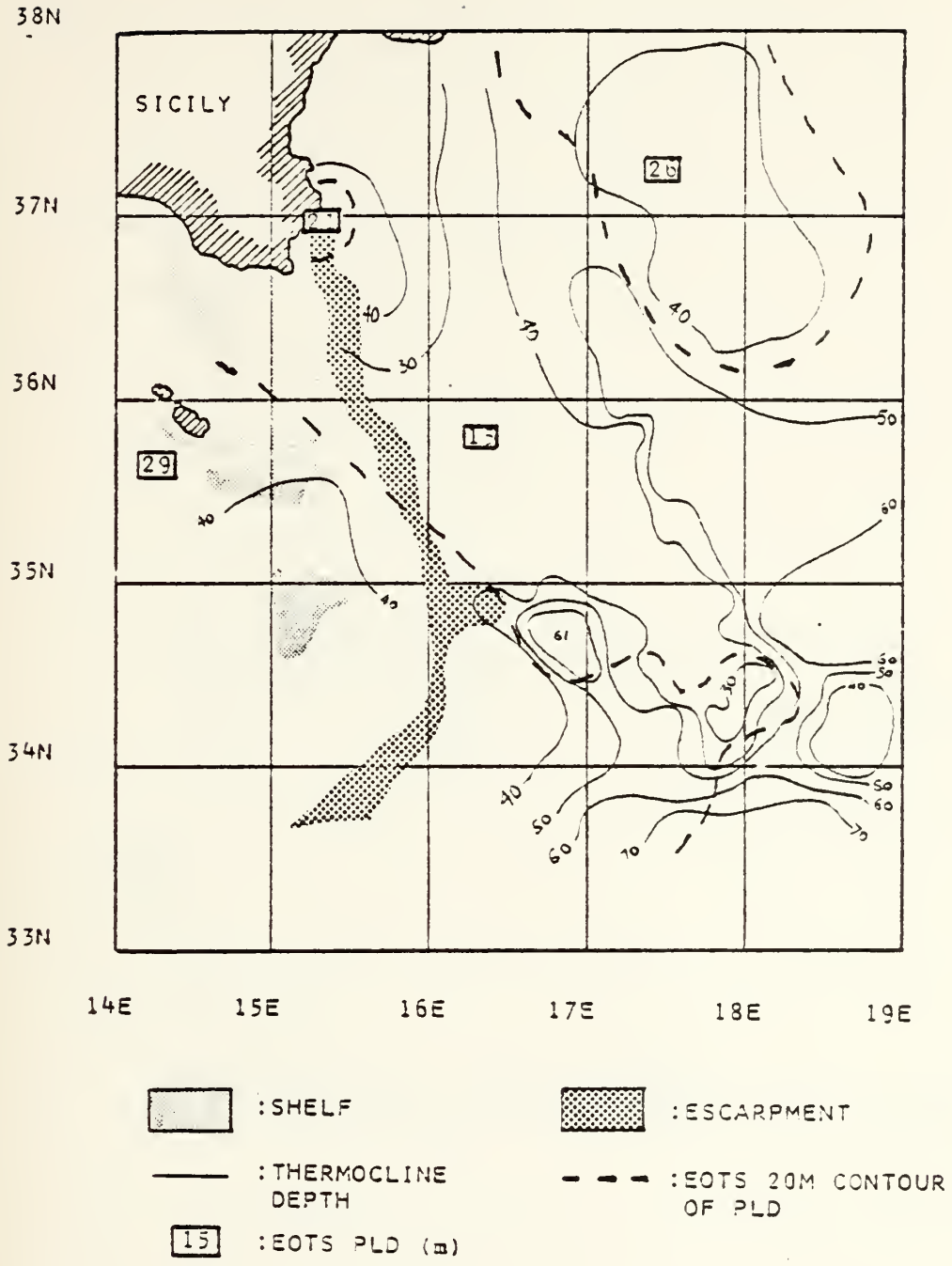

Figure 35. Thermocline depth. Variability is large in Zone I. An area of shallow thermocline depth crossed the region, and fits reasonably well with the flow of surficial water from the Strait of Sicily.

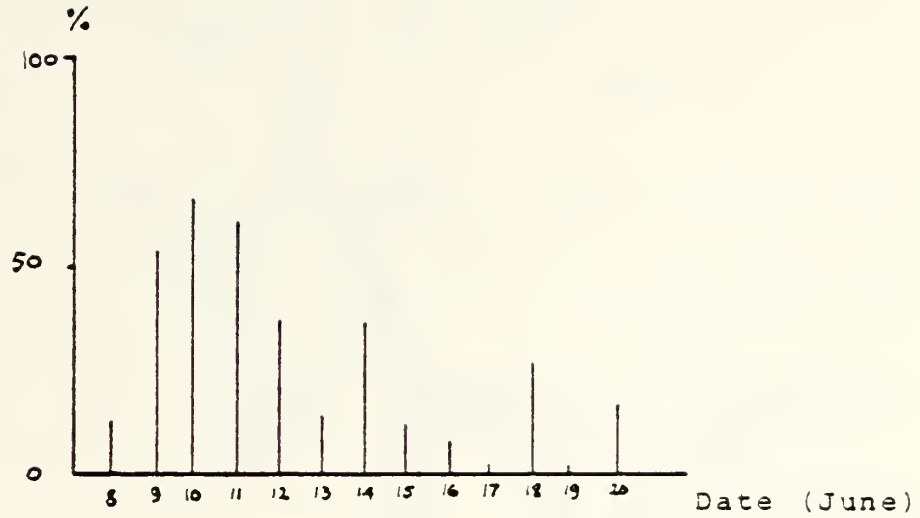

a)

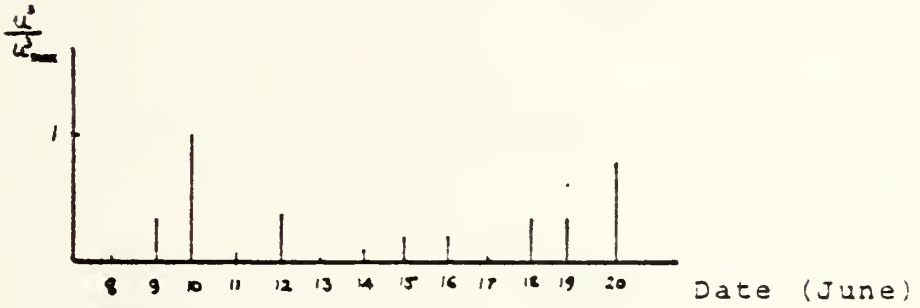

b)

Figure 36. Time distribution of surface ducts a) daily frequency of occurrence of a surface duct b) normalized cube of the daily average surface wind speed.

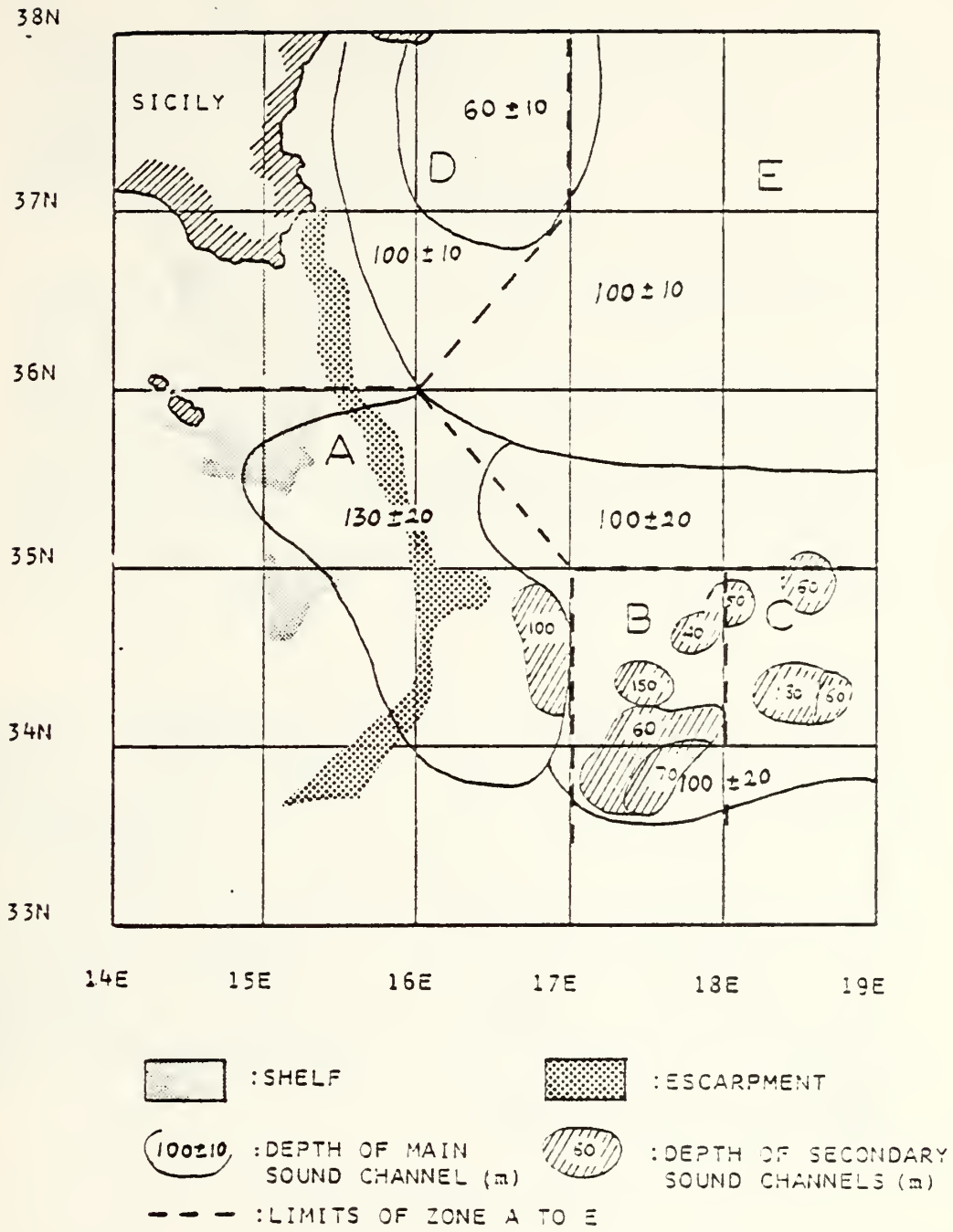

Figure 37. June 8 to 20: distribution and depth of sound channels. The main sound channel is shallower than average in Zone D and deeper in Zone A. Secondary sound channels are present only in Zones B,C, and the SE part of Zone A.

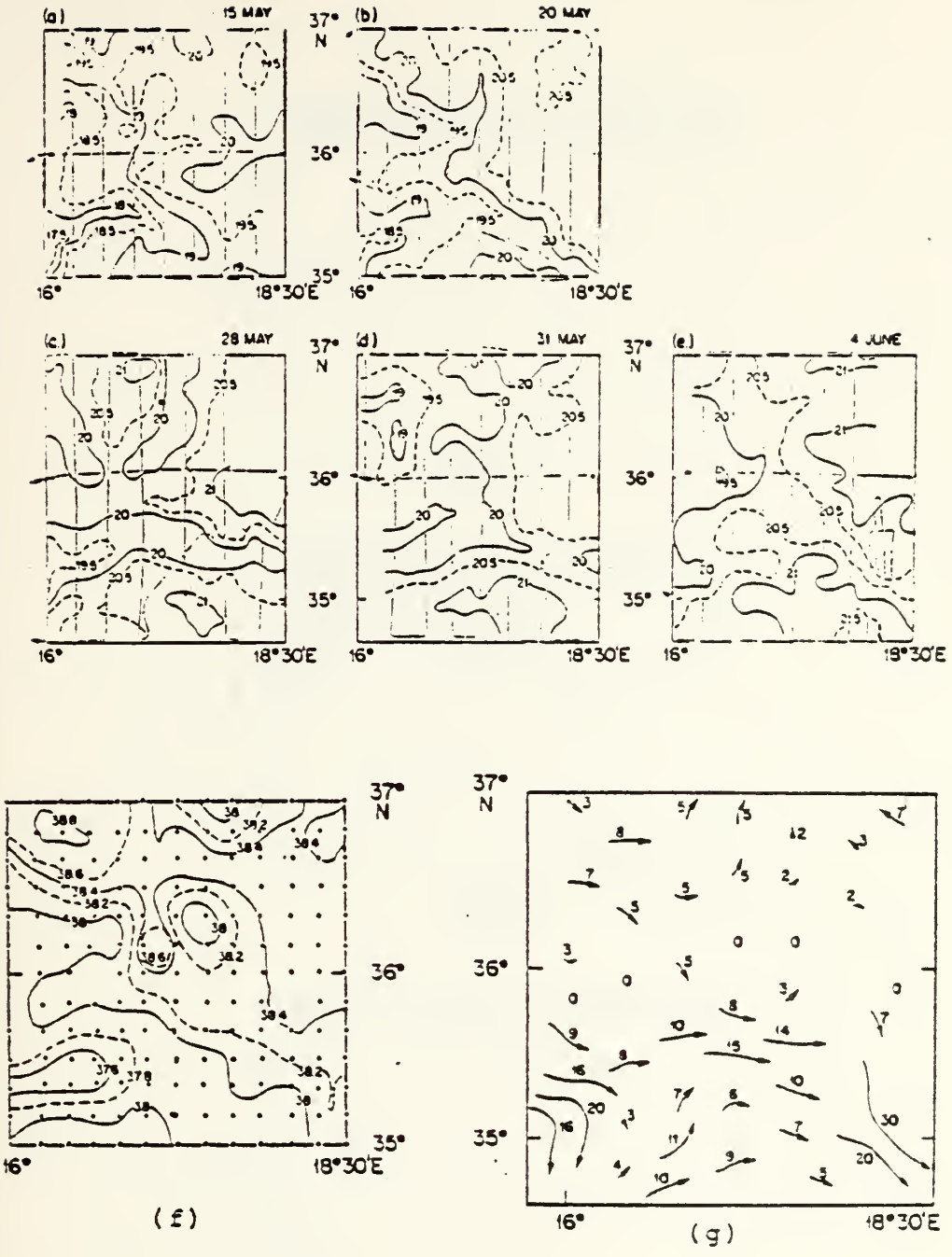

(from Saunders, 1972)

Figure 38. Horizontal temperature, salinity and geostrophic current from MILOC-68 area and ART measurements a to e) Series of ART measurements for the 15 May to 4 June period, showing the development of a "tongue" of cold water flowing eastward. f) surface salinity g) geostrophic currents relative to 200db.

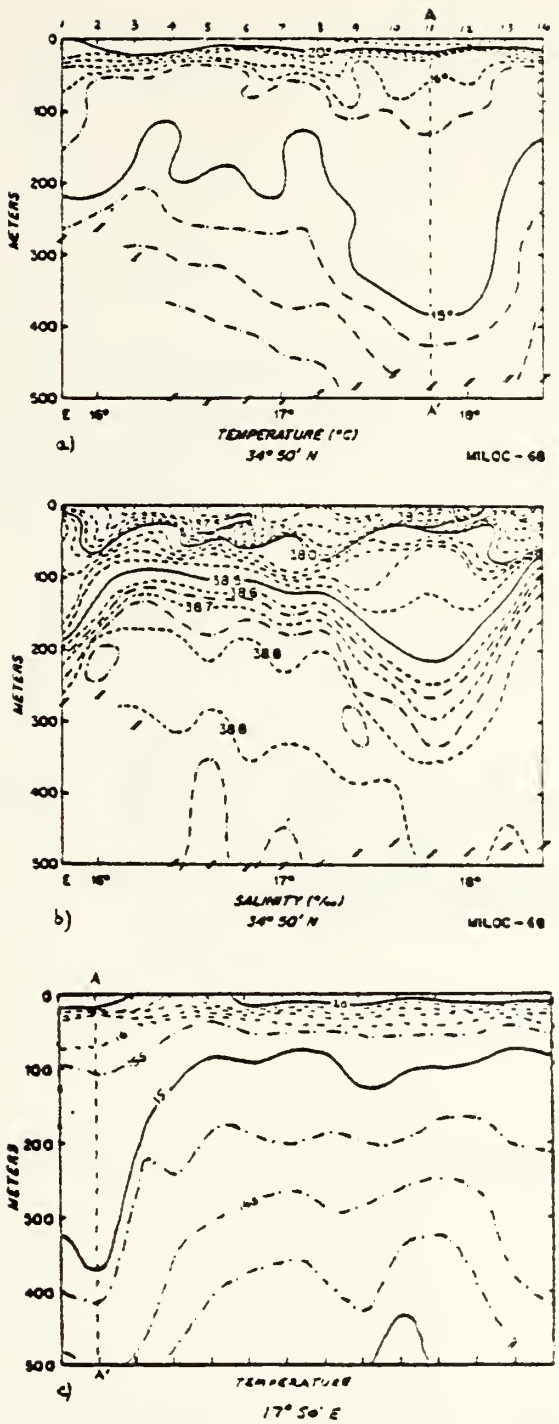

(a and b from Miller, 1972)

Figure 39. Eddy transect from MILOC-68 data a) EW temperature transect along 34°50'N b) EW salinity transect along 34°50'N c) NS temperature transect along 17°50'N, which intersects (a) at AA', the center of the eddy.

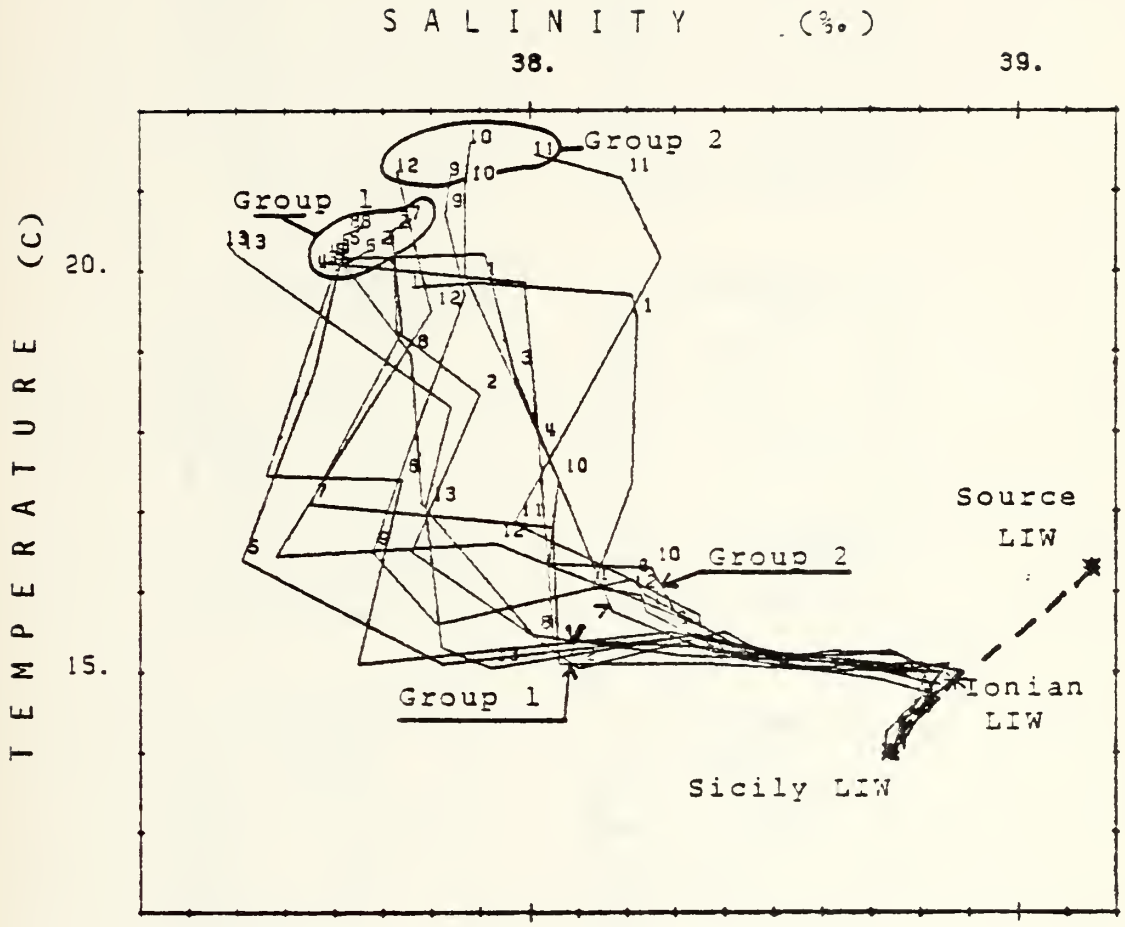

Figure 40. TS diagram from transect along 34°50'N (MILOC-68). The numbers indicate tha profile index (Fig. 39-a). Two groupings: profiles 1 to 8 and profiles 9 to 12, are clearly seen at the surface, and can be traced at the 50 to 100m level, giving an indication of different water composition. The composition of LIW at its source, in the Ionian Sea and in the Strait of Sicily is indicated.

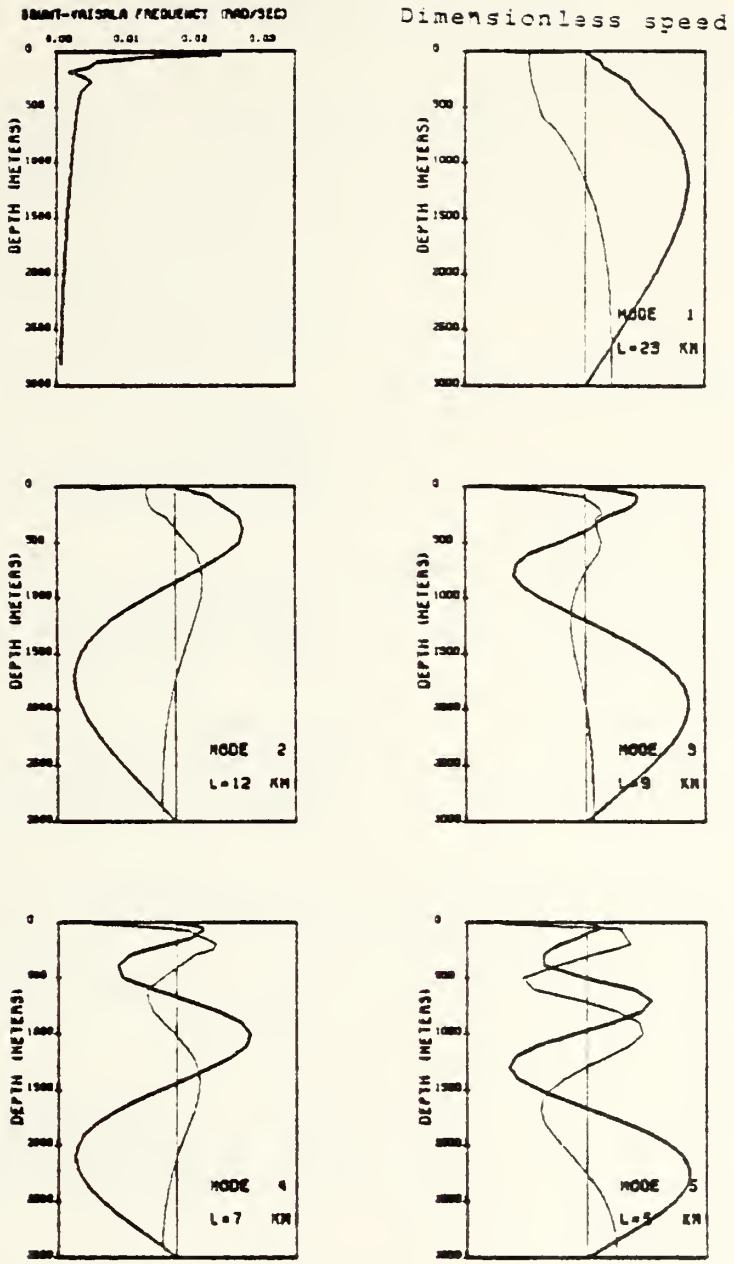

Figure 41. Brunt-Vaisala profile and baroclinic wave solutions for modes 1 to 5. The thick lines represent vertical motion profiles, the thin lines represent horizontal motion profiles. L is the modal baroclinic radius of deformation. See section K.C.2 for discussion.

INITIAL DISTRIBUTION LIST

		No. Copies
1.	Defense Technical Information Center Cameron Station Alexandria, Virginia 22314	2
2.	Library, Code 0142 Naval Postgraduate School Monterey, California 93940	2
3.	Professor C. N. K. Mooers, Chairman, Code 68Mr Department of Oceanography Naval Postgraduate School Monterey, California 93940	2
4.	Professor R. J. Renard, Chairman, Code 63Rd Department of Meteorology Naval Postgraduate School Monterey, California 93940	1
5.	Dr. R. H. Bourke, Code 68Bf Department of Oceanography Naval Postgraduate School Monterey, California 93940	1
6.	L. V. Laurent Monsaingeon Etat-Major de la Marine (EMM/MAT/SSM) 2, rue Royale 75200 Paris Naval, France	10
7.	Director Naval Oceanography Division Naval Observatory 34th and Massachusetts Avenue NW Washington, DC 20390	1
8.	Commander Naval Oceanography Command NSTL Station Bay St. Louis, Missouri 39522	1
9.	Commanding Officer Naval Oceanographic Office NSTL Station Bay St. Louis, Missouri 39522	1

10. Commanding Officer 1
Fleet Numerical Oceanography Center
Monterey, California 93940

11. Commanding Officer 1
Naval Ocean Research and Development Activity
NSTL Station
Bay St. Louis, Missouri 39522

12. Commanding Officer 1
Naval Environmental Prediction Research Facility
Monterey, California 93940

13. Chairman, Oceanography Department 1
U.S. Naval Academy
Annapolis, Maryland 21402

14. Chief of Naval Research 1
800 N. Quincy Street
Arlington, Virginia 22217

15. Office of Naval Research (Code 480) 1
Naval Ocean Research and Development Activity
NSTL Station
Bay St. Louis, Missoui 39522

16. Scientific Liaison Office 1
Office of Naval Research
Scripps Institution of Oceanography
La Jolla, California 92037

17. Library 1
Scripps Institution of Oceanography
P.O. Box 2367
La Jolla, California 92037

18. Library 1
Department of Oceanography
University of Washington
Seattle, Washington 98105

19. Library 1
CICESE
P.O. Box 4803
San Ysidro, California 92073

20. Library 1
School of Oceanography
Oregon State University
Corvallis, Oregon 97331

21. Commander 1
Oceanographic Systems Pacific
Box 1390
Pearl Harbor, Hawaii 96860

22. Commanding Officer 1
Naval Oceanography Commander Center, Rota
Box 31
Fleet Post Office
San Francisco, California 09540

23. SACLANT ASW Research Center 2
(1 for R.F.J. Winterburn, Environmental
Data Support)
Viale San Bartolomeo 400
I- 19026- LA SPEZIA- Italy

24. Dr. S. A. Piaczek (Code 322) 1
Naval Ocean Research and Development Activity
NSTL Station
Bay St. Louis, Missouri 39522

25. Dr. A. R. Robinson 1
Division of Engineering and Applied Physics
Harvard University
Cambridge, Massachusetts 02138

26. Prof. L. A. Mysak 1
Mathematics Department
121-1984 Mathematics Road
University of British Columbia
Vancouver, British Columbia, V6T1Y4, Canada

27. Dr. O. M. Johannessen (Arctic Chair), Code 68 1
Department of Oceanography
Naval Postgraduate School
Monterey, California 93940

28. Dr. A. R. Miller 1
Associated Scientists
P.O. Box 721
Woods Hole, Massachusetts 02543

29. LCDR C. R. Dunlap, Code 68Du 2
Department of Oceanography
Naval Postgraduate School
Monterey, California 93940

30. Professor G. Cantin, Code 69Ci — 1
Department of Mechanical Engineering
Naval Postgraduate School
Monterey, California 93940

31. Dr. D. S. Yost, Code 56Yo — 1
Department of National Security Affairs
Naval Postgraduate School
Monterey, California 93940

32. Monsieur l'Amiral — 3
Chef d'Etat-Major de la Marine
2, rue Royale
75200 Paris Naval, France

33. Monsieur le Capitaine de Vaisseau — 2
Commandant le CEPMAN
BP 38, 83800 Toulon Naval, France

34. Capitaine de Vaisseau (e.r.) Beydon — 1
Meteorologie Nationale (Meteo/Maritime)
92106 Boulogne Billancourt Cedex, France

35. Meteorologie Nationale — 1
SMM/Documentation
2, Avenue Rapp
75340 Paris Cedex 07, France

36. Monsieur l'Ingenieur en Chef de l'Armement — 1
Directeur de l'EPSHOM
B.p. 426
29275 Brest Cedex, France

37. Monsieur le Directeur — 1
Centre de Meteorologie Spatiale
(pour Mlle Philippe)
22300 Lannion, France

38. Museum d'Histoire Naturelle — 2
(1 pour Prof. P. Tchernia)
Laboratoire d'Oceanographie Physique
43-45, rue Cuvier
75281 Paris Cedex 05, France

Thesis
M6816
c.1

195426

Monsaingeon
Ocean thermal analysis and related naval operational considerations in the Ionian Sea - June 1980.